NACA TN 4365

NATIONAL ADVISORY COMMITTEE FOR AERONAUTICS

TECHNICAL NOTE 4365

LARGE-SCALE WIND-TUNNEL TESTS OF AN AIRPLANE MODEL WITH AN UNSWEPT, ASPECT-RATIO-10 WING, TWO PROPELLERS, AND AREA-SUCTION FLAPS

By James A. Weiberg, Roy N. Griffin, Jr.,
and George L. Florman

Ames Aeronautical Laboratory
Moffett Field, Calif.

NACA

Washington

September 1958

NATIONAL ADVISORY COMMITTEE FOR AERONAUTICS

TECHNICAL NOTE 4365

LARGE-SCALE WIND-TUNNEL TESTS OF AN AIRPLANE MODEL WITH AN UNSWEPT, ASPECT-RATIO-10 WING, TWO PROPELLERS, AND AREA-SUCTION FLAPS

By James A. Weiberg, Roy N. Griffin, Jr.,
and George L. Florman

SUMMARY

An investigation was made to determine the effects of a propeller slipstream on the lift obtainable and the flow requirements for suction applied to the porous area of a trailing-edge flap on a model of a twin-engine airplane having a high-aspect-ratio, thick, straight wing.

The lift increment produced by the propeller slipstream increased approximately in proportion to the slipstream velocity. The propeller slipstream had no effect on the suction flow requirements, but the suction pressures required increased with thrust coefficient approximately in proportion to the slipstream velocity.

Comparisons with the results of tests on the same model but having a combination slot suction and blowing boundary-layer-control system (Arado) on the trailing-edge flaps and ailerons indicated considerably lower suction flow requirements for the area-suction flaps.

INTRODUCTION

The development of power plants having high ratios of power to weight has made possible the reduction or elimination of the distance required for take-off and landing by employing the power plant to generate lift. In one system large flaps are immersed in a propeller slipstream. This system was investigated in reference 1 on a model of a twin-engine propeller-driven airplane with trailing-edge flaps. The effectiveness of the flaps was improved by application of boundary-layer control through a combination slot suction and blowing system (Arado).

Improved flap effectiveness also can be achieved by preventing separation of the boundary layer with suction distributed through a porous area along the flap leading edge. It has been shown (ref. 2)

that the power requirements for such applications are low. The purpose of the present investigation was to determine the effectiveness of the latter type boundary-layer-control system when operated in a propeller slipstream and to compare the flow requirements of the two systems (Arado and area suction).

For this investigation, the model of reference 1 was modified to incorporate area suction on the flaps and ailerons. The lift and suction power requirements were measured for various flap and aileron deflections throughout a range of propeller thrust coefficients. To obtain a basis for evaluating the effects of the propeller slipstream, tests were also made of the model with the propellers and nacelles removed. The tests were made in the Ames 40- by 80-foot wind tunnel.

NOTATION

b wing span, ft

c wing chord, measured parallel to plane of symmetry, ft

$\bar{c}$ wing mean aerodynamic chord, $\frac{2}{S}\int_0^{b/2} c^2 dy$, ft

c_n section normal-force coefficient, $\frac{1}{c}\int_0^{c} P\,dx\cos\alpha$

C_D drag coefficient, $\frac{\text{drag}}{q_\infty S}$

$C_{D'}$ drag plus thrust coefficient, $C_D + T_{C'}$

C_L lift coefficient, $\frac{\text{lift}}{q_\infty S}$

C_m pitching-moment coefficient computed about the moment center shown in figure 2, $\frac{\text{pitching moment}}{q_\infty S\bar{c}}$

C_l rolling-moment coefficient computed about wind axis, $\frac{\text{rolling moment}}{q_\infty Sb}$

C_n yawing-moment coefficient, $\frac{\text{yawing moment}}{q_\infty Sb}$

C_Y side-force coefficient, $\frac{\text{side force}}{q_\infty S}$

C_Q flow coefficient, $\frac{Q}{V_\infty S}$

D propeller diameter, ft

h maximum thickness of propeller blade section, in.

i_t tail incidence, deg

J propeller advance ratio, $\frac{V_\infty}{nD}$

n propeller rotational speed, rps

p static pressure, lb/sq ft

P pressure coefficient, $\frac{p - p_\infty}{q_\infty}$

q dynamic pressure, lb/sq ft

Q volume of air removed through porous surface, based on standard density, cu ft/sec

s chordwise extent of porous surface measured along surface, ft

S wing area, sq ft

S' wing area spanned by flaps or ailerons, sq ft

T_C' thrust coefficient, $\frac{\text{thrust}}{q_\infty S}$

v suction air velocity, fps

V velocity, fps

w propeller blade width, in.

x distance along the wing chord from the leading edge, parallel to the plane of symmetry, ft

y spanwise distance measured perpendicular from fuselage center line, ft

α angle of attack of fuselage center line, deg

β propeller blade angle at 0.75 blade radius, deg

δ movable surface deflection measured in plane normal to hinge line, deg

Δp pressure drop across porous material, lb/sq ft

Subscripts

a aileron

d duct

e external

f flap

L left

min minimum

R right

s slipstream

u uncorrected for tunnel-wall effects or strut interference

∞ free-stream conditions

MODEL AND APPARATUS

The model is shown in figure 1(a) and represents a twin-engine propeller-driven airplane having a high-aspect-ratio (A = 10), thick (t/c = 0.17), straight wing. The wing was twisted 4.8° between root and tip sections with the root section at 8.3° incidence with respect to the fuselage center line. For some of the tests, the nacelles and propellers on the model were removed. The model thus tested is shown in figure 1(b) The geometric dimensions and areas of the model are given in figure 2 and table I. Flush orifices were installed in the left wing for measuring external surface pressures. A simulated leading-edge flap was used on the model for some of the tests. When installed, the flap extended along the full span of the wing except in the regions occupied by the fuselage and by the nacelles. The flap was a chord-extension type and thus increased the wing area by approximately 8 percent.

The model tested was that used for the tests reported in reference 1 modified to incorporate area-suction flaps. Also, for the present tests, the length of the fuselage was increased 8.19 inches ahead of the $0.25\overline{c}$ and 16.35 inches aft of the $0.25\overline{c}$.

Flaps and Ailerons

The slotted-type trailing-edge flaps and ailerons on the wing were hinged at the 0.75 wing-chord station and the upper surface over the hinge line was constructed of a porous material. Details of the flaps and ailerons are shown in figure 3. To simulate a plain flap, the flap slot was closed for some of the tests by extending the wing upper-surface skin until it met the flap.

The permeable material used in the porous area was a composite arrangement of a fibrous-glass mat (ref. 3) sandwiched between two perforated steel sheets having 0.125-inch-diameter perforations staggered on 0.187-inch centers (33 holes per sq in., approximately 40-percent open area). The outer perforated sheet formed the surface of the flap. This type of porous material arrangement, described in more detail in reference 4, was of uniform porosity throughout. The air-flow resistance of the porous material is given in figure 4. Various extents of porous area were obtained by closing portions of the porous surface with a nonporous tape.

The suction pressure required to induce flow through the porous material was provided by a centrifugal compressor driven by a variable-speed electric motor located in the fuselage. Air was drawn through the porous material into ducts in the flaps and ailerons and then through ducting from each end of the flaps and ailerons into a ducting system in the wing to a plenum chamber and the compressor in the fuselage. The exhaust air from the compressor was discharged into the fuselage from which it entered the tunnel air stream through a slot (approximately 2.5 sq ft) in the afterportion of the bottom of the fuselage. The forces exerted on the model by this exhaust air were negligible. The ducting in the flaps and ailerons was large enough to reduce the dynamic pressure of the induced air to sufficiently low values to insure uniform internal static pressure across the span of the flaps or ailerons. Flush orifices were used to measure the internal static pressures in the ducts.

The flow quantity was controlled by valves in the ducts and by the compressor speed.

Propellers

The propellers were made from four-bladed Aeroproducts propellers (hub designation A-542-B1, blade designation H20-156-23M5) modified by

cutting off the tips (no tip plan-form rounding) to give a propeller diameter of 6.75 feet. The geometric blade characteristics of the modified propellers are shown in figure 5. The blade angle at 0.75 blade radius was set at 29.5°. This blade angle was chosen to allow the propellers to absorb the maximum power output of the drive motors at the maximum propeller rotational speed determined from considerations of propeller strength. Both propellers were rotated in a clockwise direction (viewed from the rear).

Each propeller was driven through a gearbox by a variable-speed electric motor. The gearbox and motor were housed in the engine nacelles shown in figure 1(a).

TEST METHODS

In most tests the angle of attack was varied while the tunnel speed, the suction flow quantity, and the propeller rpm were held constant. For some configurations, the critical suction flow requirements[1] for the flaps and ailerons were determined by varying the flow quantity while the angle of attack, the tunnel speed, and propeller thrust were held constant.

The tests were made at free-stream velocities from 72 to 93 feet per second (q_∞ from 6 to 10 lb/sq ft), corresponding to Reynolds numbers of 2.0 to 2.6 million based on the mean aerodynamic chord of the model of 4.73 feet.

Thrust Calibration

A calibration was made to determine the propeller thrust for a given condition of tunnel free-stream velocity and propeller rotational speed. The calibration was made with the model with flaps and ailerons undeflected and with the model at the angle of attack for zero lift. Measurements were made of the drag force for various values of propeller rotational speed and tunnel dynamic pressure. The gross propeller thrust (with slipstream effect neglected) was assumed to be the difference between the measured drag force with propeller operating and with propeller removed. The propeller thrust thus determined was converted to a dimensionless coefficient by means of the relationship $T_C' = \text{thrust}/q_\infty S$. The propeller rotational speed was converted to the usual dimensionless form of propeller advance ratio, $J = V_\infty/nD$. The variation of T_C' with J is shown in figure 6 (for the 29.5° blade used in the tests) and for the

[1]The critical suction flow coefficient, $C_{Q_{crit}}$, is defined as in reference 2 as the flow coefficient above which only small gains in lift are obtained for large increases in flow coefficient.

purposes of this report was assumed to be independent of the angle of flow into the propeller as affected by angle of attack, wing lift, and flap deflection. In the tests, propeller rotational speed and tunnel dynamic pressure were set to give the value of J required (fig. 6) to obtain the desired thrust coefficient T_C'.

The force data presented in the figures include the direct propeller thrust and normal forces as well as the aerodynamic forces, except that the thrust coefficient T_C' has been added to the measured drag force for all test conditions with propellers operating ($T_C' \cos \alpha$ was assumed equal to T_C').

Flow Quantity

The suction flow quantities were determined independently for each flap and aileron by thin plate orifices, and by total and static pressure tubes in the ducts. A standard ASME orifice meter (ref. 5) was used to calibrate this flow measuring instrumentation. The flow quantity was regulated by valves in the ducts which were adjusted to give equal flow quantities from each flap and aileron.

CORRECTIONS

Corrections for the influence of the tunnel wall were applied to the data as follows:

$$\alpha = \alpha_u + 0.41\ C_L$$

$$C_D = C_{D_u} + 0.0073\ C_L^2$$

$$C_m = C_{m_u} + 0.0147\ C_L \text{ (tail on only)}$$

where the subscript u denotes uncorrected values. No corrections were made for strut tares or strut interference.

ACCURACY OF DATA

Low free-stream tunnel dynamic pressures were used in order to obtain high thrust coefficients without exceeding the limitations of the power available from the propeller drive motors; this affected the accuracy of the test data. An estimate of the accuracy of the data is given in the following table. The values given are the maximum deviation from an average and can be attributed primarily to fluctuations of the wind-tunnel balance system resulting from unsteady air loads, and to the error

in setting and maintaining a given frequency input to the propellers and hence propeller rpm and thrust. These values were determined at an angle of attack of the model below that for $C_{L_{max}}$. The table also gives values of the least reading on the scales. These values are the minimum forces (converted to coefficients for $q = 6$ lb/sq ft) which can be read on the scales without interpolation.

Coefficient	Maximum deviation	Least reading on scales
C_L	0.03	0.01
C_D	.03	.002
$C_{D'}$	.05	
C_m	.07	.049
C_Y	.02	.002
C_n	.003	.0005
C_l	.01	.002
C_Q	.0001	.0001
$T_{C'}$	.05	.001

RESULTS AND DISCUSSION

Aerodynamic Characteristics

The basic longitudinal aerodynamic characteristics of the model for various flap deflections with and without suction are presented in figures 7(a) to 7(k) with nacelles and propellers on, and in figures 8(a) to 8(e) with propellers and nacelles removed. Data are also presented in these figures for symmetrically deflected ailerons in combination with the deflected flaps. The data in figure 7 are for various values of propeller thrust coefficient (held constant while the angle of attack was varied). The porous area on the flaps and ailerons for the data in figures 7 and 8 was located as shown in the following table:

δ_f or δ_a, deg	Forward edge of porous area[1]	Aft edge of porous area[1]
30,40,60	0	3.0
70	-2.2	3.0

[1]Percent chord measured along surface of flap or aileron from reference point shown in figure 3.

These porous openings are equal to or greater than the opening required to obtain maximum lift at a given angle of attack with minimum suction quantity.

The data in figures 7 and 8 for $C_{Q_a} = 0$ were obtained with the valves closed in the suction ducts to the ailerons. Data for both $C_{Q_a} = 0$ and $C_{Q_f} = 0$ are with the suction pump not operating. For the data with suction on, the suction quantity was maintained at a value above $C_{Q_{crit}}$.

Lift due to flap deflection.- The increment of lift (above the plain-wing value) resulting from flap deflection is shown in figure 9(a) for the model with nacelles off, and in figure 9(b) with nacelles on and the propellers operating at zero thrust. The values shown are for an angle of attack of zero but are nearly constant up to maximum lift. The data with nacelles on were obtained by an extrapolation to zero thrust of the data in figure 7 (replotted as C_L vs. T_C'). A lift increment for a flap deflection of 60° with nacelles on and propellers removed included in figure 9(b) shows close agreement with the propeller-on data extrapolated to zero thrust. Comparison of the data in figures 9(a) and 9(b) shows that the addition of the nacelles with the propellers operating at zero thrust did not appreciably affect the lift increment due to flap deflection.

A flap lift increment computed by the method of reference 6 assuming linear flap effectiveness[2] is compared with the experimentally measured values in figure 9. The experimental data in the figure are for the model with tail on whereas the computed values are for wing alone with the assumption the flap does not extend across the fuselage. It is assumed that the lift carried by the tail does not affect the lift increment due to flap deflection.

The lift increments developed by the flaps were considerably below the values predicted by the theory. The application of suction to the flaps greatly increased the flap lift increments; however, the values were only 75 percent of those computed from the theory. This may have been a consequence of the inability of suction to completely suppress flow separation on the flap. Such a conclusion is supported by the pressure distributions shown in figure 10 for the flap deflected 60° with suction. The relatively constant pressures near the trailing edge and the failure of the pressures to completely recover at the trailing edge (for angles of attack below that for maximum lift) are indicative of flow separation (ref. 7).

To determine if the slot between the flap and the wing in any way affected the ability of the suction to control flow separation, values of flap lift increment were obtained with the slot closed by extending the wing upper-surface skin until it met the flap. The lift increments obtained with this simulated plain flap (fig. 9(a)) were approximately the same as those with the slotted flap.

[2]The computed lift increments in figure 9 are based on a lift effectiveness parameter $d\alpha/d\delta$ of 0.61, giving a $dC_L/d\delta$ of 0.029.

Lift due to thrust.- The increase in C_L at $\alpha_u = 0$ and in $C_{L_{max}}$ with T_C' is shown in figure 11.

One method developed for predicting this lift increase from propeller operation is given in reference 10. This method is based on lifting line theory and is limited to moderate thrust coefficients. The lift increase due to thrust determined by this method is dependent on the ratio of the propeller diameter to the chord of that portion of the wing immersed in the propeller slipstream. For a wing chord small in comparison to the slipstream diameter, the lift increase is proportional to the dynamic pressure in the slipstream. As the wing chord is increased in relation to the slipstream diameter, the lift due to the slipstream is reduced to a limiting condition which is proportional to the slipstream velocity. The lift due to slipstream computed by the methods of reference 10 for the two limiting conditions is compared with the experimental data in figure 12 for flaps undeflected and deflected 60°. The values presented in the figure are the lift increments above the plain wing value for an angle of attack of 0°.

For flaps undeflected, the experimentally measured lift increase was approximately proportional to the slipstream velocity. For the wing chord to slipstream diameter of these tests, this result appears to be in agreement with the predictions of reference 10.

With flaps deflected 60° (with suction), the measured lift increment due to thrust coefficient is below the theoretical value at low thrust coefficients. As was shown previously, this difference was primarily due to the inability of area suction to completely eliminate flow separation on the flap. With increasing thrust coefficient, the flap lift increment was increased, giving closer agreement with the computed value. The improved flap lift increment at the high thrust coefficients appeared to be a result of a reduction of flow separation on the flaps as indicated by the pressure distributions of figure 13. This reduced flow separation is indicated by the improved pressure recovery at the trailing edge of the portions of the flap in the propeller slipstream at the high thrust coefficients.

Although the slipstream enables the flap with suction to achieve attached flow, the slipstream is not sufficiently powerful to reattach the flow without boundary-layer control on the flap, as indicated by the pressure distributions in figure 14.

Lift due to aileron deflection.- The use of area suction on the ailerons enables consideration of the use of drooped ailerons to increase lift. The extent of the lift realized from a 30° symmetrical deflection of the ailerons is shown in figure 15. The lift increments in this figure are for an angle of attack of zero but are nearly constant up to maximum lift and appear to be unaffected by flap deflection (fig. 15(a)) or thrust coefficient (fig. 15(b)).

Effect of a leading-edge flap.- With the application of boundary-layer control to the trailing-edge flap, the additional load induced over the forward portion of the airfoil increases the problem of maintaining attached flow at the leading edge at high angles of attack. The pressure distributions in figure 10 for the model with suction on the deflected flap show that as the angle of attack was increased beyond that for maximum lift, a loss in leading-edge peak pressures occurred with a redistribution of pressures along the chord into a more or less flattened form. This type of pressure change, as well as the abrupt loss in lift following maximum lift, is indicative of a leading-edge type of stall (ref. 7).

This flow separation from the leading edge of an airfoil can be delayed, as shown in reference 11, by some form of camber near the leading edge, such as a leading-edge flap or drooped leading edge. To see if the above reasoning regarding the limitation to maximum lift by leading-edge flow separation was correct, the model was tested with the simulated leading-edge flap (fig. 3). The results are presented in figures 16 and 17. Apparently, leading-edge flow separation was contributing to the stall since the addition of the nose flap resulted in approximately a 4° increase in the angle of attack for maximum lift. Part of the gain in maximum lift shown in figures 16 and 17 is the result of the 8-percent increase in wing area when the nose flap was added.

Longitudinal stability and control.- The effectiveness of the horizontal tail for longitudinal control is shown in figure 18. The tail effectiveness as indicated by $(dC_m/di_t)_{\alpha = 4^\circ}$ was -0.06 and was relatively unaffected by thrust (fig. 18(d)).

The data in figure 18(c) indicate that the use of variable horizontal-tail incidence for longitudinal control may be limited at high flap deflections and high thrust coefficients. Longitudinal control at low angles of attack for these high flap deflections and thrust coefficients may require tail angles of attack which exceed that for maximum lift of the section. The resulting stall of the tail causes the abrupt change in pitching-moment curve slope at low lift coefficients shown in figure 18(c).

The longitudinal stability of the model as affected by flap deflection, boundary-layer control, and thrust is shown by comparison of the data in figures 7 and 8.

Lateral control.- The aerodynamic characteristics of the model with the ailerons asymmetrically deflected are shown in figure 19. The rolling moment due to aileron deflection (from fig. 19) is shown in figure 20. The aileron deflections in this figure are the total asymmetrical deflection measured from a symmetrically drooped position of 30°. As an indication of the relative effectiveness of the ailerons, the rolling moment due to aileron deflection computed by the methods of reference 12 is shown in figure 20 for comparison with the measured values.

With suction ($C_{Q_{a_L}}$ = 0.0008) the aileron effectiveness was approximately equal to the theoretical value at lift coefficients below 2.0 but decreased to approximately 75 percent of the theoretical value at a lift coefficient of 4.0. Without suction, the effectiveness was approximately 55 percent of the theoretical value. The aileron effectiveness appeared to be relatively unaffected by thrust coefficient.

Flap Suction Requirements

Porous opening.- An extensive investigation was made to determine the effect of the position and extent of the porous area on the flap lift increment and suction quantity required for a flap deflection of 60° (ailerons deflected 30°) and a T_C' of 1.2. The primary effect of variations in location or extent of the porous area was to alter the value of $C_{Q_{crit}}$. The results indicated that there was a critical location and extent of the porous area to obtain the full value of $\Delta C_{L_{crit}}$ for the least $C_{Q_{crit}}$. It was found that for minimum $C_{Q_{crit}}$, the leading edge of the porous area should be roughly at the chordwise location of the peak external pressure over the flap and the porous area should extend approximately 3-percent chord downstream of the pressure peak. Progressively moving the leading edge of the porous area downstream of the pressure peak or reducing the chordwise extent of the porous area to less than 3-percent chord aft of the pressure peak resulted in, first, an increase in $C_{Q_{crit}}$ and then an inability to maintain attached flow on the flap. In general, extending the porous area upstream of the pressure peak or downstream more than 3-percent chord increased $C_{Q_{crit}}$ but did not increase $\Delta C_{L_{crit}}$. These results are in qualitative agreement with other data obtained on suction flaps (refs. 2 and 4).

The location and extent of the porous area which gave maximum lift with lowest suction quantity were also determined for flap deflections of 40° and 70°. In general, the results were similar to those obtained for 60° flap deflection. The location of the forward edge of the porous area coincided roughly with the peak external pressure on the flap. The extent of the porous area increased with flap deflection as shown in the following table:

δ_f, deg	Extent of porous opening[1]
40	1.5
60	3.0
70	3.8

[1]Percent chord measured along surface of flap from reference point shown in figure 3.

This variation of extent of porous opening was in qualitative agreement with the results of other tests on suction flaps (e.g., ref. 2).

Suction quantity.- The suction flow requirements of the flap are shown in figure 21 for propellers and nacelles removed and for various values of thrust, angle of attack, and flap and aileron deflection. This figure shows that the critical suction flow coefficient $C_{Q_{crit}}$ is primarily a function of flap deflection independent of thrust coefficient and angle of attack and is unaffected by aileron deflection. The results of other tests of suction flaps (refs. 2 and 4) also showed flap deflection to be the primary variable governing the critical suction flow coefficient.

Suction pressure.- The suction pressures in the flap duct (for the left wing panel) required to obtain $C_{Q_{crit}}$ are presented in figure 22. The suction pressure is a function of the external surface pressure and the flow resistance of the material in the porous area. The peak external pressures on the flap (at the leading edge of the porous area) are included in figure 22. The magnitude of the external pressures was dependent on the thrust coefficient and flap deflection, and varied with the spanwise position on the flap. A rough estimate of the variation of peak external pressure on the portion of the flap in the propeller slipstream with thrust coefficient can be obtained by multiplying the pressure at zero thrust by the ratio of the slipstream velocity to free-stream velocity determined from simple momentum theory. This ratio is shown in figure 22(c) for comparison with the measured values. The data in figure 23 show that the external pressures on the flap were a minimum at span stations behind the propeller and increased for stations outside the slipstream. Since the duct in the flap is uncompartmented, the duct pressure must be at least equal to the minimum external pressure on the flap.

Aileron Suction Requirements

The suction requirements for the ailerons are shown in figure 24. This figure shows the variation of rolling-moment coefficient with suction flow coefficient for the left aileron for asymmetrically-deflected ailerons. The suction pressures in the left aileron duct for $C_{Q_{crit}}$ are given in the following table:

δ_{a_L}, deg	δ_{a_R}, deg	$(P_{d_{crit}})_L$
50	10	-4.1
60	0	-4.5

The aileron flow requirements were determined with the flaps deflected 60° with a flap suction flow coefficient of 0.0028 and the propellers operating at a thrust coefficient $T_{C'}$ of 1.15. The data show trends similar to that obtained on the flaps in that $C_{Q_{crit}}$ and $P_{d_{crit}}$ increased with deflection. However, the magnitude of $C_{Q_{crit}}$ and $P_{d_{crit}}$ for the ailerons was considerably less than the values for the flaps. The reason for this difference is not known.

Comparison With the Arado System

Since the basic wing of the model used in the investigation of the Arado type boundary-layer-control flaps reported in reference 1 was the same as that used with the area-suction flaps in this investigation, it is possible to obtain a fairly reliable comparison of the relative merits of these two types of boundary-layer control. However, in making this comparison, it should be noted that the chords and hinge-line locations of the two flaps are different, as is shown in the following table:

Flap	Chord, percent	Hinge-line location, percent chord
Area suction	34.7	75
Arado	25	81.4

The spans of the two flaps were the same. For the Arado type boundary-layer-control system, the inboard 73 percent of the flap span contained a suction slot. A blowing slot extended over the remainder of the flap and over the ailerons.

A comparison of the variation of lift coefficient with flow coefficient for the two systems is shown in figure 25. The comparison is made between the Arado model with propellers windmilling and the area-suction flap model with propellers and nacelles removed. The flow coefficients in figure 25 are based on the wing area spanned by the flaps or ailerons. The flow coefficients for the Arado system are for equal quantities of air flow through the suction and blowing slots. For the area-suction flaps, the flow coefficient for the ailerons was held constant at a value of $Q/S'V_\infty = 0.0023$. The data in figure 25 show that the suction quantities required for a given lift increment were considerably greater for the Arado type boundary-layer-control system than for the area-suction flaps and ailerons. To obtain a lift coefficient of 2.0 (approximately $C_{L_{crit}}$) with the area-suction flaps required a combined flow coefficient as defined by $Q/S'V_\infty$ of 0.003. For the ailerons, $Q/S'V_\infty$ was assumed equal to 0.001. For the Arado system, the flow coefficient required to obtain a lift coefficient of 2.0 was almost five times the combined value for the area-suction flaps and ailerons. With large flow quantities, the

lift increments obtained with the Arado boundary-layer-control system are larger than for the area-suction flaps, primarily as a result of the lift contributed by the blowing portions of the Arado flaps and ailerons. The spanwise variations of normal-force coefficient for the two systems are compared in figure 26. For the Arado system, the normal-force coefficient in the region of the ailerons with a blowing slot is greater than the inboard flap portion of the wing with a suction slot. For the wing with area-suction flaps and ailerons, the lift provided by the ailerons is a smaller part of the total wing lift.

The maximum lift coefficient for both wings was approximately 2.8 and appeared to be limited by flow separation from the wing leading edge.

CONCLUSIONS

The following conclusions are drawn from the results of the investigation reported herein.

1. The propeller slipstream had no effect on the suction flow requirements but the suction pressure required increased with thrust coefficient approximately in proportion to the slipstream velocity.

2. The lift increment produced by the propeller slipstream increased approximately in proportion to the slipstream velocity.

3. With the propellers and nacelles removed, lift increments due to flap deflection with suction were obtained that were approximately 75 percent of values predicted from linear theory. The inability to attain the theoretically predicted flap lift increments was primarily due to the inadequacy of suction applied at the leading edge of the flaps in controlling flow separation at the trailing edge.

4. The suction flow quantities for a given flap lift increment for the area-suction flap were approximately 25 percent of the flow quantities required for a combination slot suction and blowing (Arado) system. With large flow quantities, lift increments could be obtained with the Arado system that were larger than what could be obtained with the area-suction flaps.

5. With the application of boundary-layer control to the trailing-edge flaps and ailerons, maximum lift appeared to be limited primarily as a result of flow separation from the wing leading edge.

Ames Aeronautical Laboratory
National Advisory Committee for Aeronautics
Moffett Field, Calif., July 2, 1958

REFERENCES

1. Fink, Marvin P., Cocke, Bennie W., and Lipson, S.: A Wind-Tunnel Investigation of a 0.4-Scale Model of an Assault Transport Airplane With Boundary-Layer Control Applied. NACA RM L55G26a, 1956. (Supersedes NACA RM SL55G26a)

2. Cook, Woodrow L., Holzhauser, Curt A., and Kelly, Mark W.: The Use of Area Suction for the Purpose of Improving Trailing-Edge Flap Effectiveness on a 35° Sweptback Wing. NACA RM A53E06, 1953.

3. Dannenberg, Robert E., Weiberg, James A., and Gambucci, Bruno, J.: A Fibrous-Glass Compact as a Permeable Material for Boundary-Layer-Control Applications Using Area Suction. NACA TN 3388, 1955.

4. Dannenberg, Robert E., Weiberg, James A., and Gambucci, Bruno J.: Perforated Sheets as the Porous Material for a Suction-Flap Application. NACA TN 4038, 1957.

5. Anon.: ASME Power Test Codes - 1949. Supplement on Instruments and Apparatus. Part 5 - Measurement of Quantity of Materials P.T.C. 19.5, 4-1949, ASME, N. Y., 1949.

6. DeYoung, John: Theoretical Symmetric Span Loading Due to Flap Deflection for Wings of Arbitrary Plan Form at Subsonic Speeds. NACA Rep. 1071, 1952. (Supersedes NACA TN 2278)

7. McCullough, G. B., and Gault, D. E.: Examples of Three Representative Types of Airfoil Stall at Low Speed. NACA TN 2502, 1951.

8. Cahill, J. F.: Summary of Section Data on Trailing-Edge High-Lift Devices. NACA Rep. 938, 1949.

9. Kelly, Mark W., and Tolhurst, William H., Jr.: Full-Scale Wind-Tunnel Tests of a 35° Sweptback Wing Airplane With High-Velocity Blowing Over the Trailing-Edge Flaps. NACA RM A55I09, 1955.

10. Smelt, R., and Davies, H.: Estimation of Increase of Lift Due to Slipstream. R. & M. No. 1788, British, 1937.

11. Thomson, K. D.: A Review of Leading-Edge High-Lift Devices. Rep. A77, Australian Aero Res. Lab., Dept. of Supply, June 1951.

12. DeYoung, John: Theoretical Antisymmetric Span Loading for Wings of Arbitrary Plan Form at Subsonic Speeds. NACA Rep. 1056, 1951. (Supersedes NACA TN 2140)

TABLE I.- GENERAL GEOMETRIC DIMENSIONS OF THE MODEL

Dimension	Wing	Horizontal surface	Vertical surface
Area, sq ft	205.4	56.5	30.6
Span, ft	45.00	16.03	7.19
Mean aerodynamic chord, ft	4.73	3.50	4.68
Aspect ratio	9.86	4.55	1.69
Taper ratio	0.50	0.45	0.55
Geometric twist, deg	4.8° (washout)	0	0
Dihedral from reference plane, deg	0.8	0	---
Incidence from reference plane, deg	8.3	---	---
Section profile (constant)	NACA 23017	NACA 0012	NACA 0012
Root chord, ft	6.07	4.61	5.88
Tip chord, ft	3.06	2.54	2.65
Sweep of leading edge, deg	2	12	24
Tail length, ft	---	18.01	---

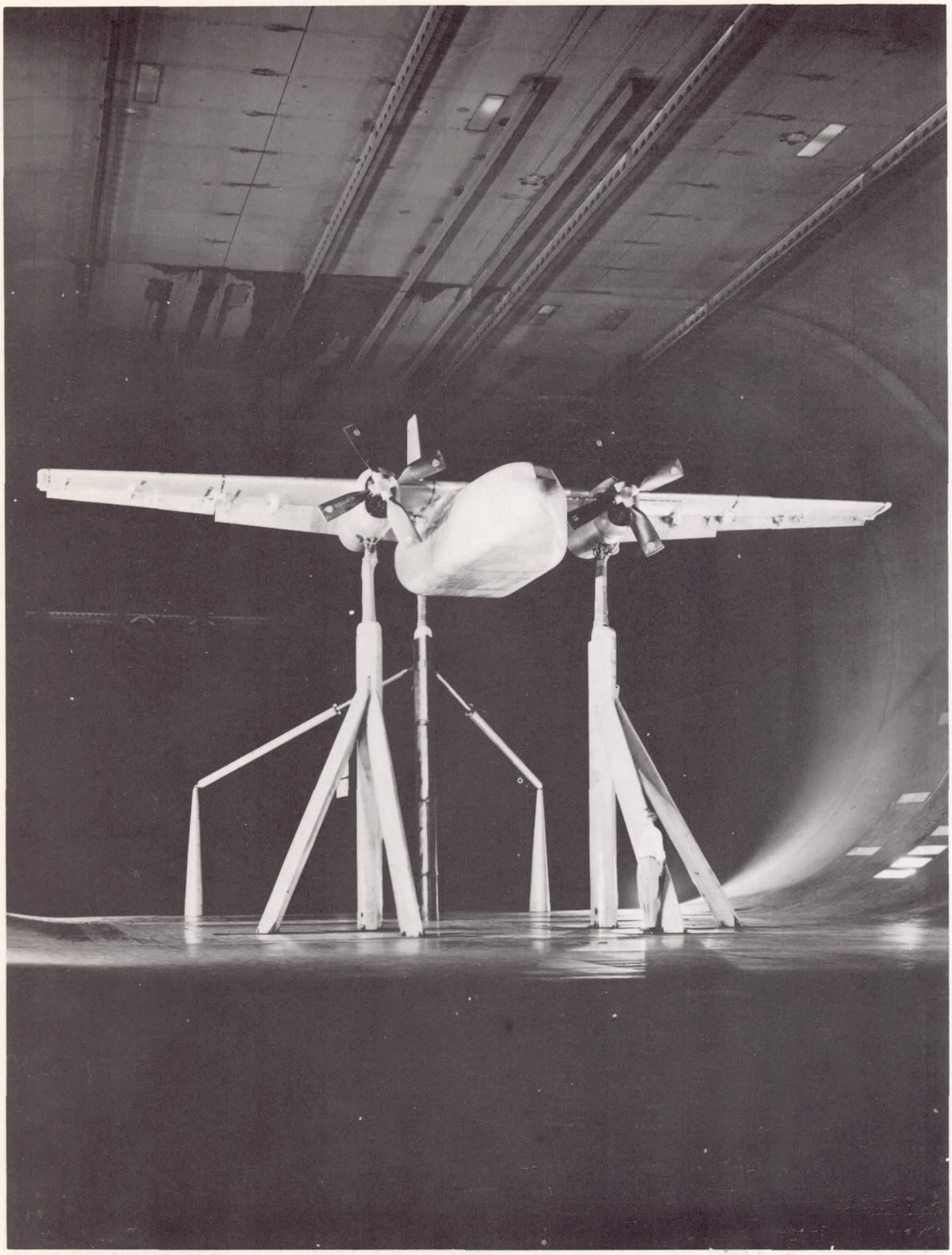

A-22323

(a) Nacelles and propellers on.

Figure 1.- The model with flaps and ailerons deflected.

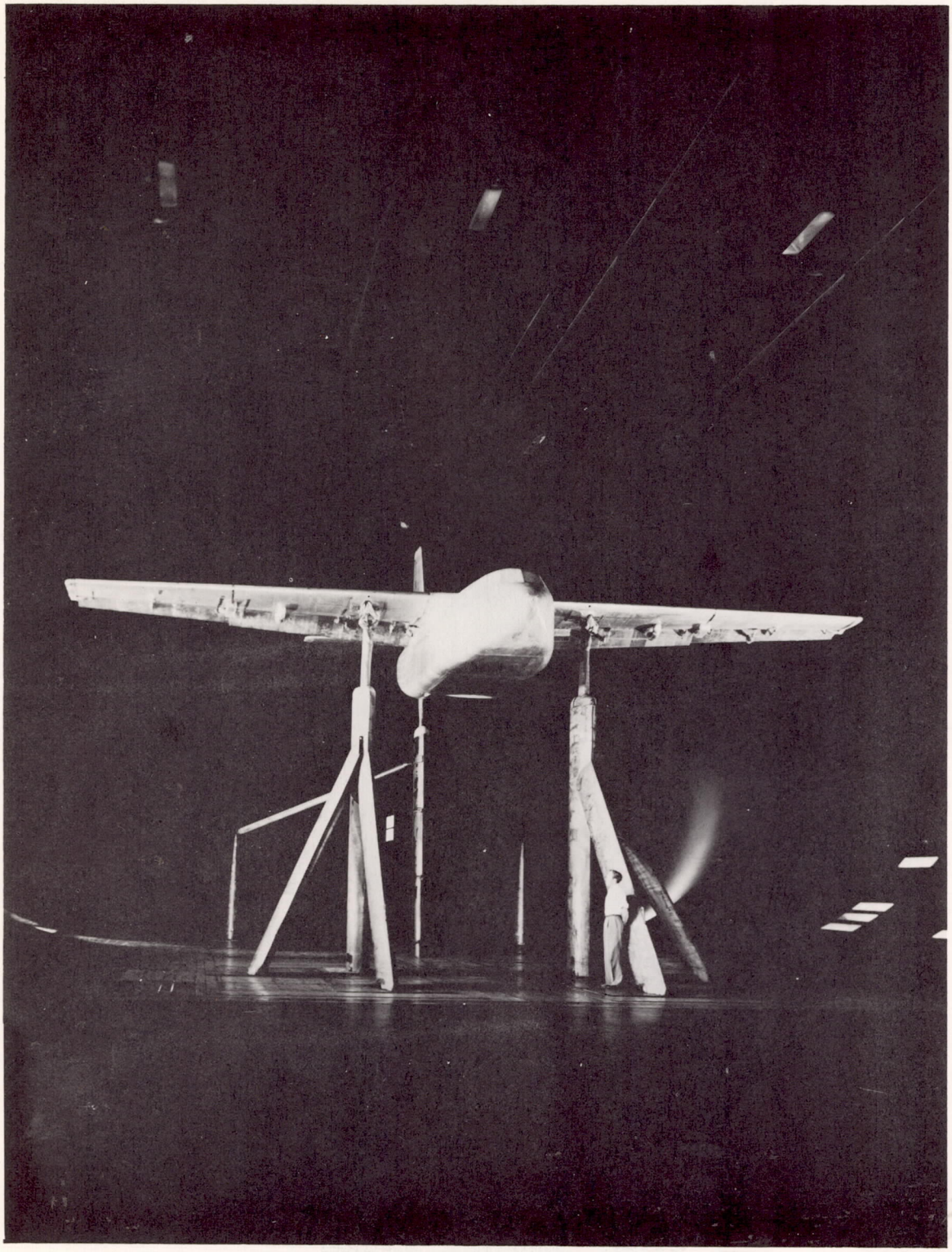

A-23114

(b) Nacelles and propellers off.

Figure 1.- Concluded.

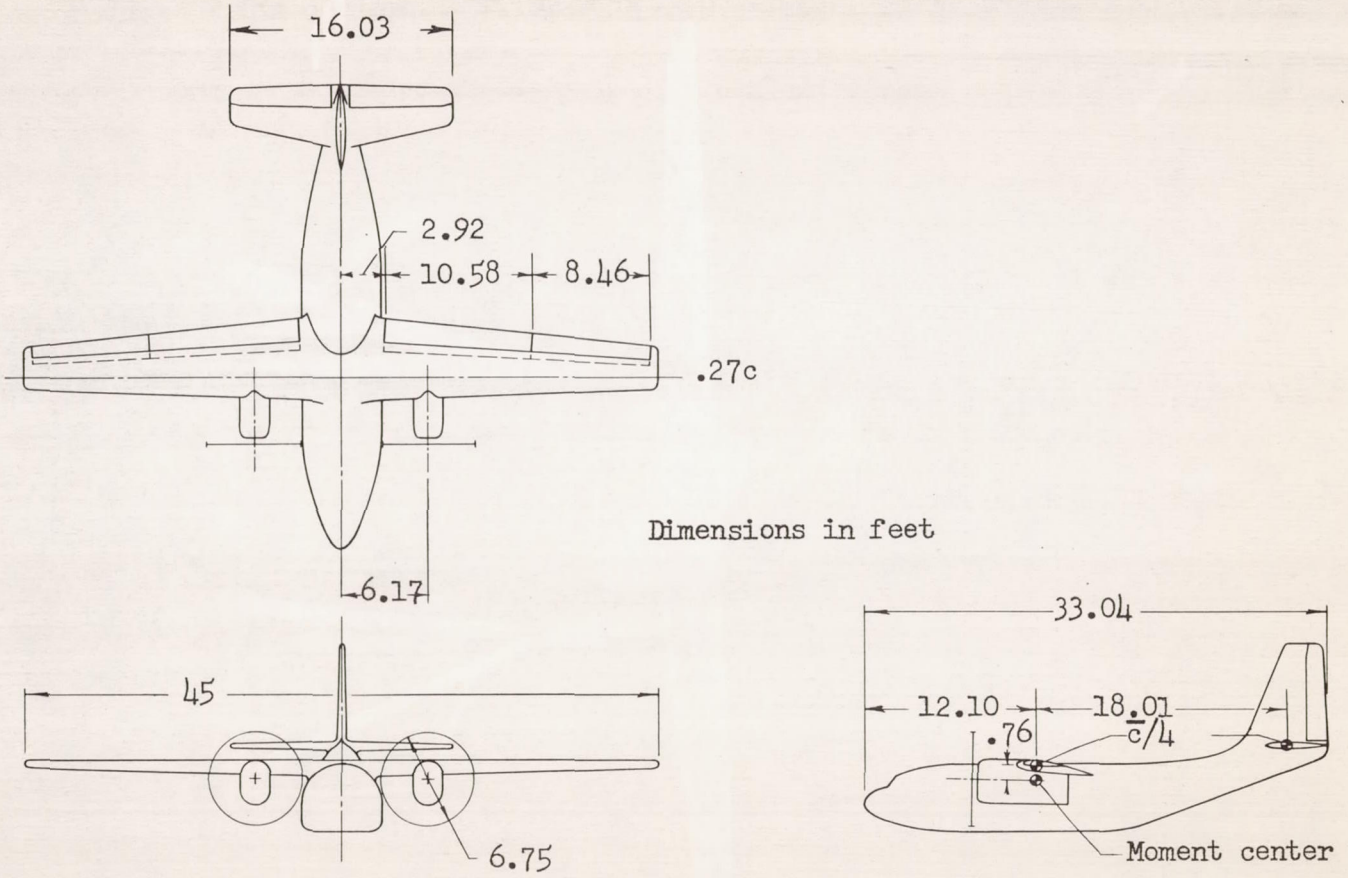

Figure 2.- Geometry of the model.

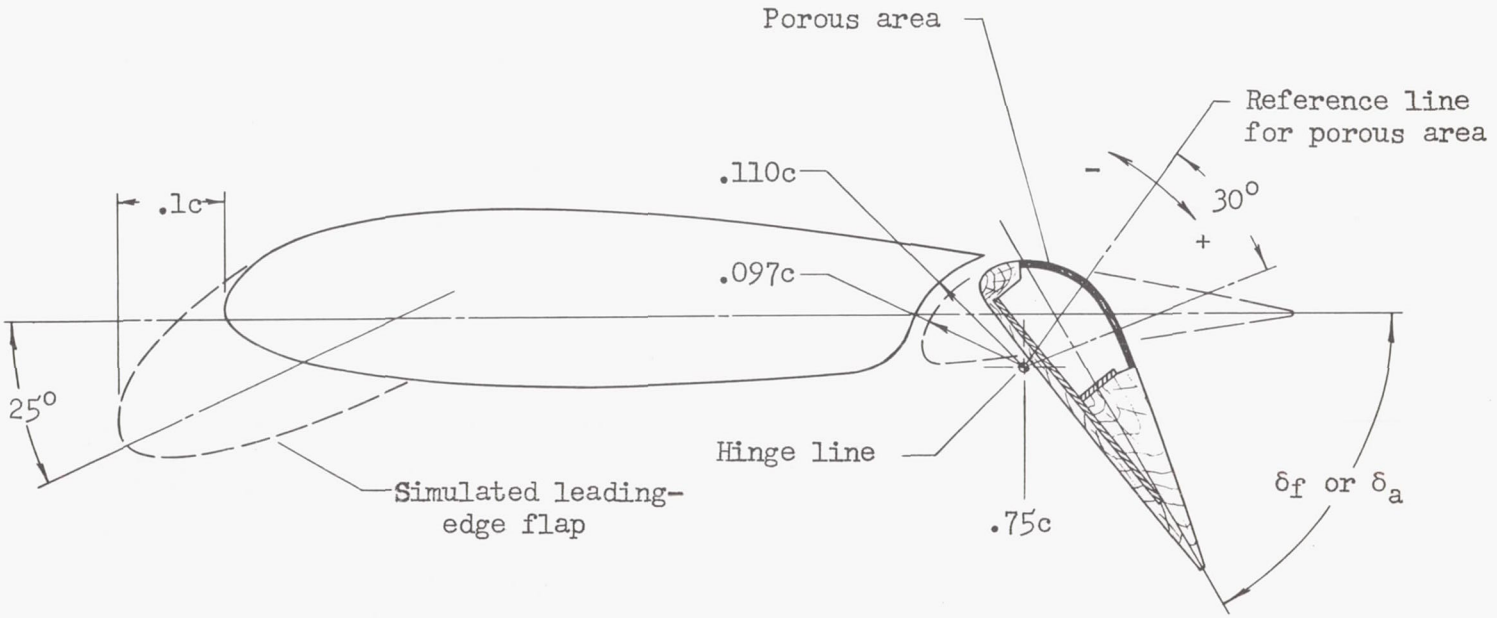

Figure 3.- Details of flaps and ailerons.

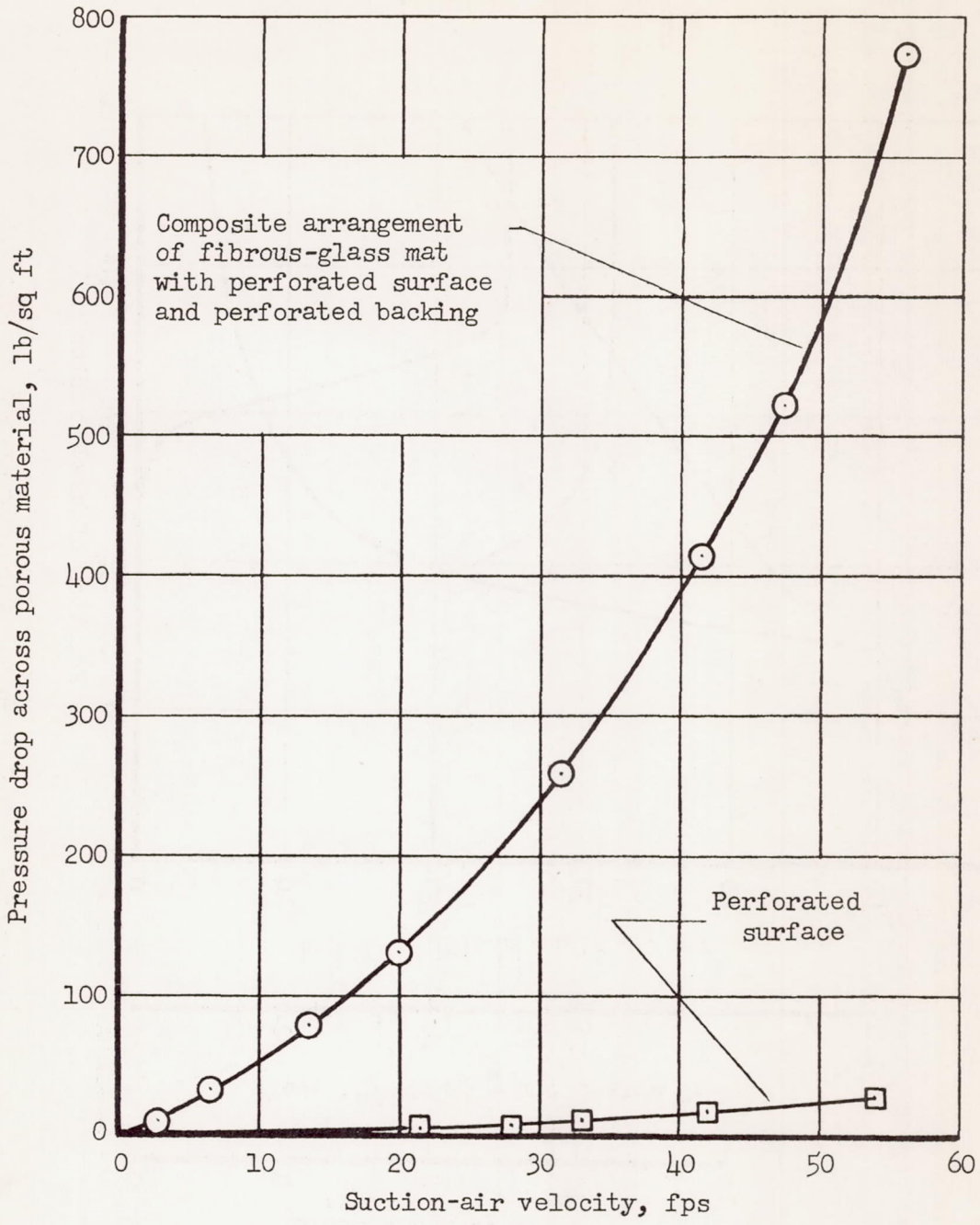

Figure 4.- Air-flow resistance characteristics of the porous material used in the flaps and ailerons.

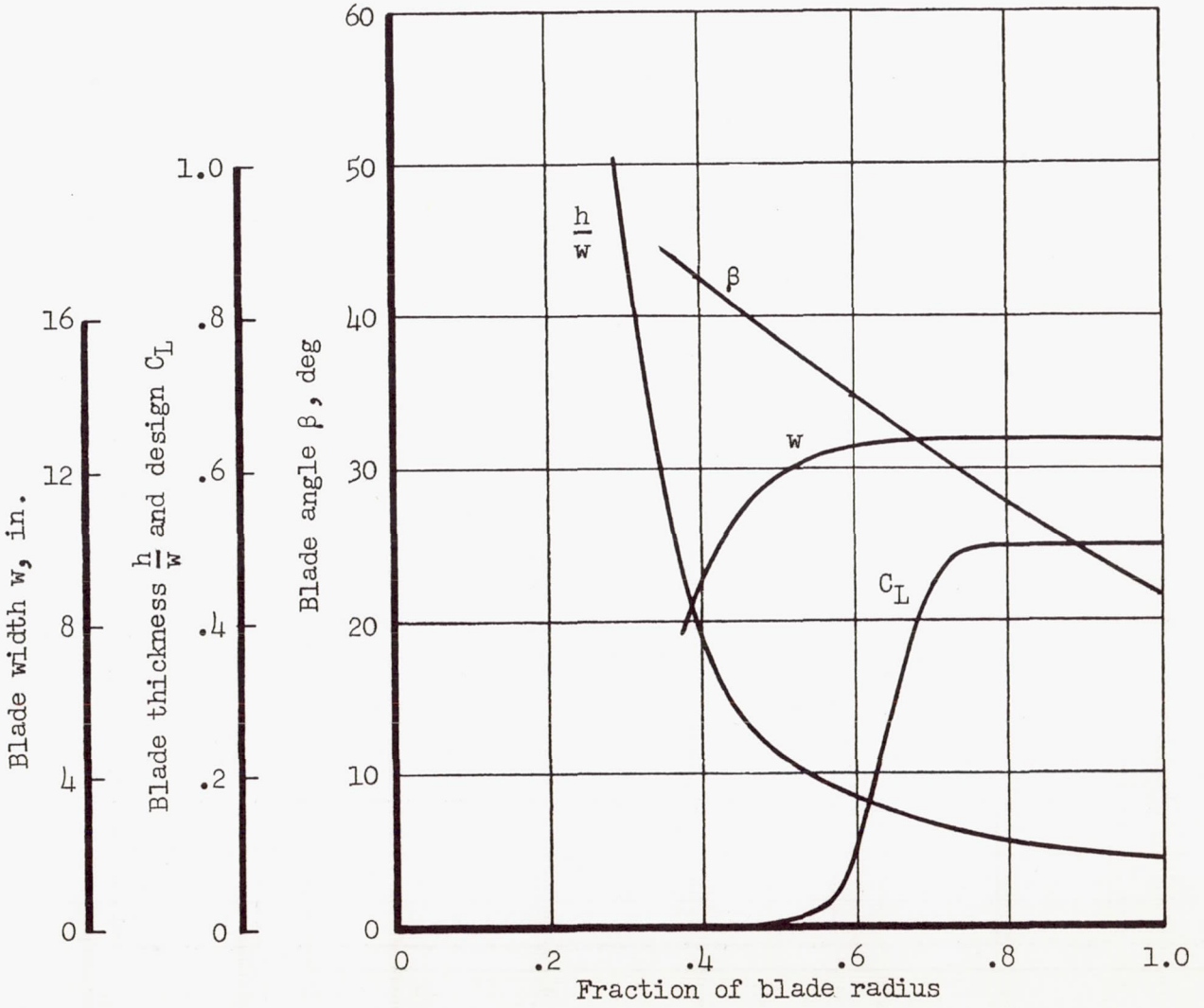

Figure 5.- Propeller-blade form curves.

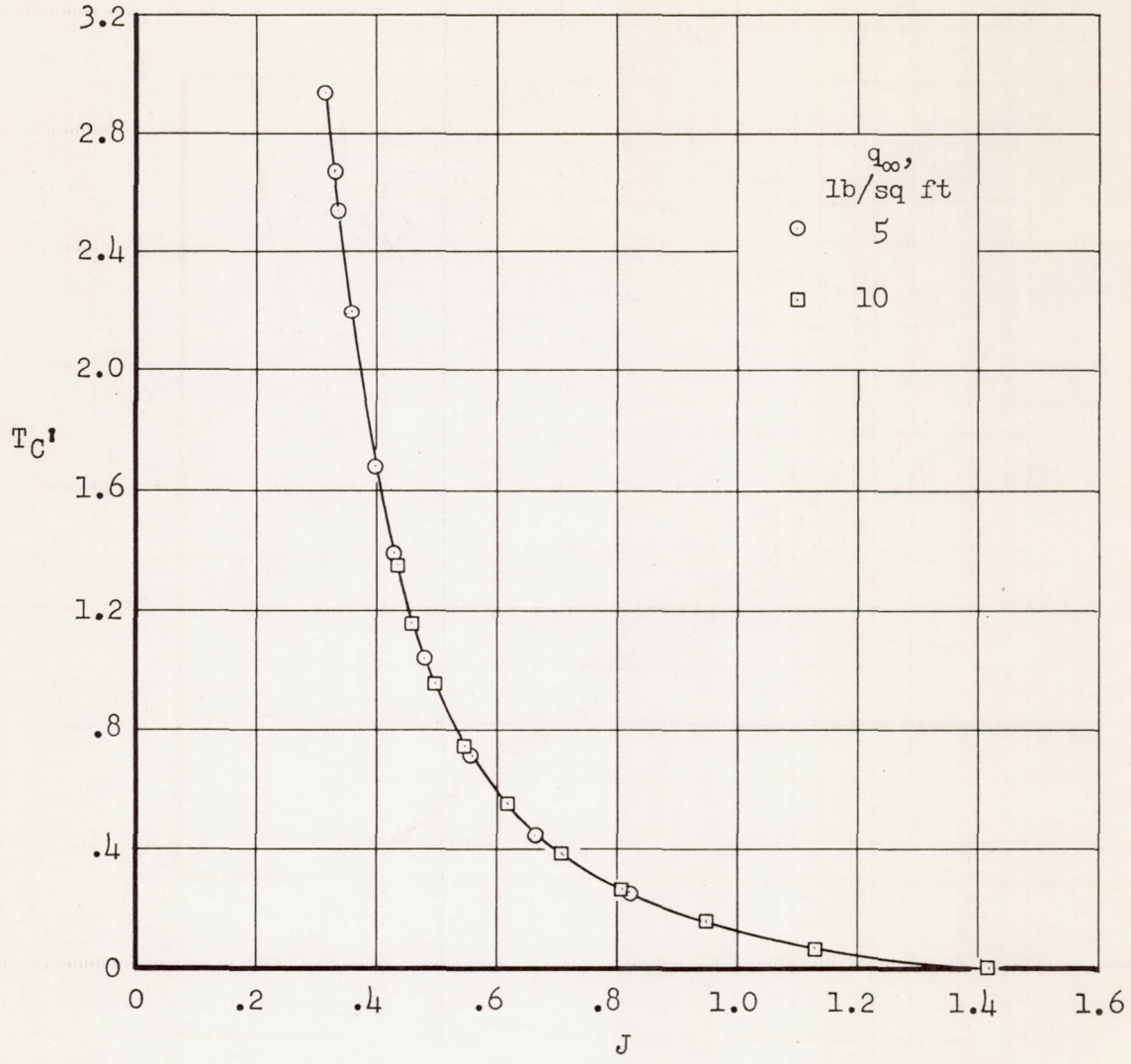

Figure 6.- Thrust characteristics.

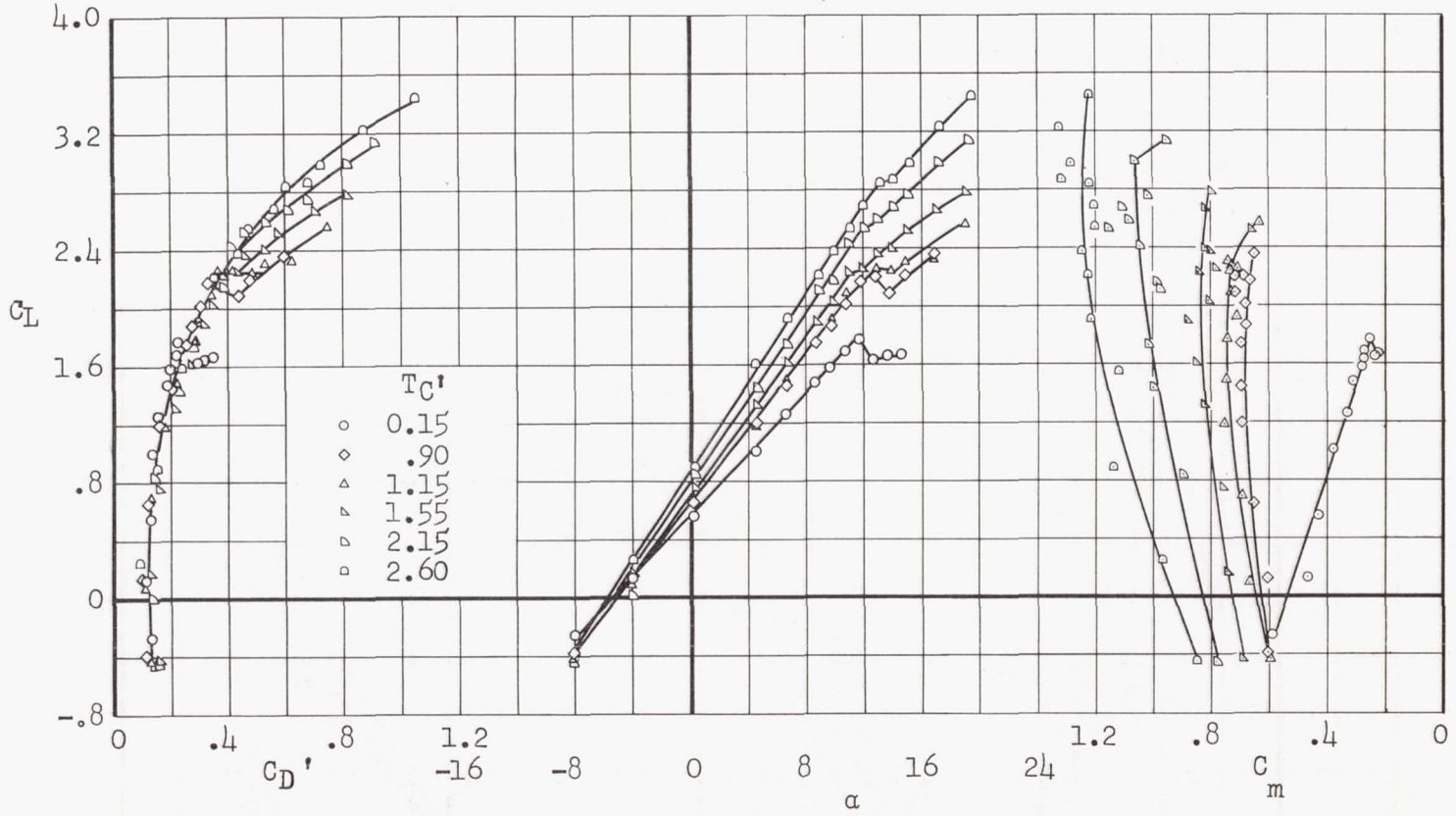

(a) $\delta_f = \delta_a = 0^\circ$; $C_{Q_f} = C_{Q_a} = 0$; $i_t = -3^\circ$

Figure 7.- Effect of thrust coefficient on the aerodynamic characteristics of the model.

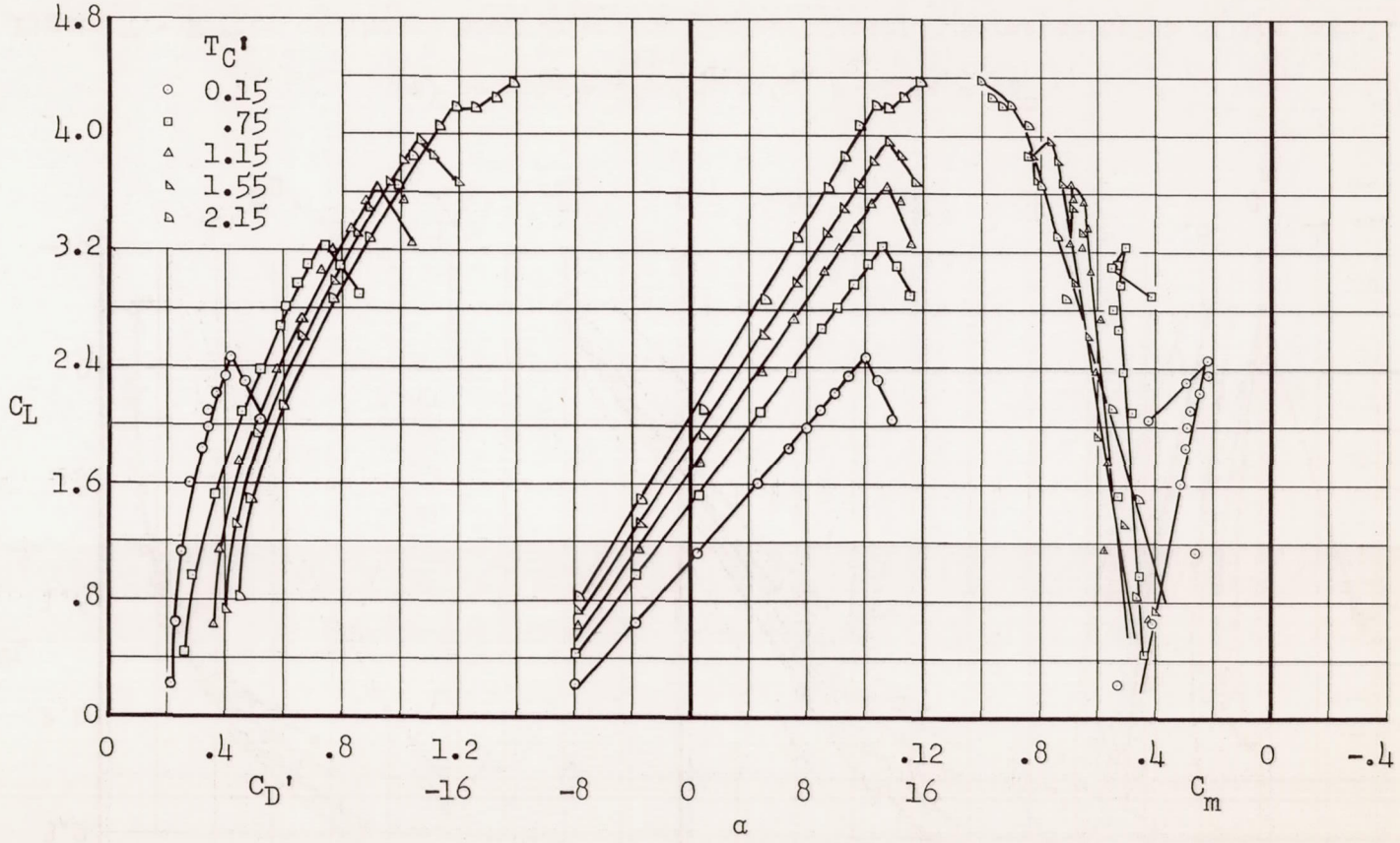

(b) $\delta_f = 40^\circ$; $\delta_a = 0^\circ$; $C_{Q_f} = C_{Q_a} = 0$; $i_t = -3^\circ$

Figure 7.- Continued.

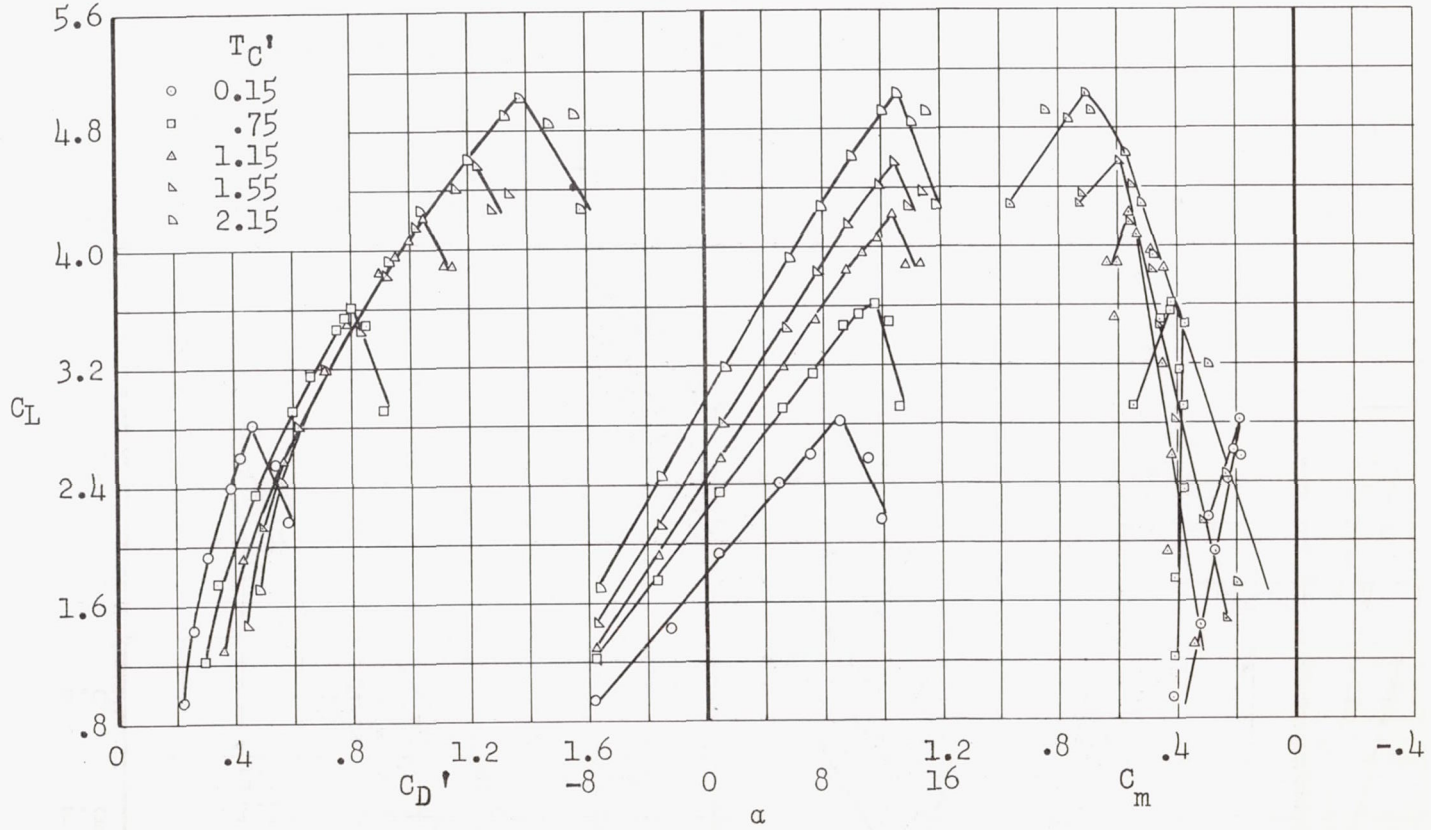

(c) $\delta_f = 40^\circ$; $\delta_a = 30^\circ$; $C_{Q_f} = 0.0033$; $C_{Q_a} = 0.0013$; $i_t = -3^\circ$

Figure 7.- Continued.

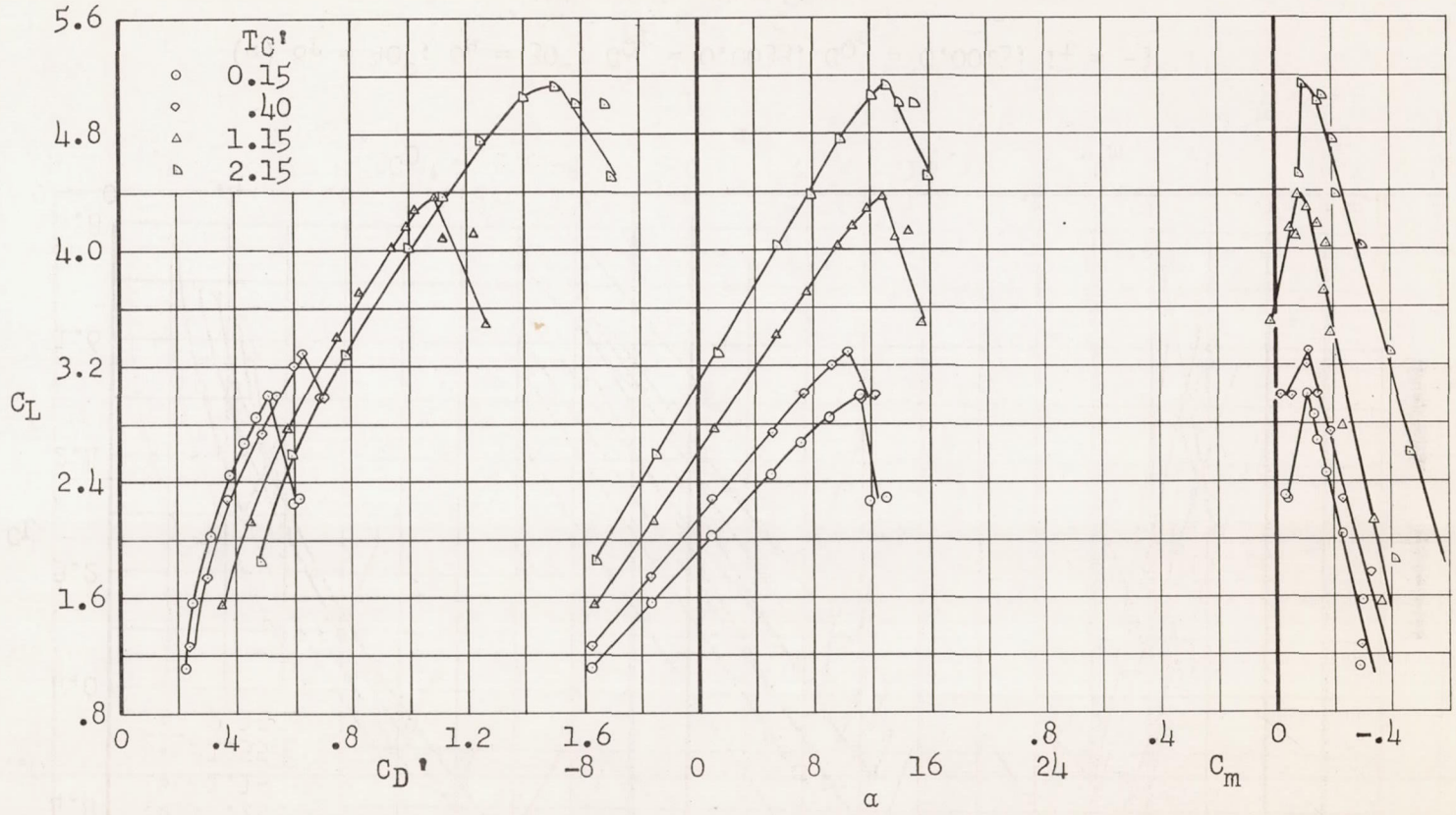

(d) $\delta_f = 40^\circ$; $\delta_a = 30^\circ$; $C_{Q_f} = 0.0028$; $C_{Q_a} = 0.0010$; tail off

Figure 7.- Continued.

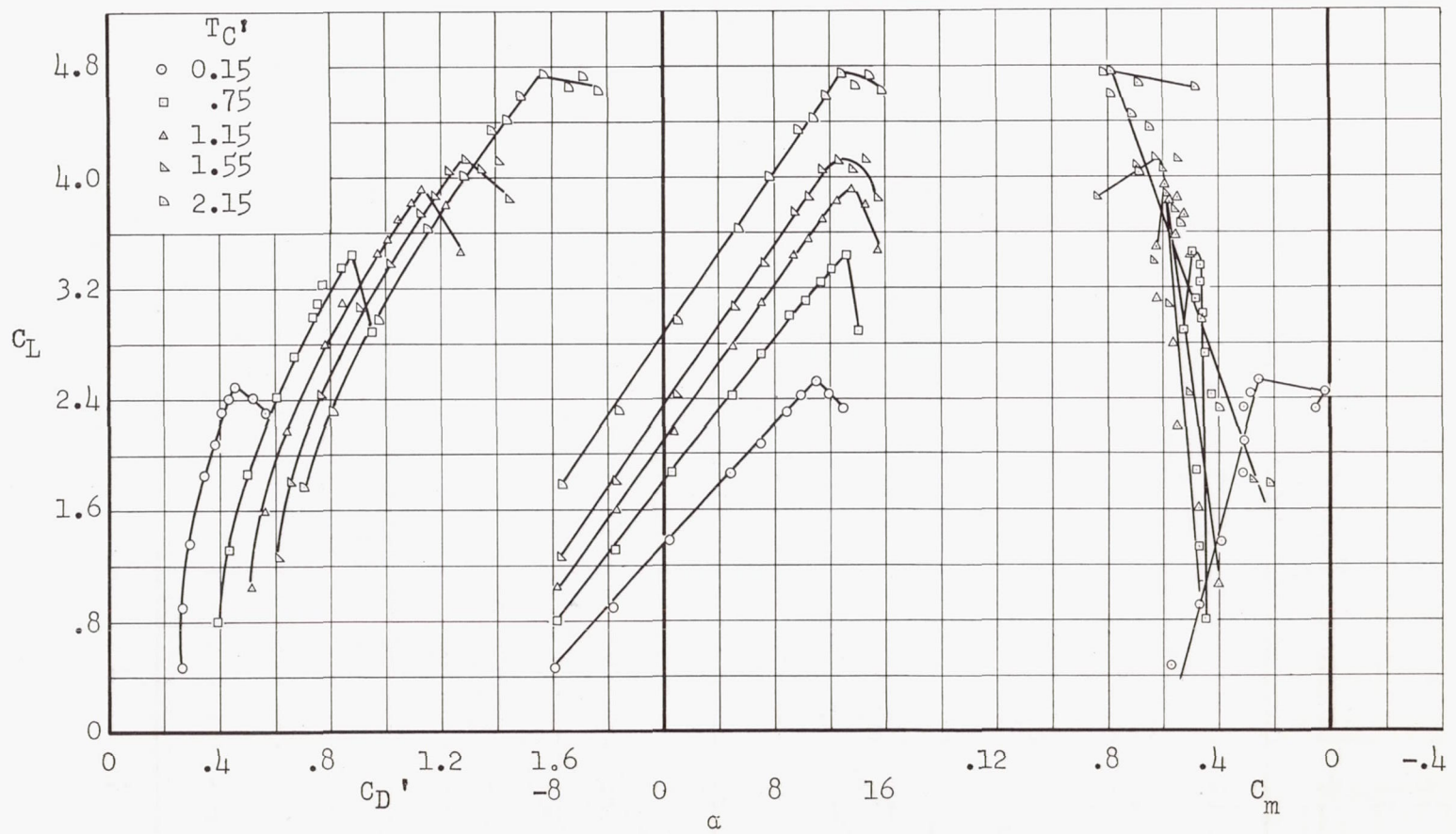

(e) $\delta_f = 60^\circ$; $\delta_a = 0^\circ$; $C_{Q_f} = C_{Q_a} = 0$; $i_t = -3^\circ$

Figure 7.- Continued.

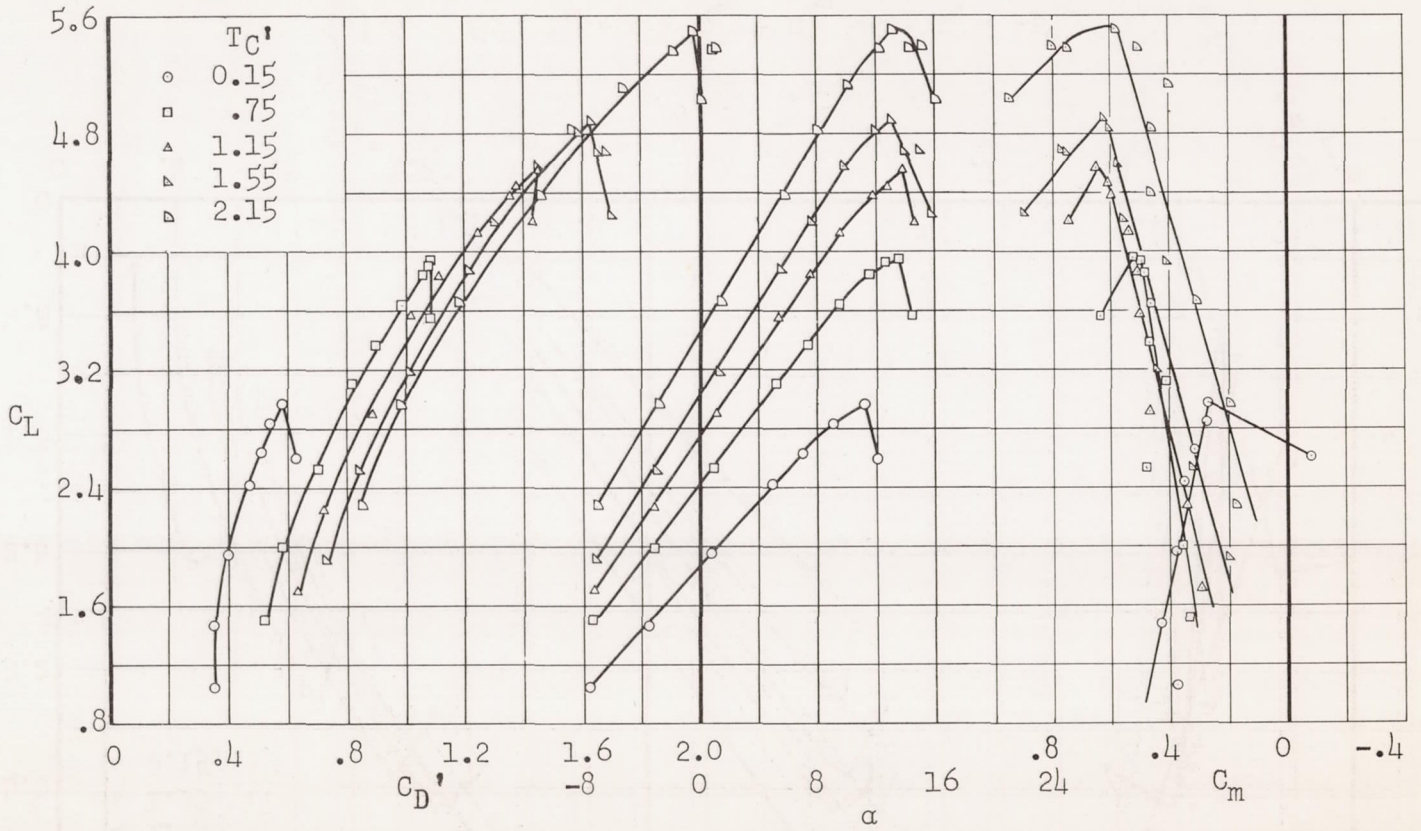

(f) $\delta_f = 60^\circ$; $\delta_a = 0^\circ$; $C_{Q_f} = 0.0030$; $C_{Q_a} = 0$; $i_t = -3^\circ$

Figure 7.- Continued.

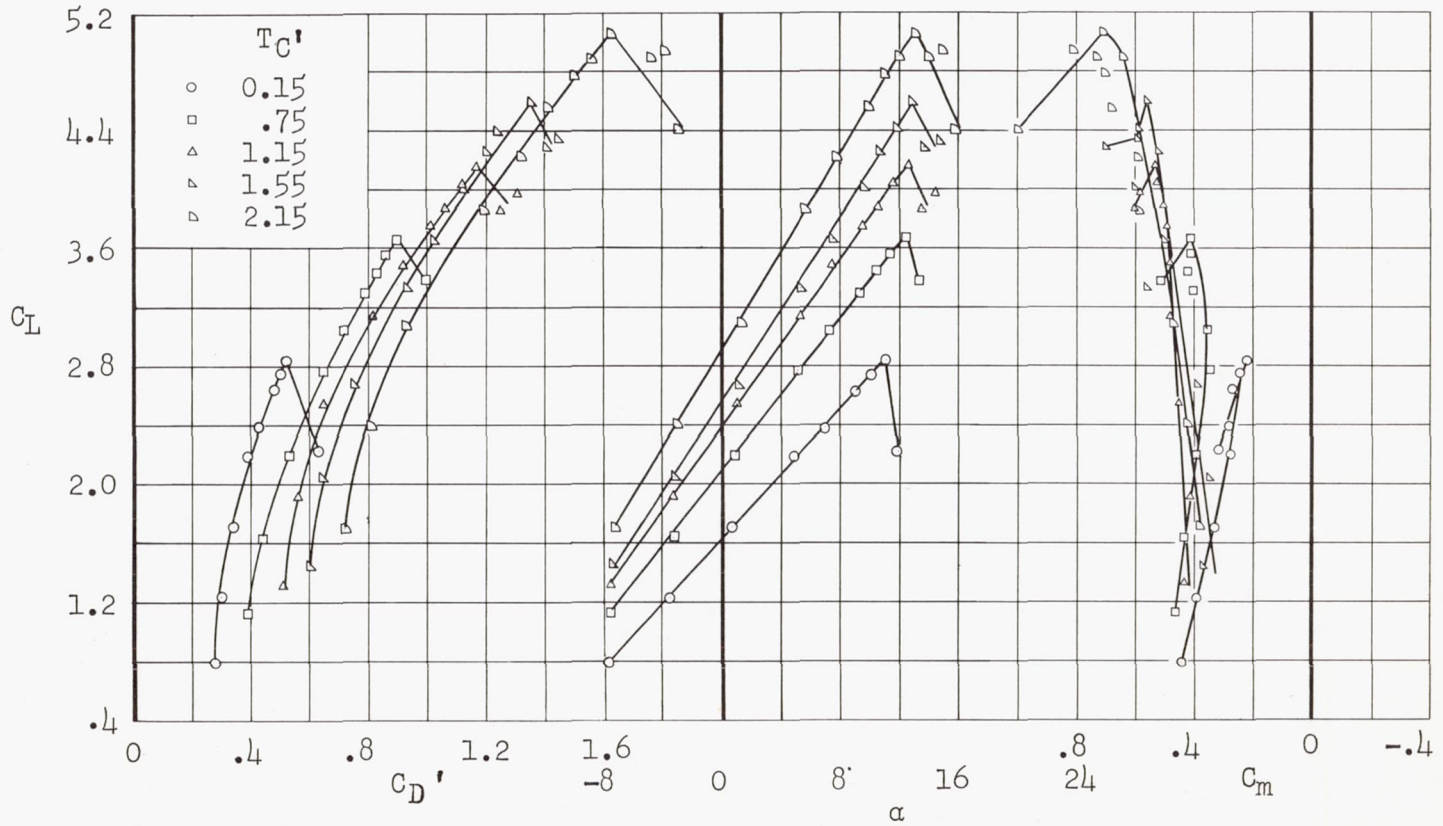

(g) $\delta_f = 60^\circ$; $\delta_a = 30^\circ$; $C_{Q_f} = C_{Q_a} = 0$; $i_t = -3^\circ$

Figure 7.- Continued.

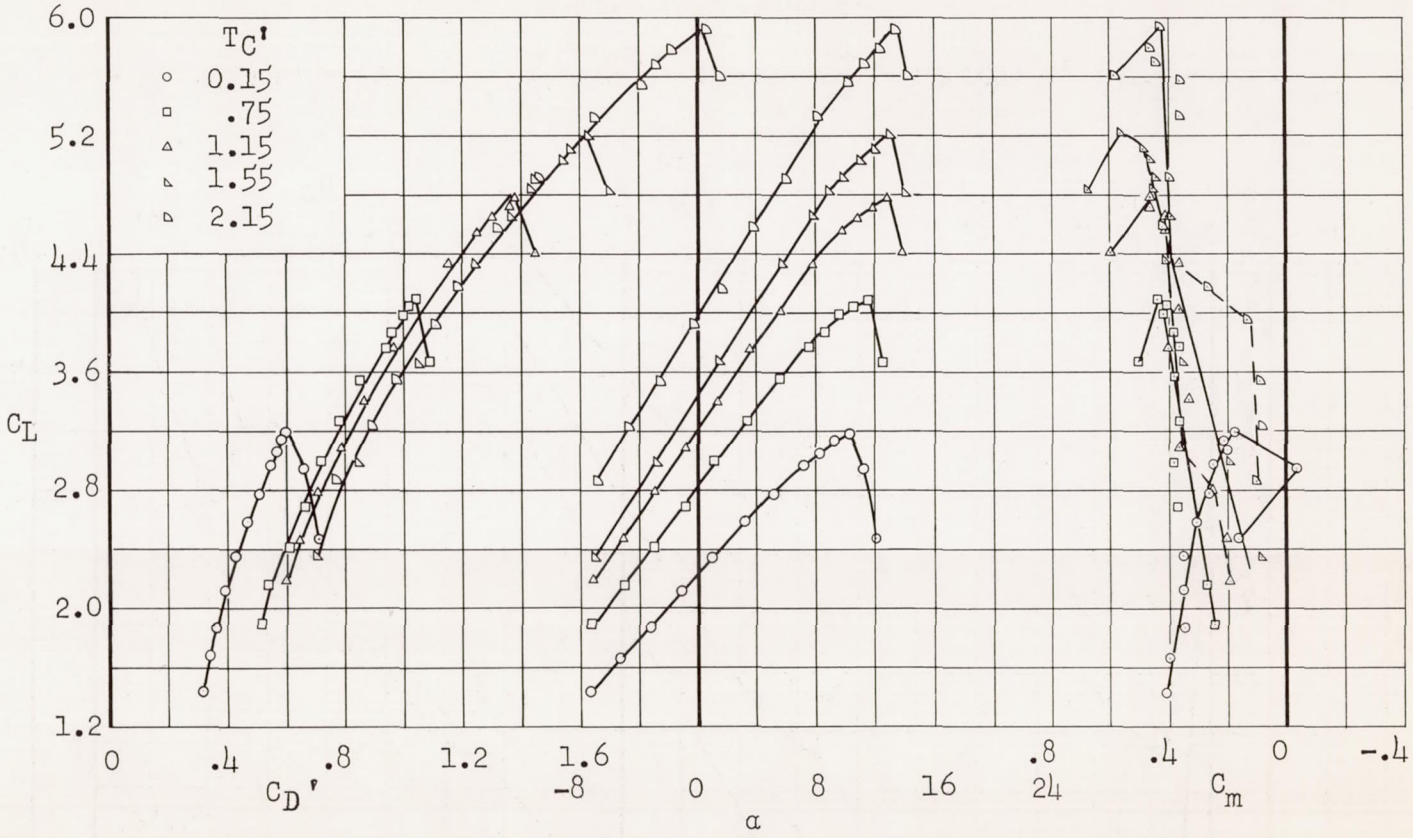

(h) $\delta_f = 60^\circ$; $\delta_a = 30^\circ$; $C_{Q_f} = 0.0033$; $C_{Q_a} = 0.0016$; $i_t = -3^\circ$

Figure 7.- Continued.

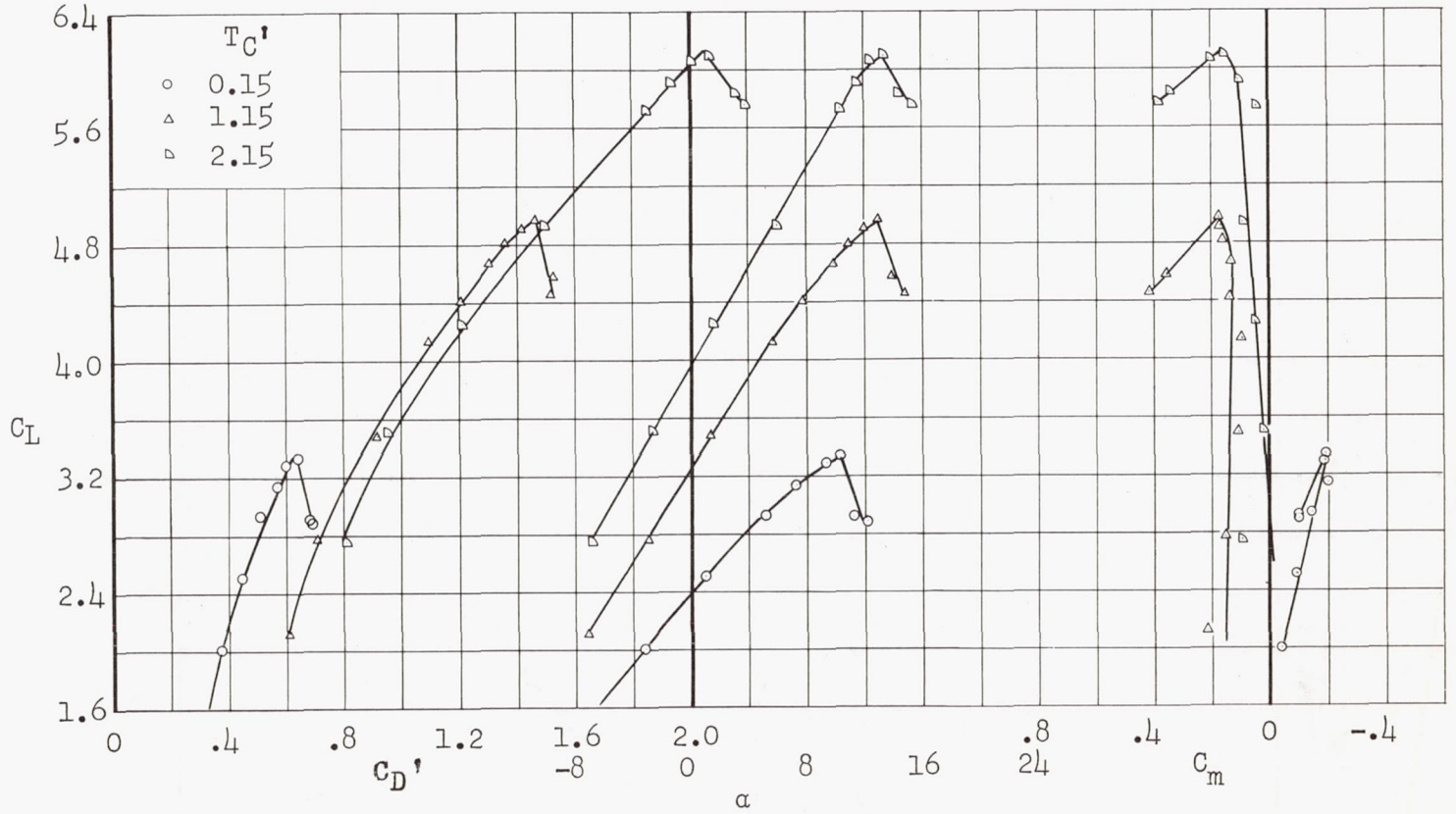

(i) $\delta_f = 60^\circ$; $\delta_a = 30^\circ$; $C_{Q_f} = 0.0027$; $C_{Q_a} = 0.0007$; $i_t = 3^\circ$

Figure 7.- Continued.

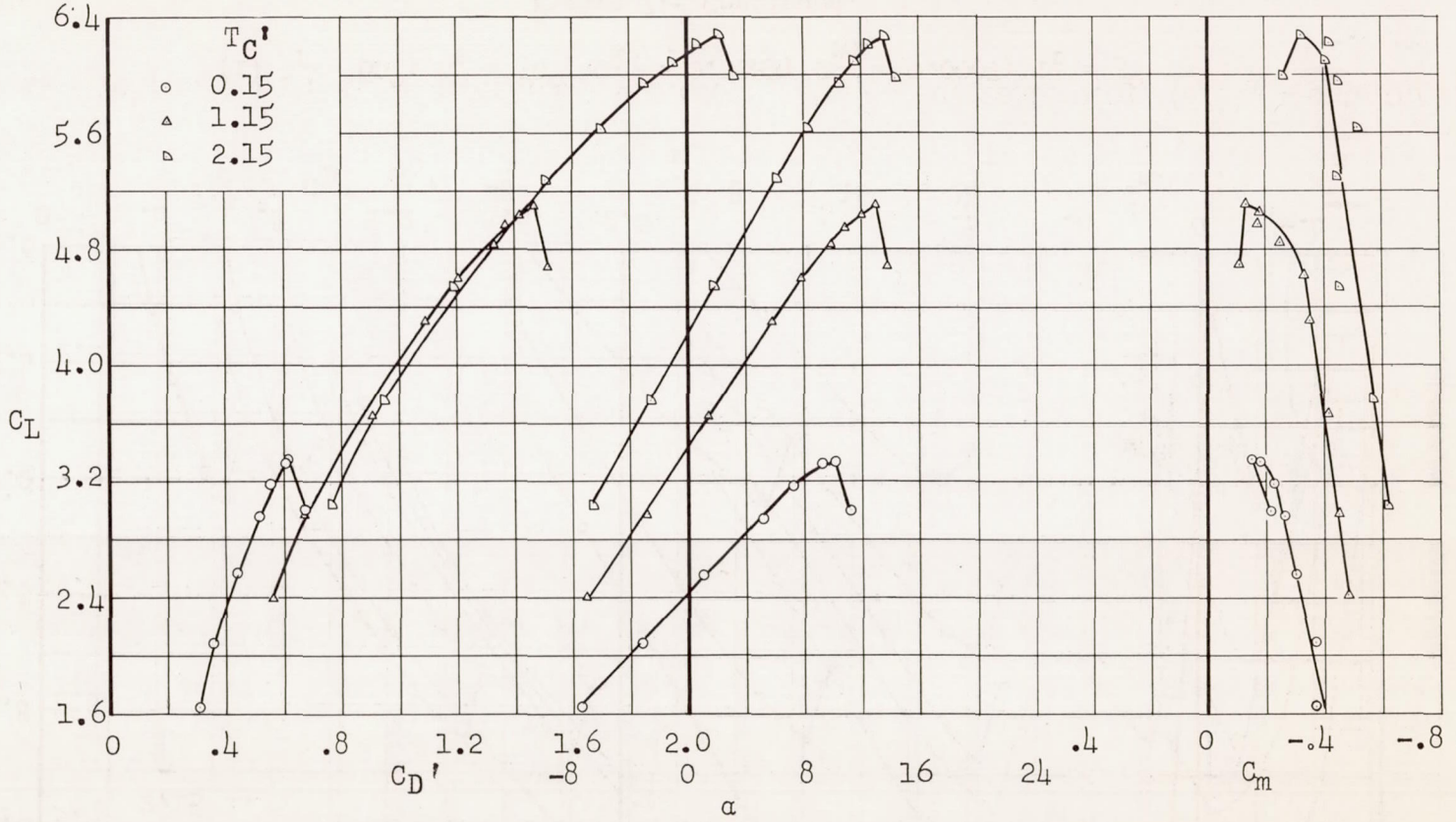

(j) $\delta_f = 60°$; $\delta_a = 30°$; $C_{Q_f} = 0.0028$; $C_{Q_a} = 0.0007$; tail off

Figure 7.- Continued.

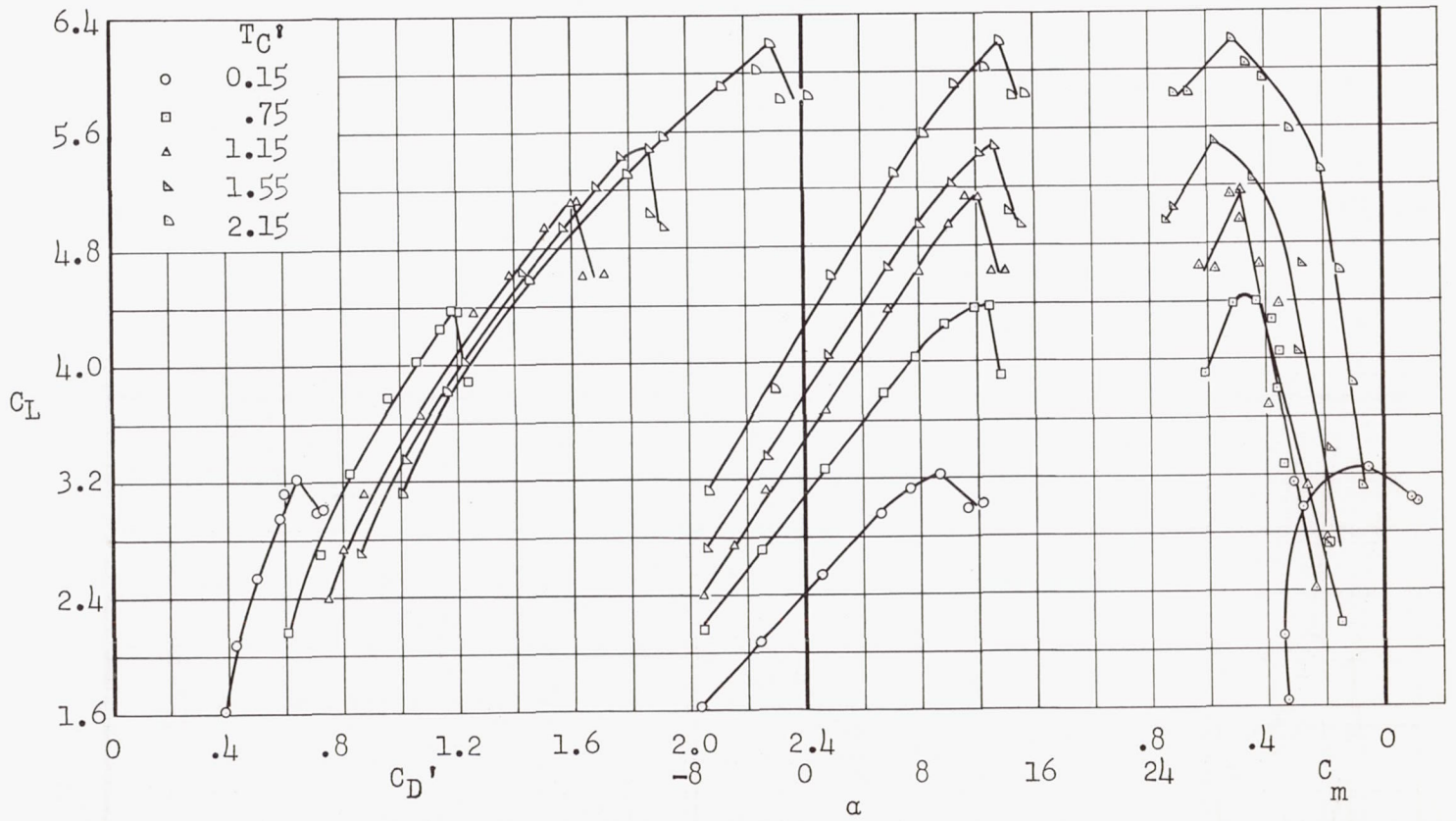

(k) $\delta_f = 70^\circ$; $\delta_a = 30^\circ$; $C_{Q_f} = 0.0028$; $C_{Q_a} = 0.0007$; $(s/c)_f$ = -0.022 to 0.03, $(s/c)_a$ = 0 to 0.03; $i_t = -3^\circ$

Figure 7.- Concluded.

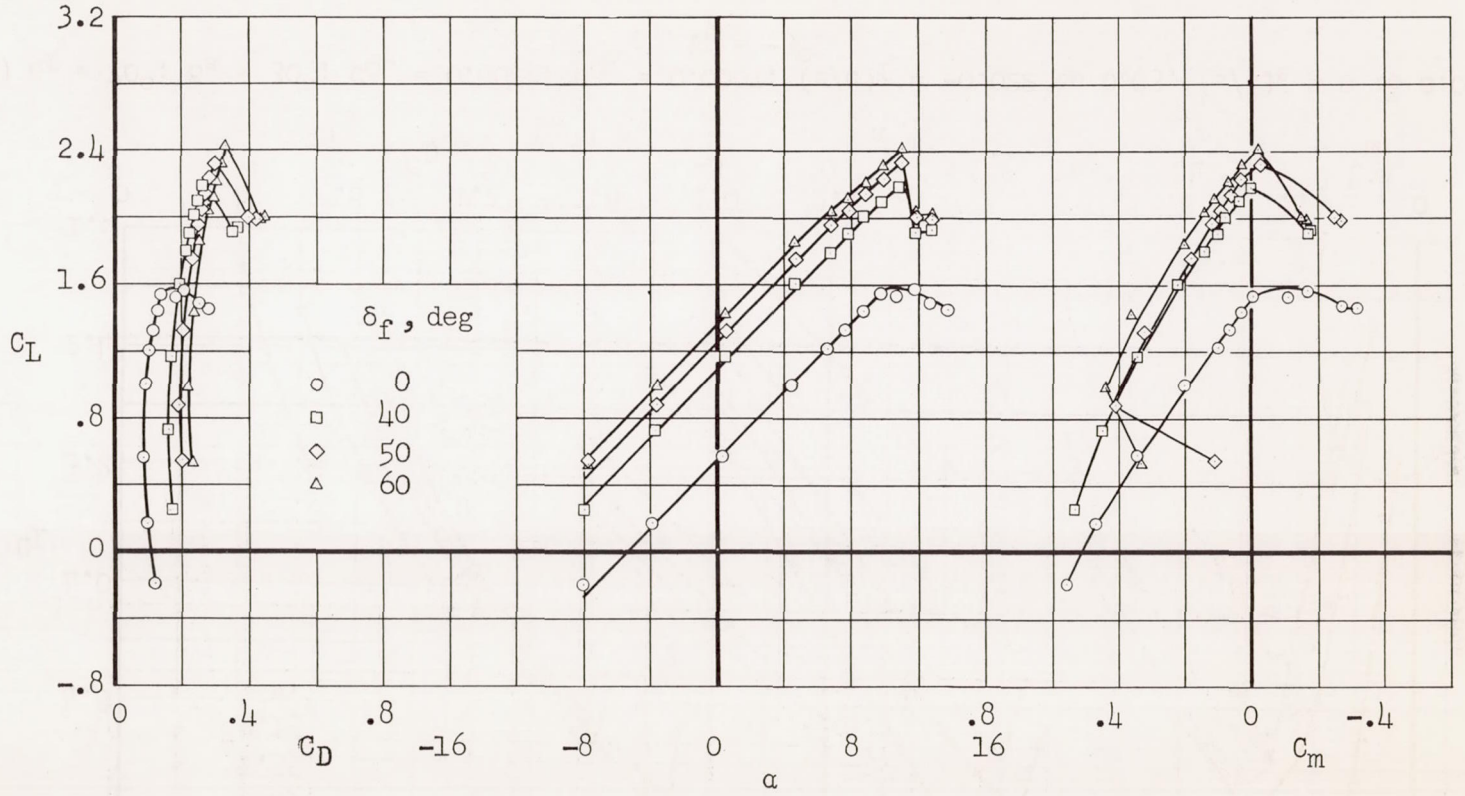

(a) $\delta_a = 0^\circ$; $C_{Q_f} = C_{Q_a} = 0$; $i_t = -3^\circ$

Figure 8.- Aerodynamic characteristics of the model with nacelles and propellers off.

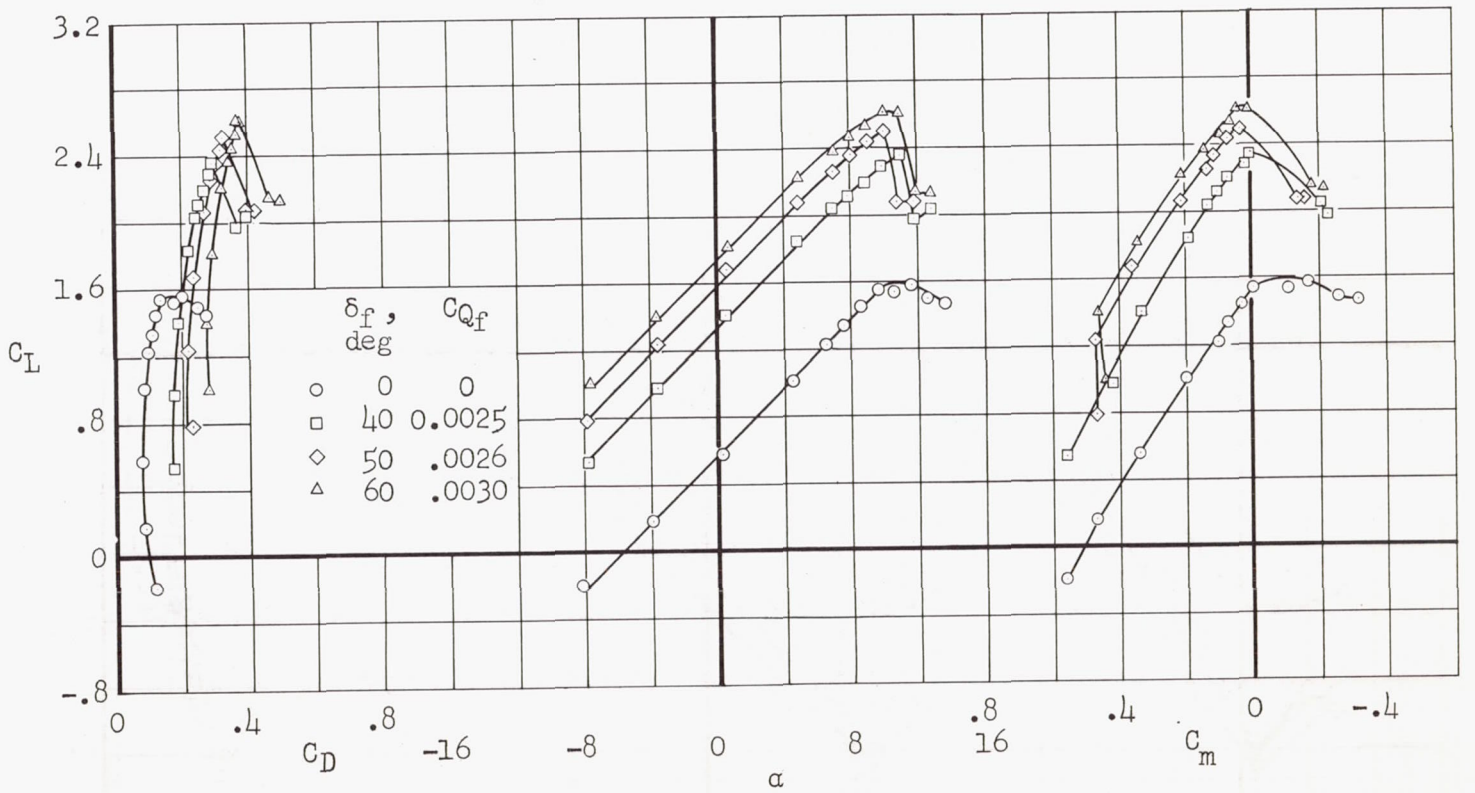

(b) $\delta_a = 0^\circ$; $C_{Q_a} = 0$; $i_t = -3^\circ$

Figure 8.- Continued.

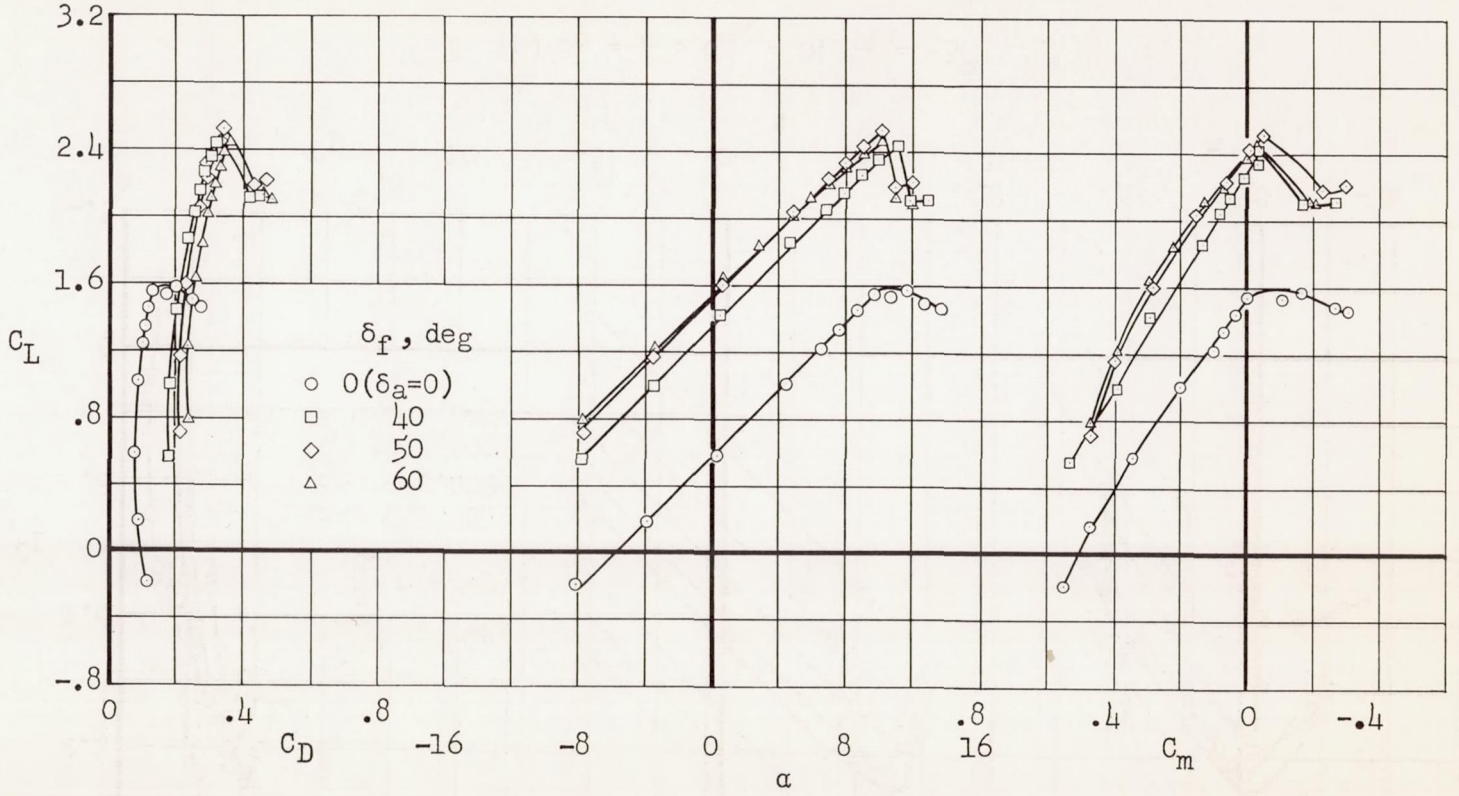

(c) $\delta_a = 30^\circ$; $C_{Q_f} = C_{Q_a} = 0$; $i_t = -3^\circ$

Figure 8.- Continued.

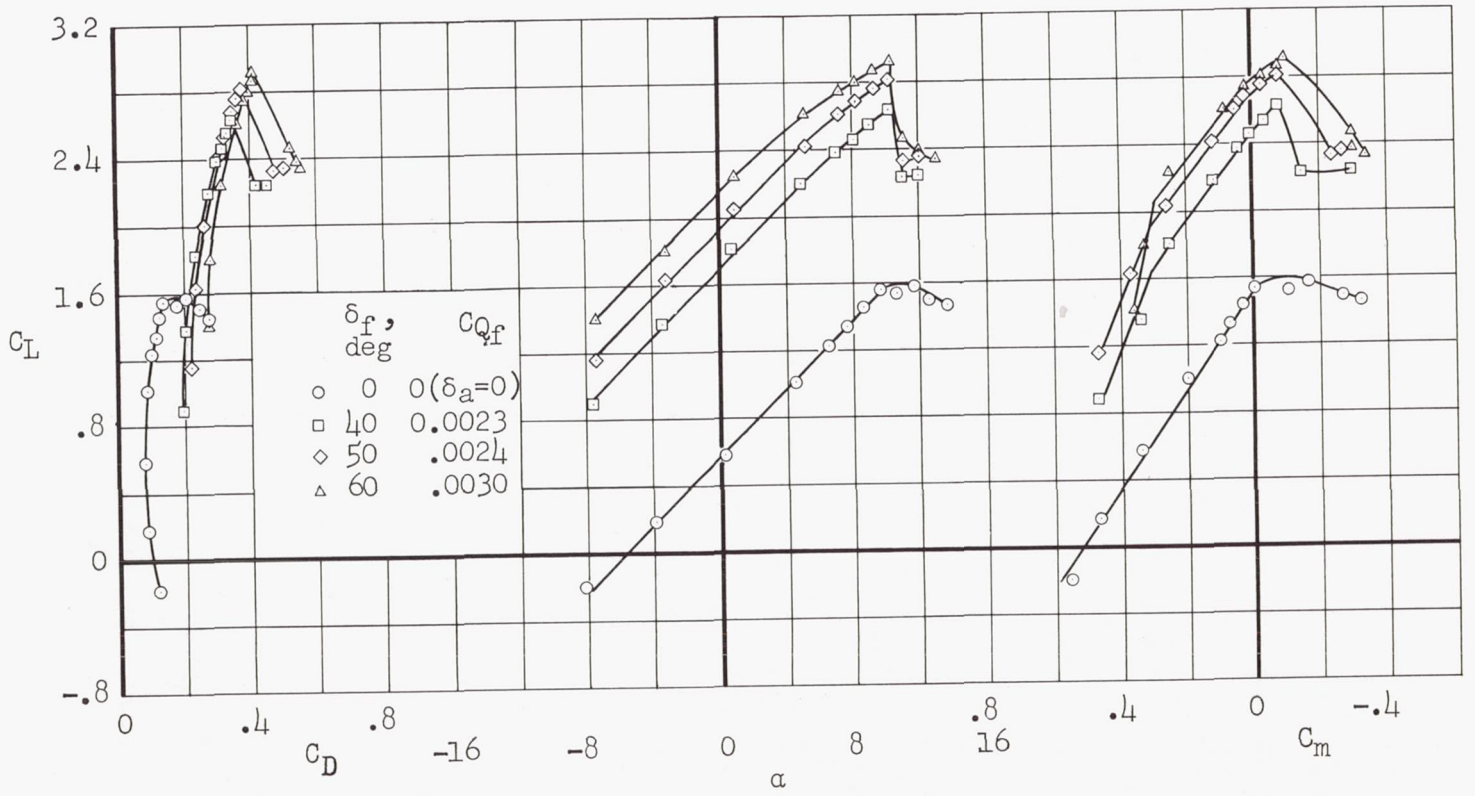

(d) $\delta_a = 30^\circ$; $C_{Q_a} = 0.0007$; $i_t = -3^\circ$

Figure 8.- Continued.

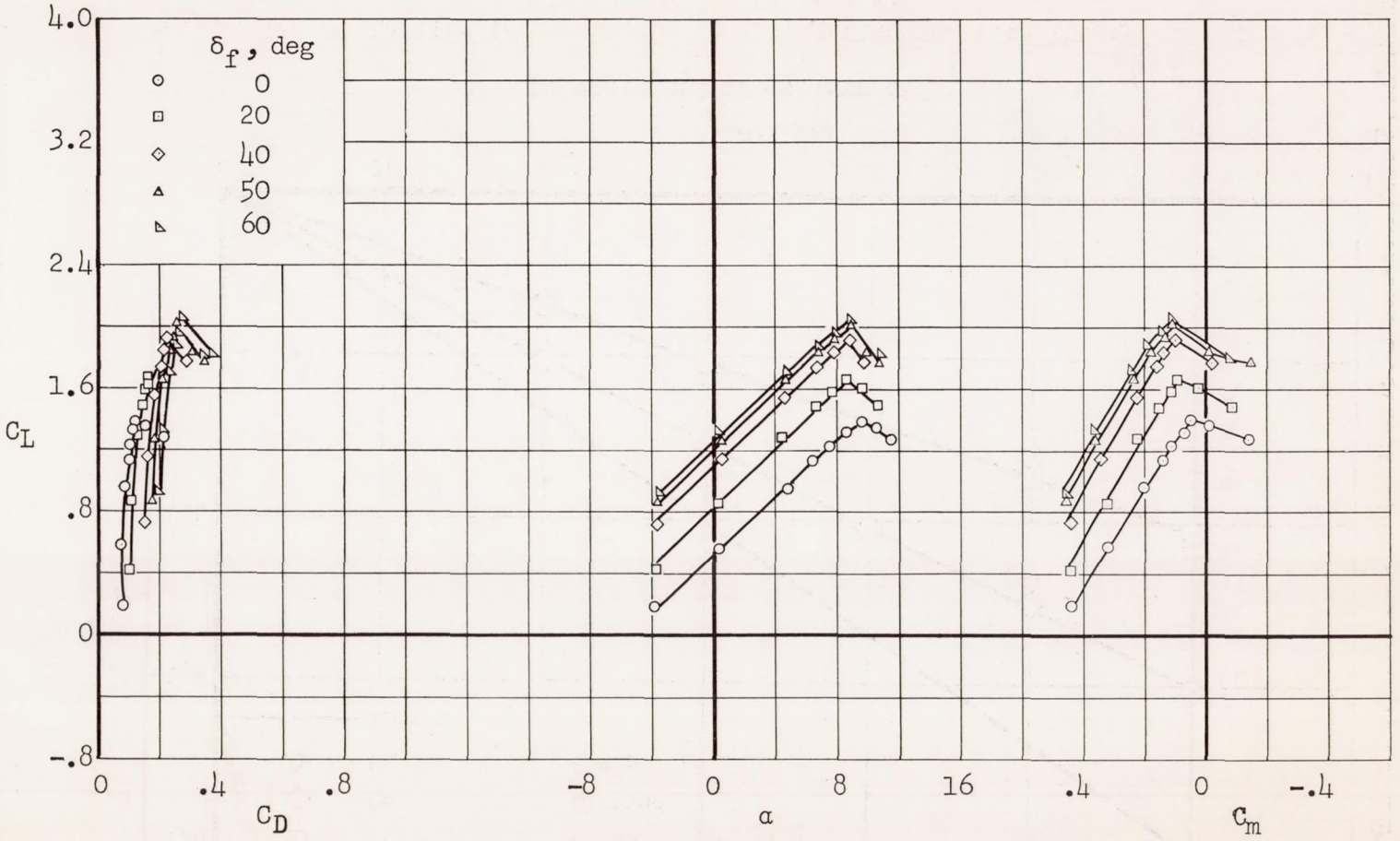

(e) $\delta_a = 0^\circ$; $C_{Q_f} = C_{Q_a} = 0$; $i_t = -3^\circ$; plain flap

Figure 8.- Concluded.

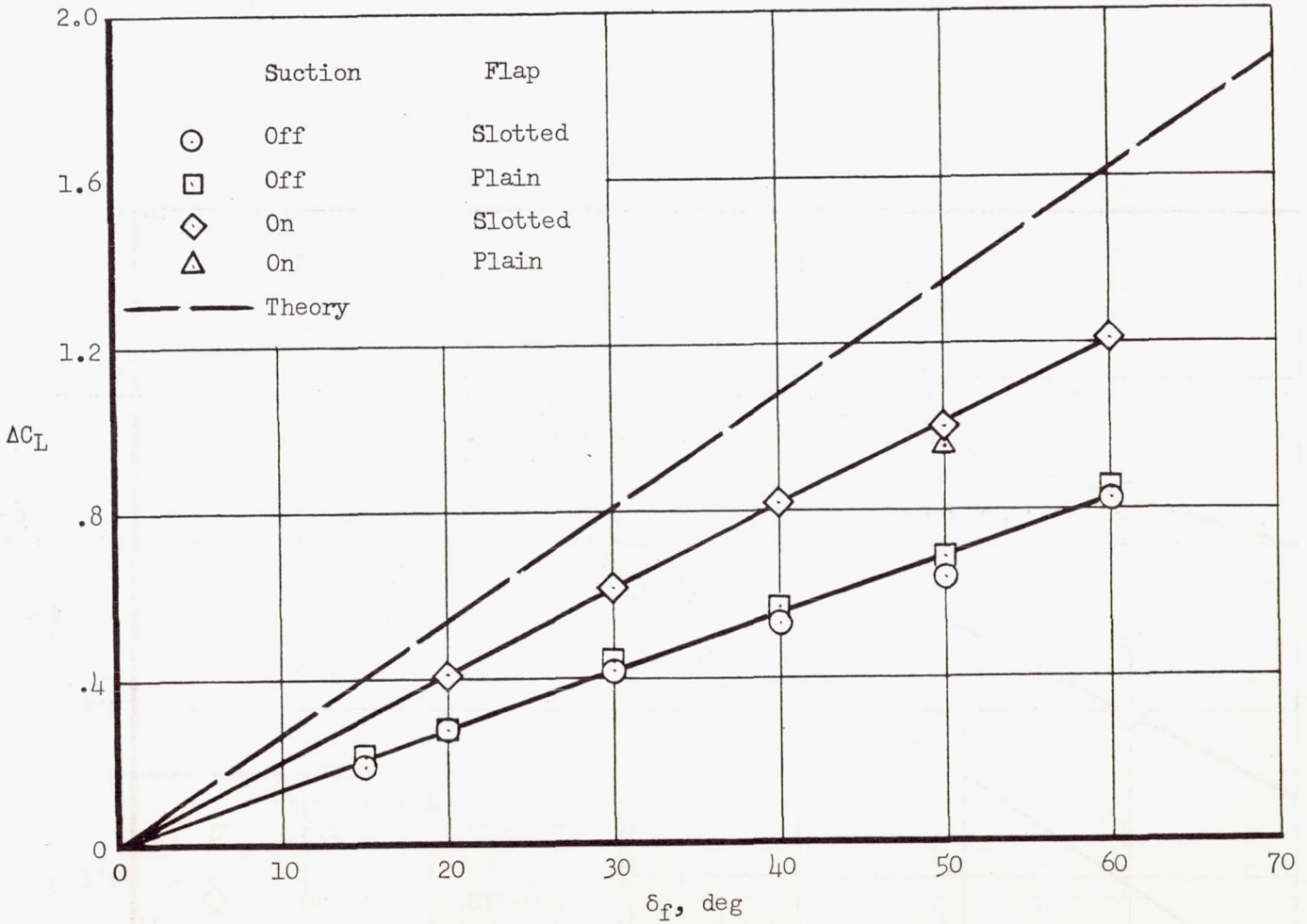

(a) Nacelles and propellers off.

Figure 9.- Comparison of the lift increment due to flap deflection with theory; $\alpha_u = 0^\circ$; $\delta_a = 0^\circ$; $C_{Q_f} = C_{Q_{crit}}$; $C_{Q_a} = 0$; $i_t = -3^\circ$.

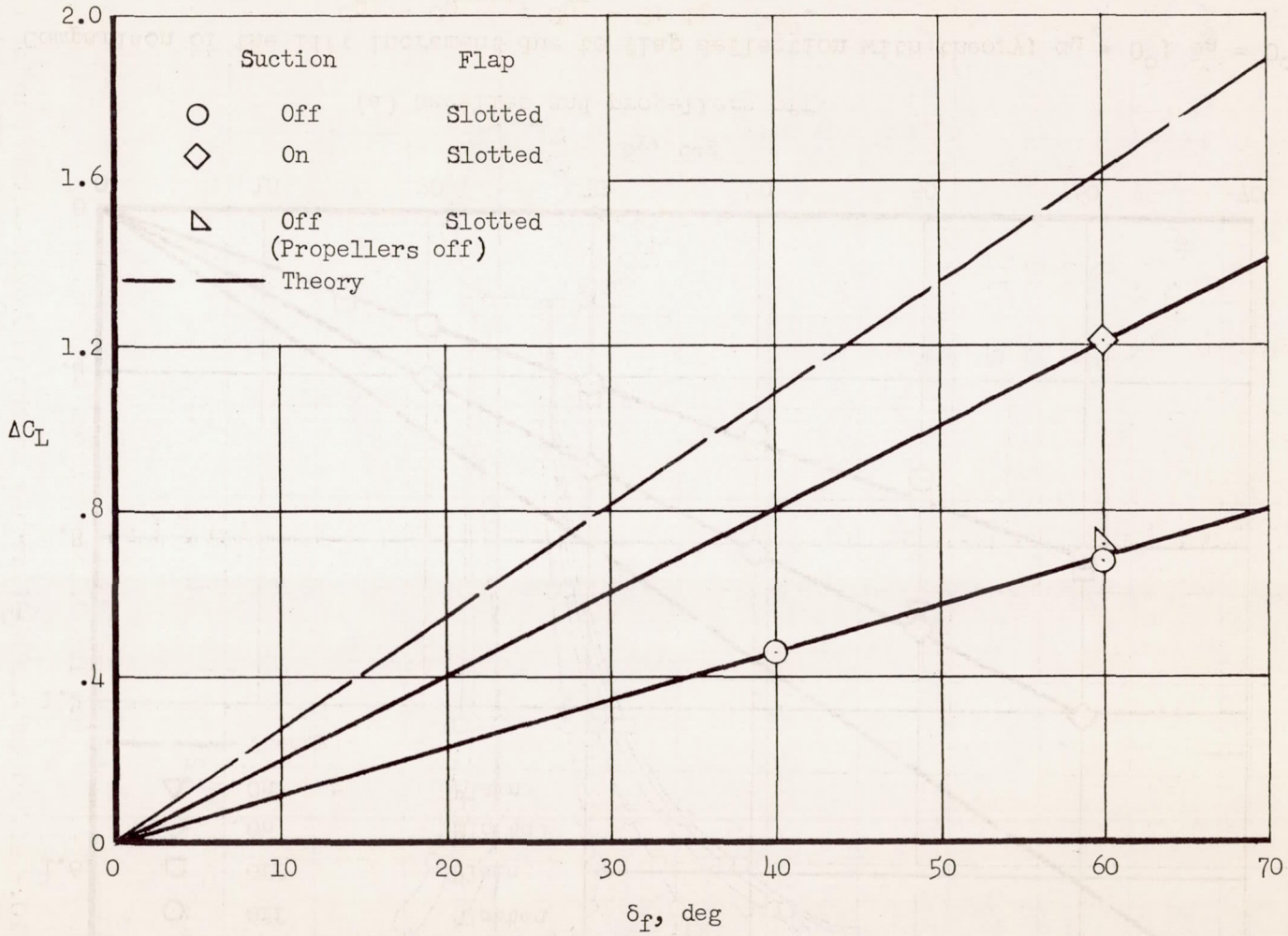

(b) Nacelles and propellers on; $T_C' = 0$.

Figure 9.- Concluded.

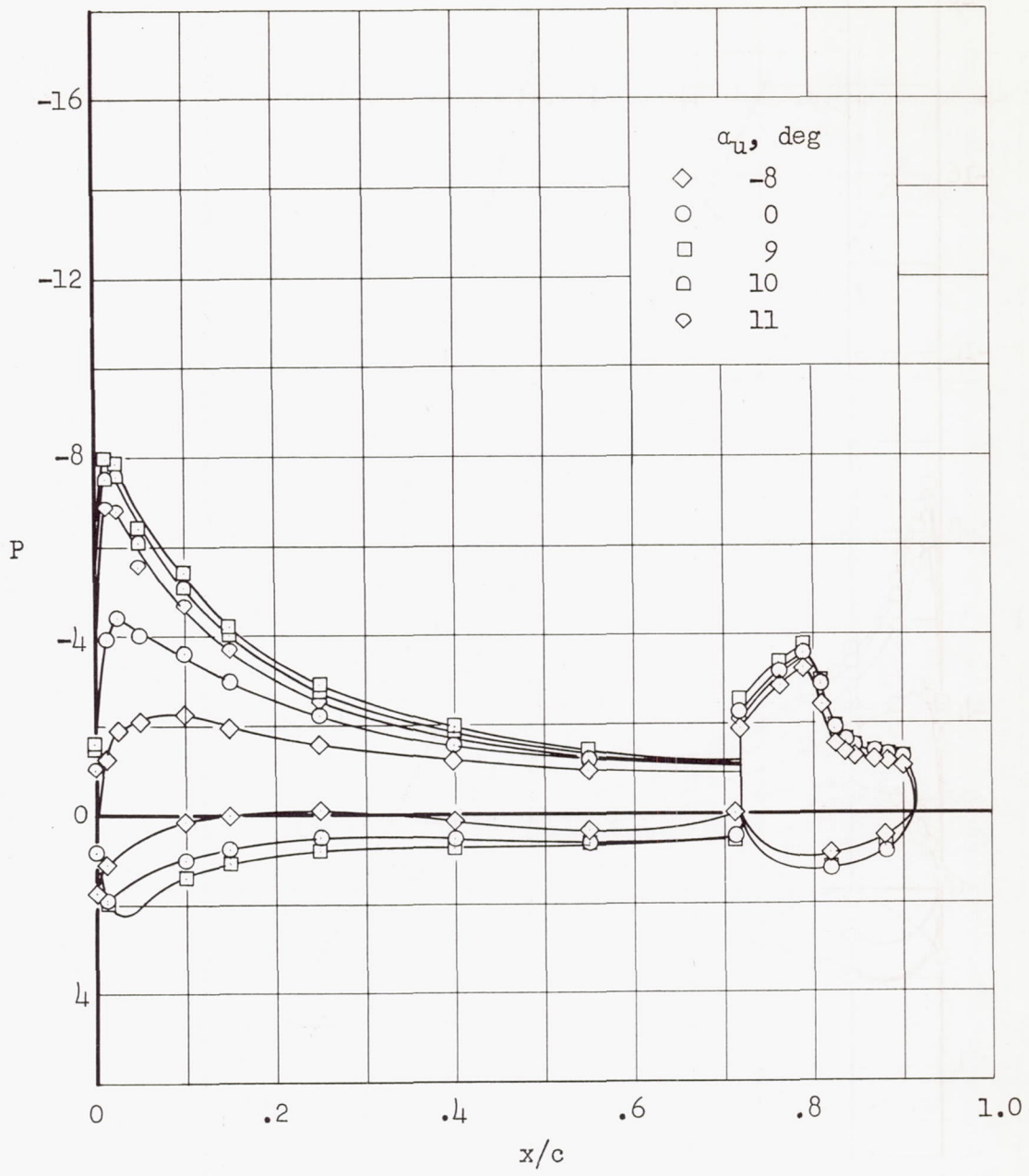

(a) The 0.150-semispan station.

Figure 10.- Effect of angle of attack on the chordwise distribution of pressures on the left wing; $\delta_f = 60^\circ$; $\delta_a = 30^\circ$; $C_{Q_f} = 0.0033$; $C_{Q_a} = 0.0016$; $i_t = -3^\circ$; $T_C' = 0.15$.

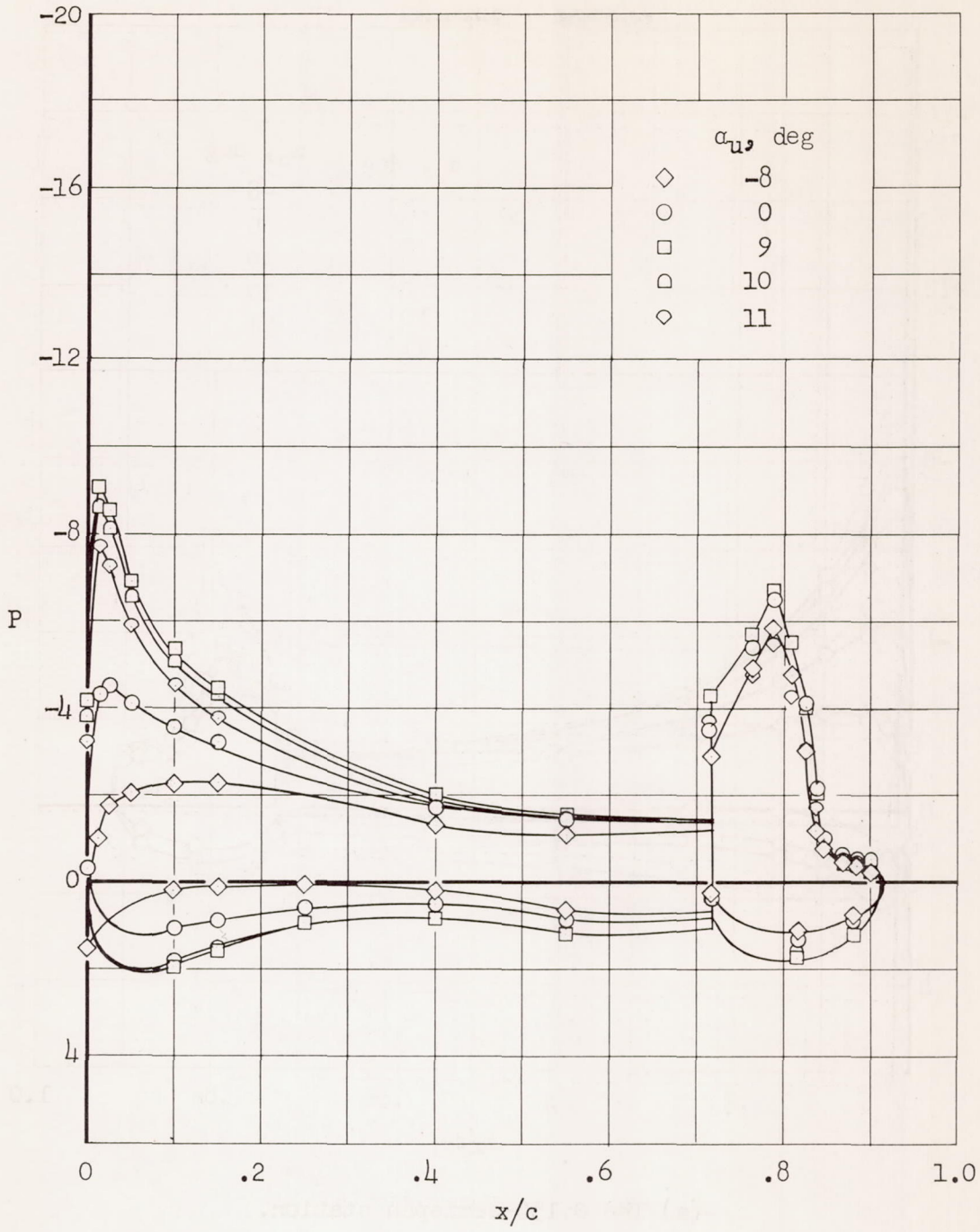

(b) The 0.186-semispan station.

Figure 10.- Continued.

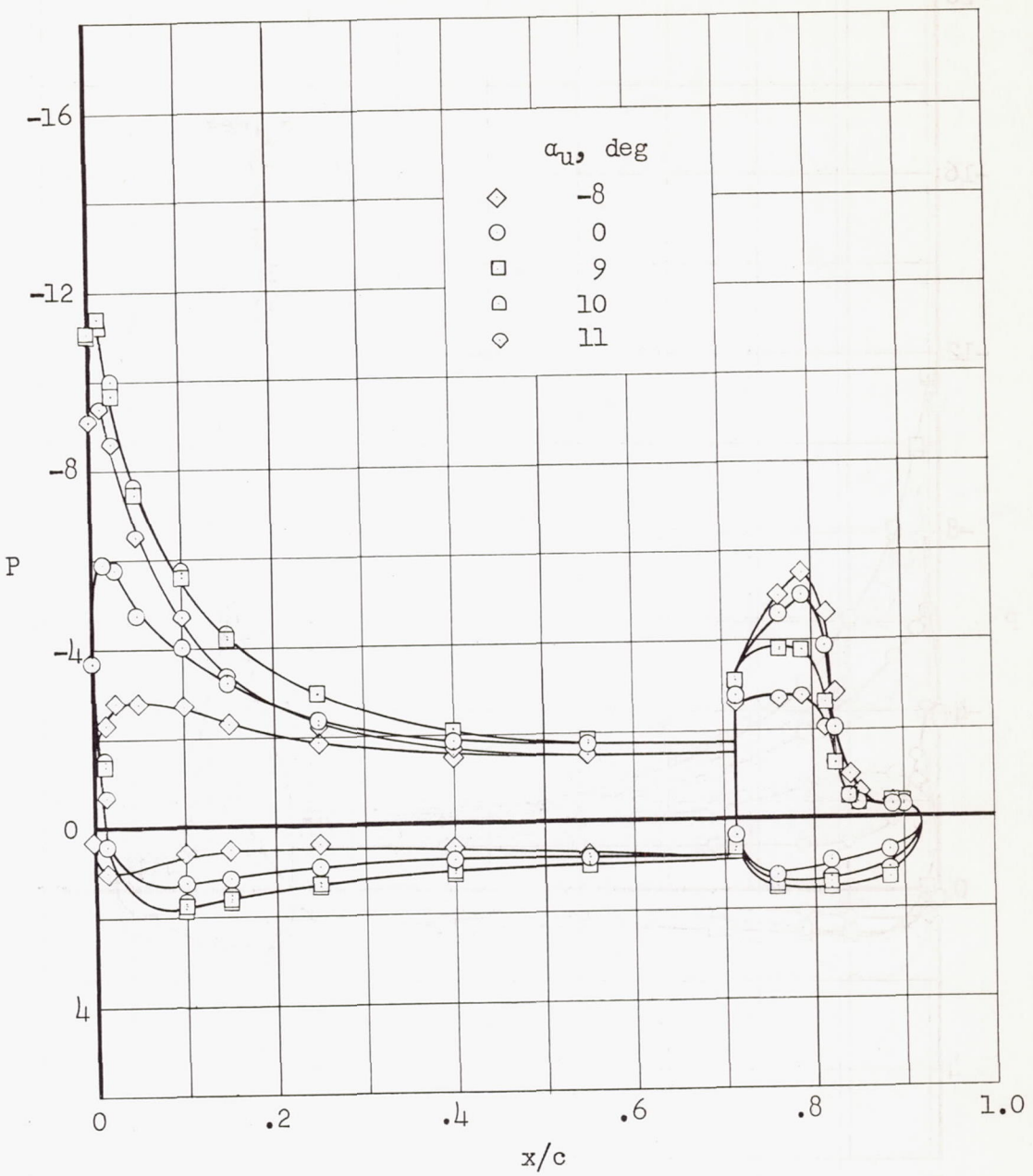

(c) The 0.343-semispan station.

Figure 10.- Continued.

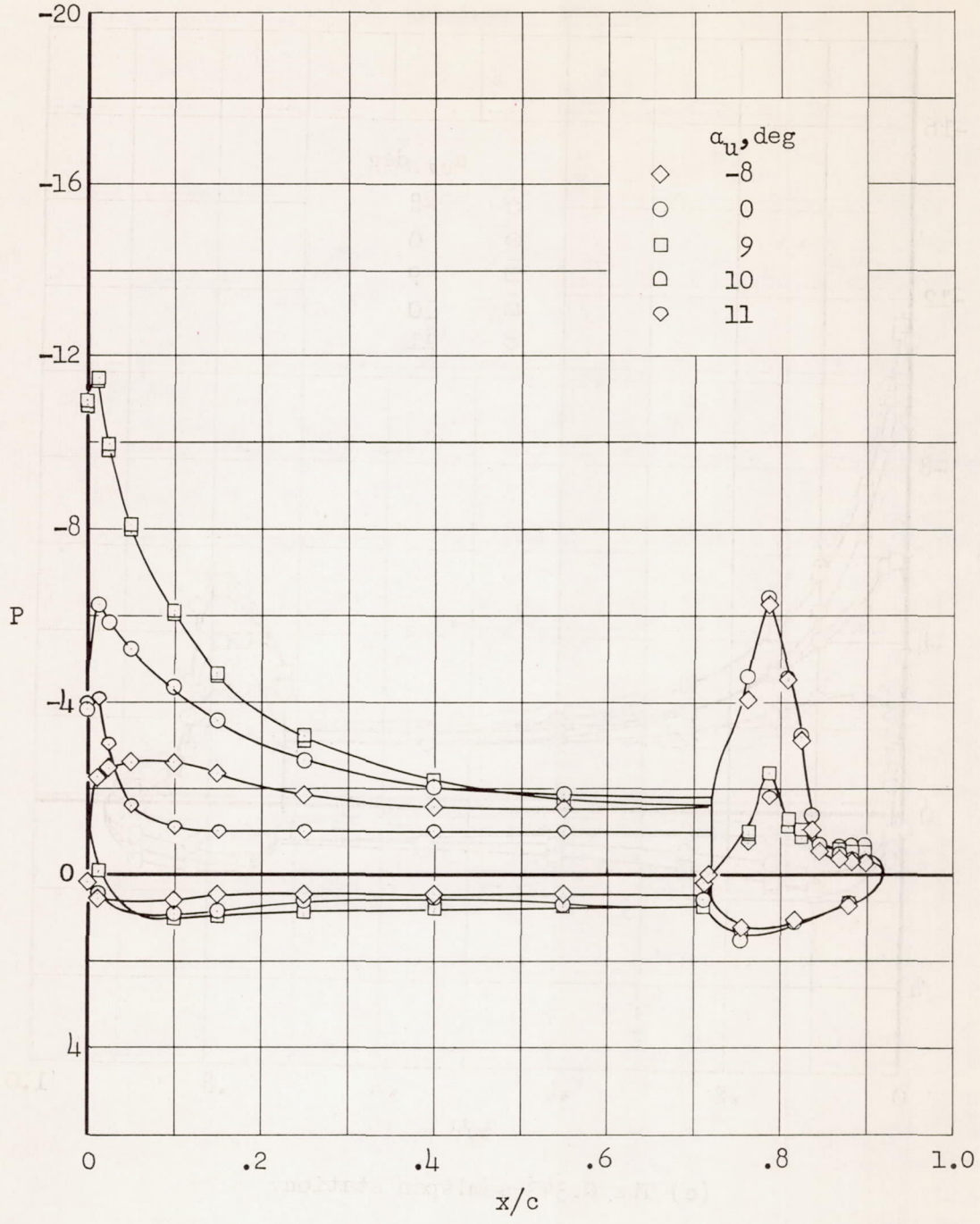

(d) The 0.454-semispan station.

Figure 10.- Continued.

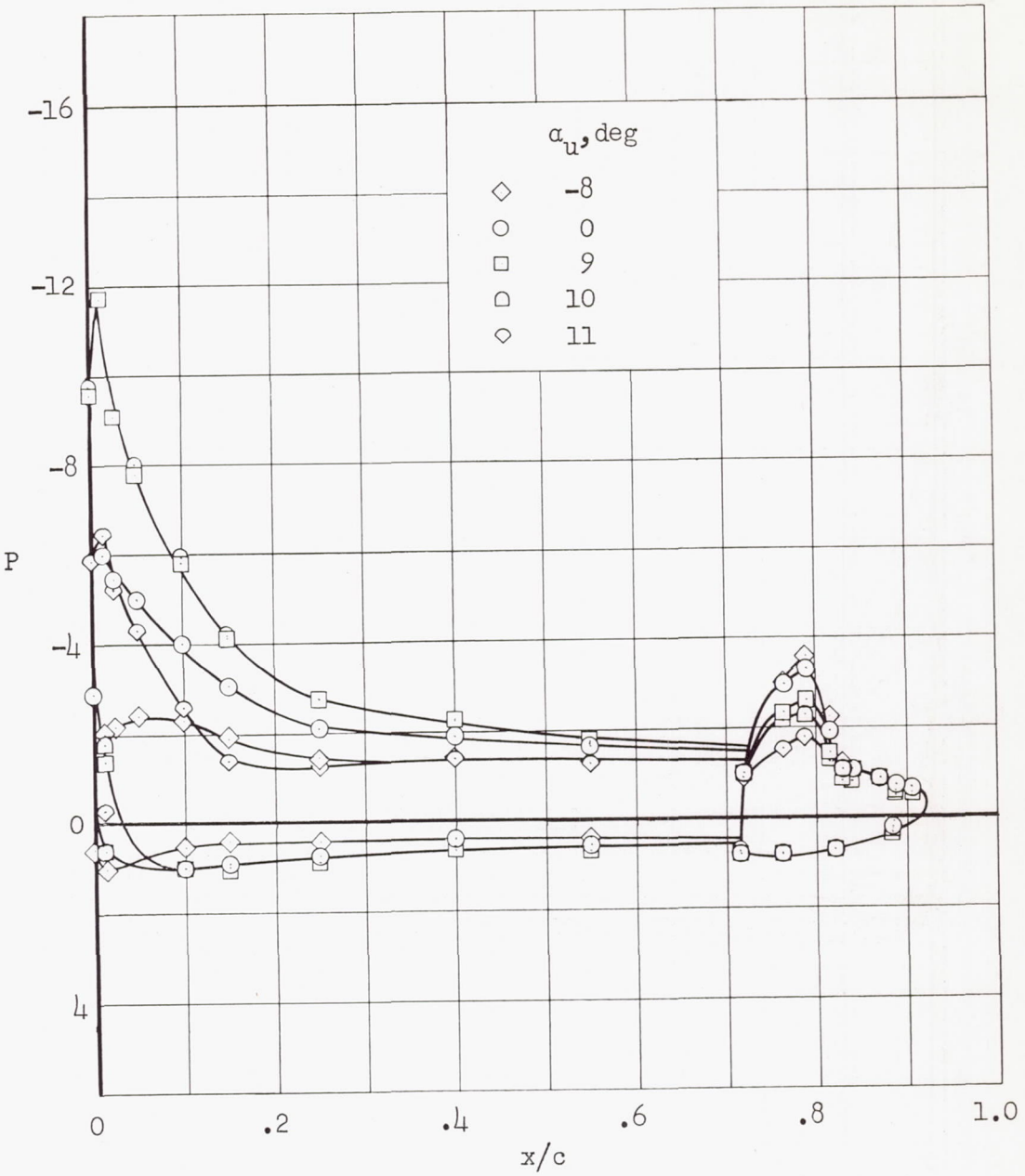

(e) The 0.583-semispan station.

Figure 10.- Continued.

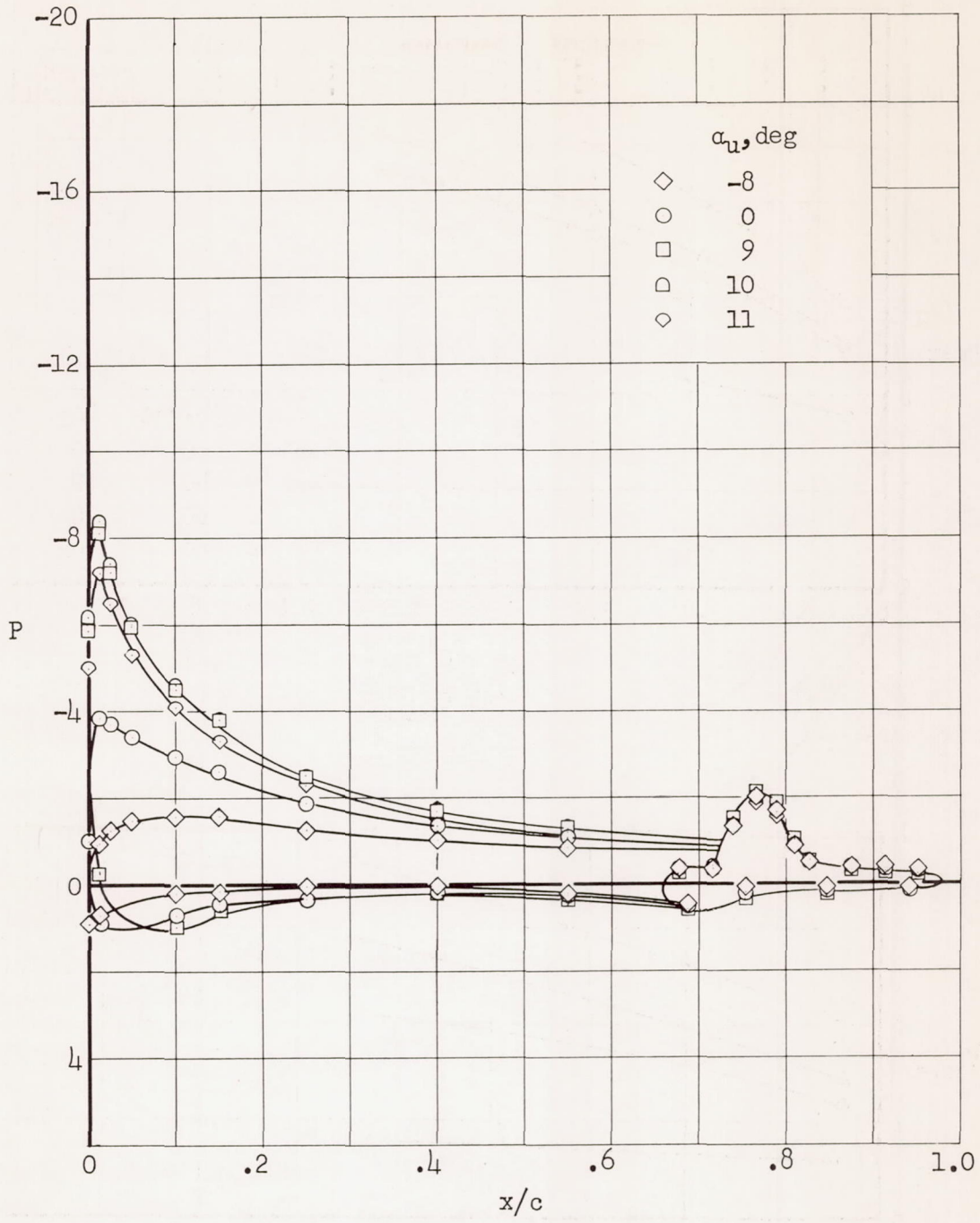

(f) The 0.799-semispan station.

Figure 10.- Concluded.

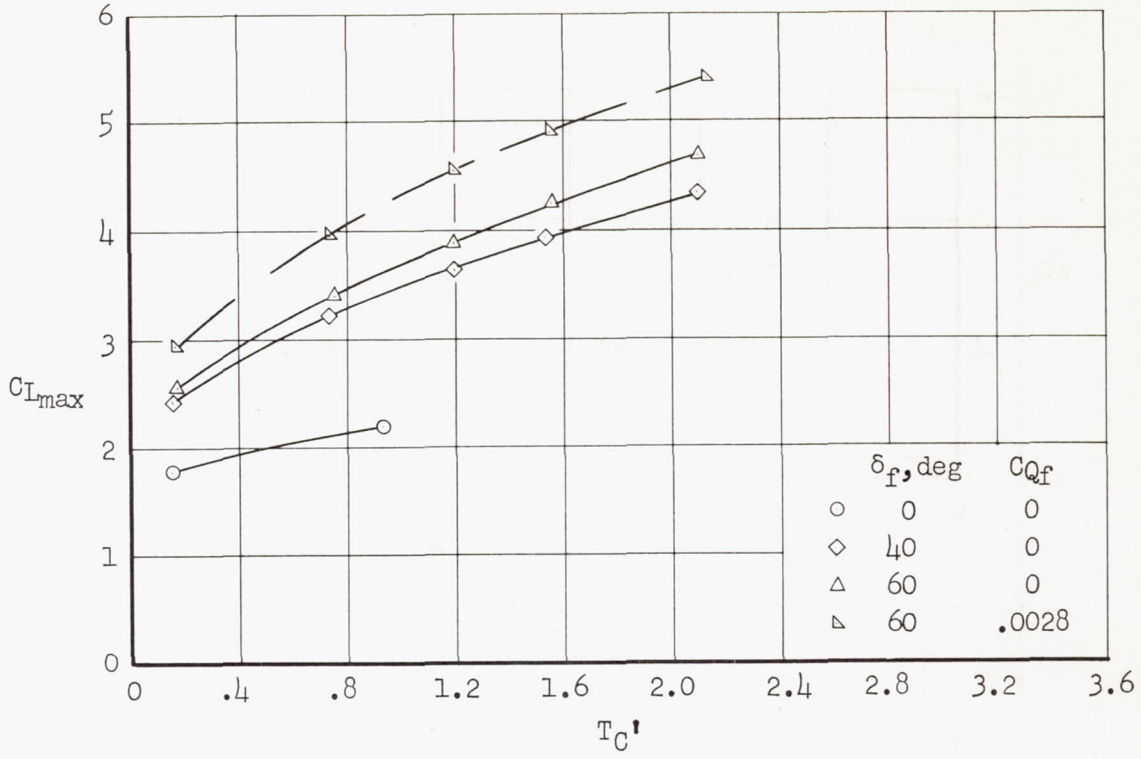

(a) $C_{L_{max}}$

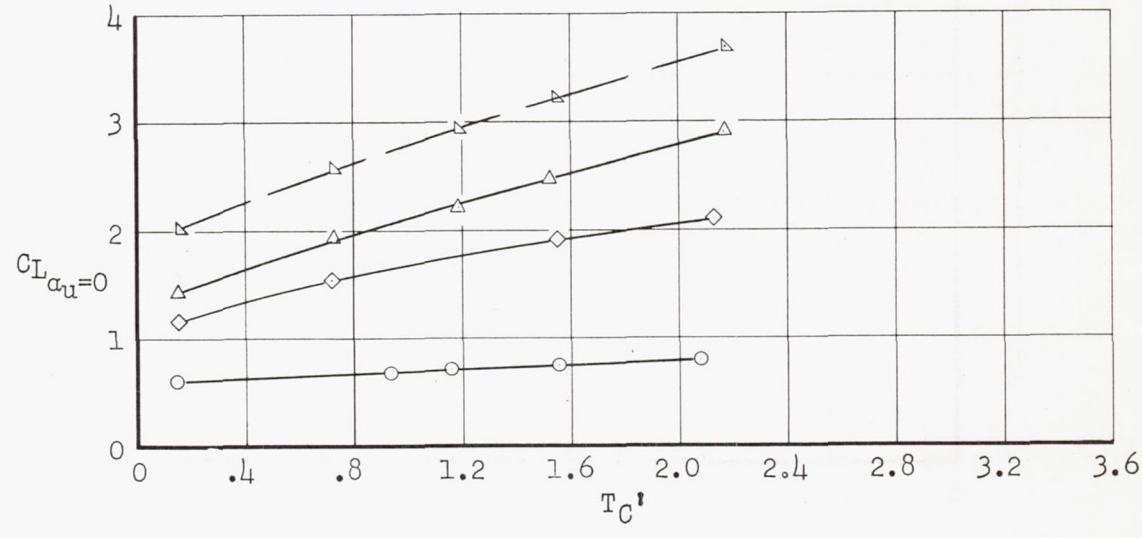

(b) $C_{L_{\alpha_u = 0}}$

Figure 11.- Effect of thrust on $C_{L_{max}}$ and C_L at $\alpha_u = 0^\circ$; $\delta_a = 0^\circ$.

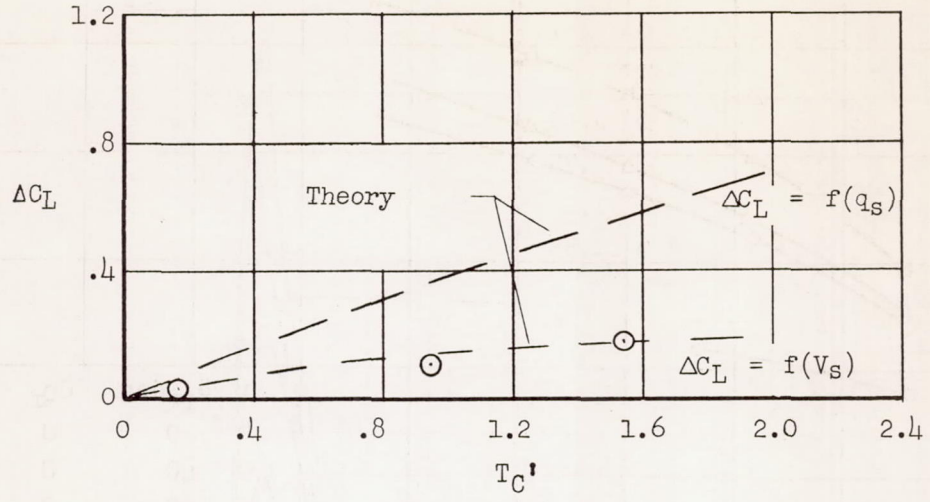

(a) $\delta_f = 0^\circ$; $C_{Q_f} = 0$; $c_n = 0.63$

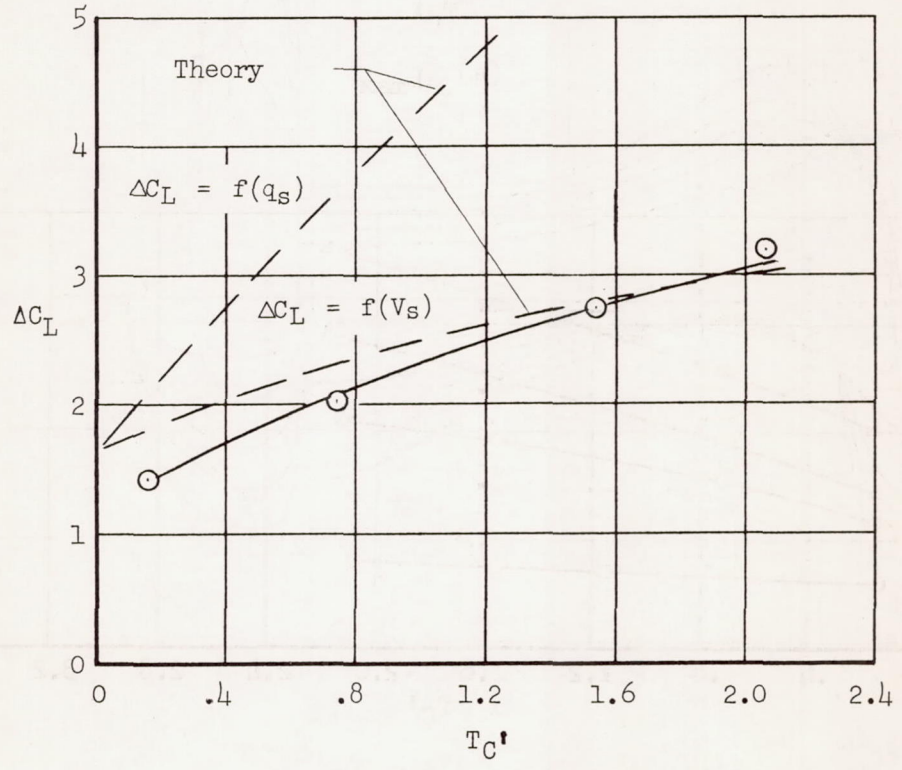

(b) $\delta_f = 60^\circ$; $C_{Q_f} = 0.0028$; $c_n = 3.20$

Figure 12.- Comparison of the lift increase due to thrust with the theory of reference 10; $\delta_a = 0^\circ$; $\alpha_u = 0^\circ$.

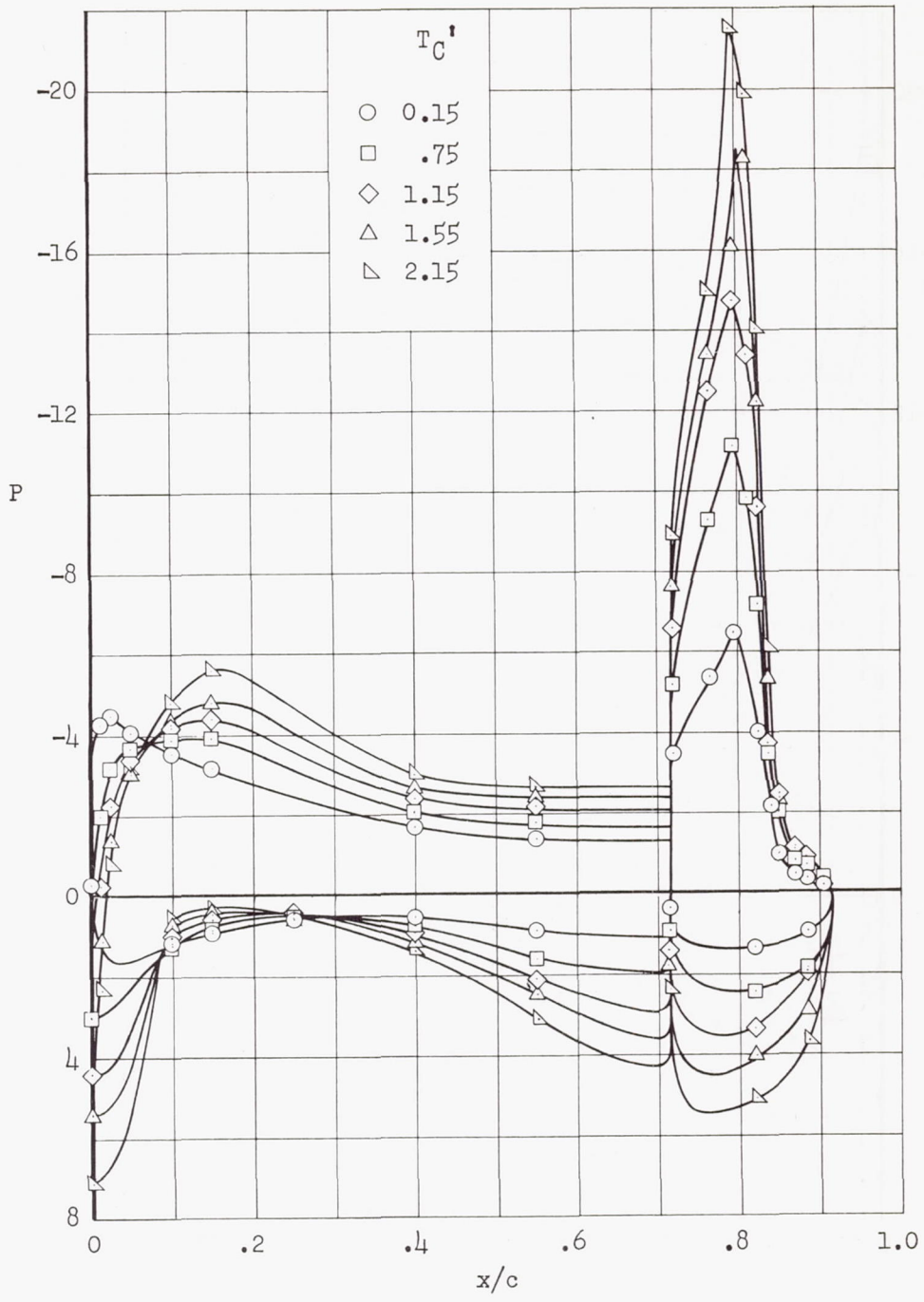

(a) The 0.186-semispan station.

Figure 13.- Effect of thrust on the chordwise distribution of pressure coefficient on the left wing; $\delta_f = 60^\circ$; $\delta_a = 30^\circ$; $C_{Q_f} = 0.0033$; $C_{Q_a} = 0.0016$; $i_t = -3^\circ$; $\alpha_u = 0^\circ$.

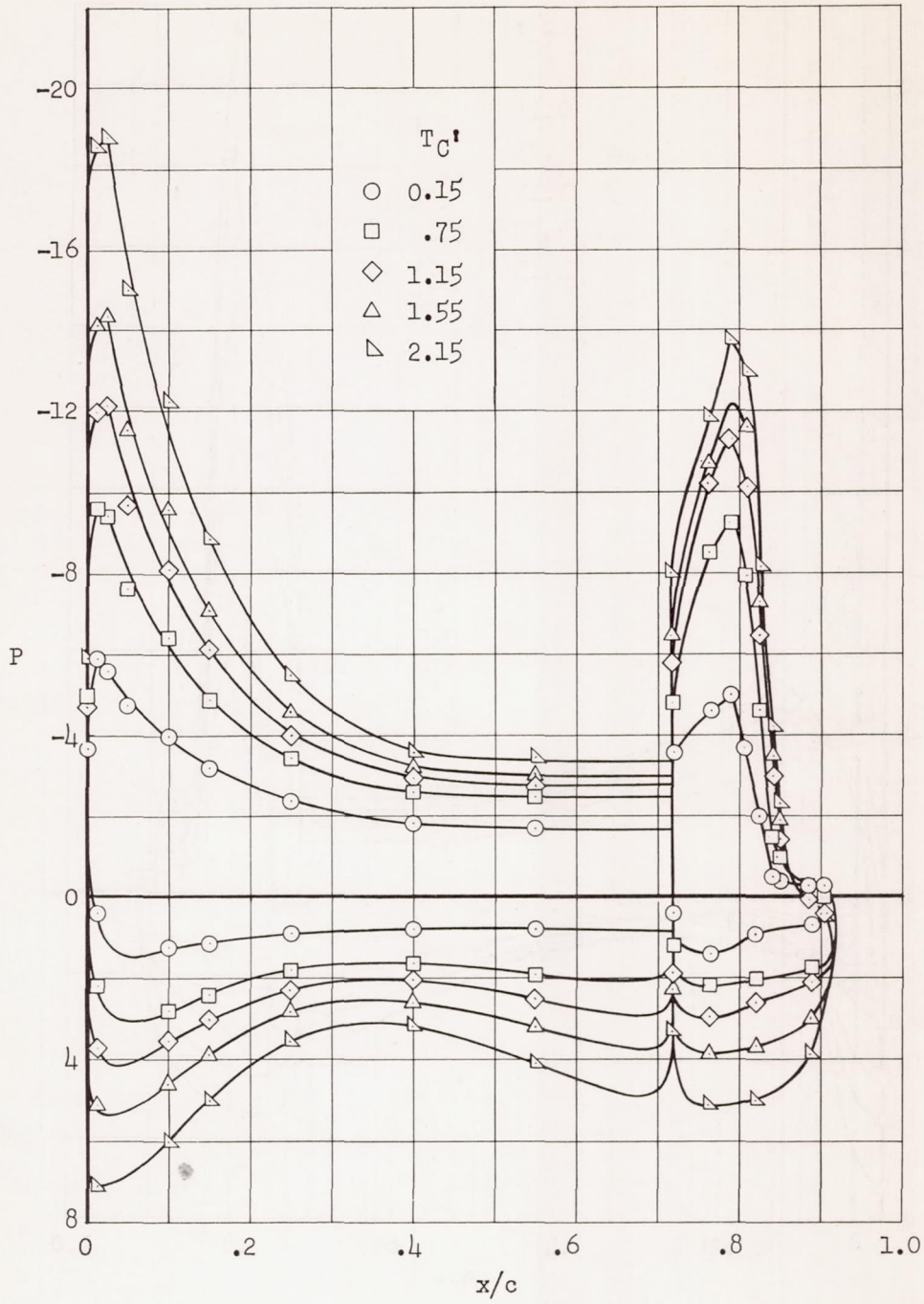

(b) The 0.343-semispan station.

Figure 13.- Continued.

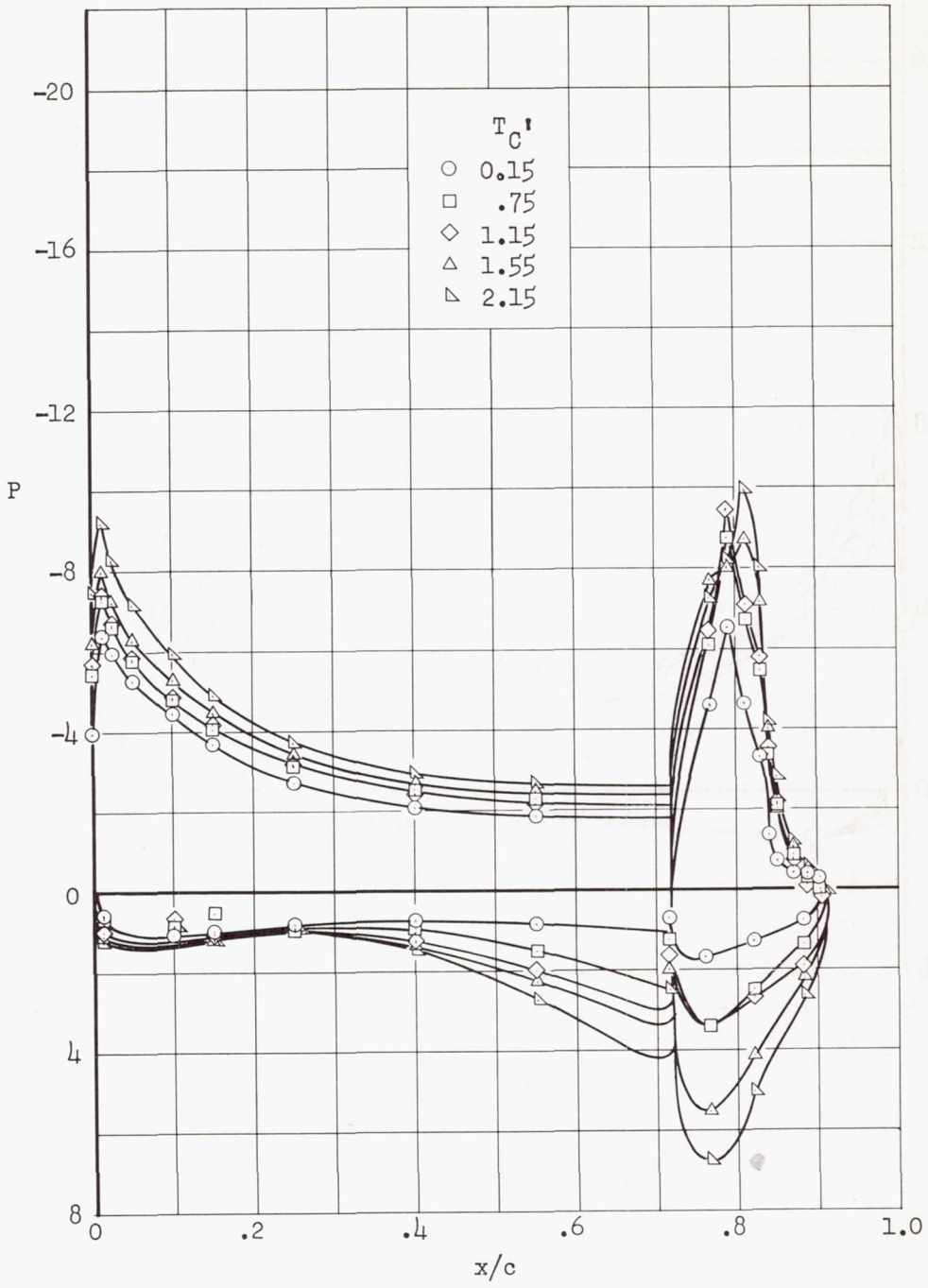

(c) The 0.454-semispan station.

Figure 13.- Continued.

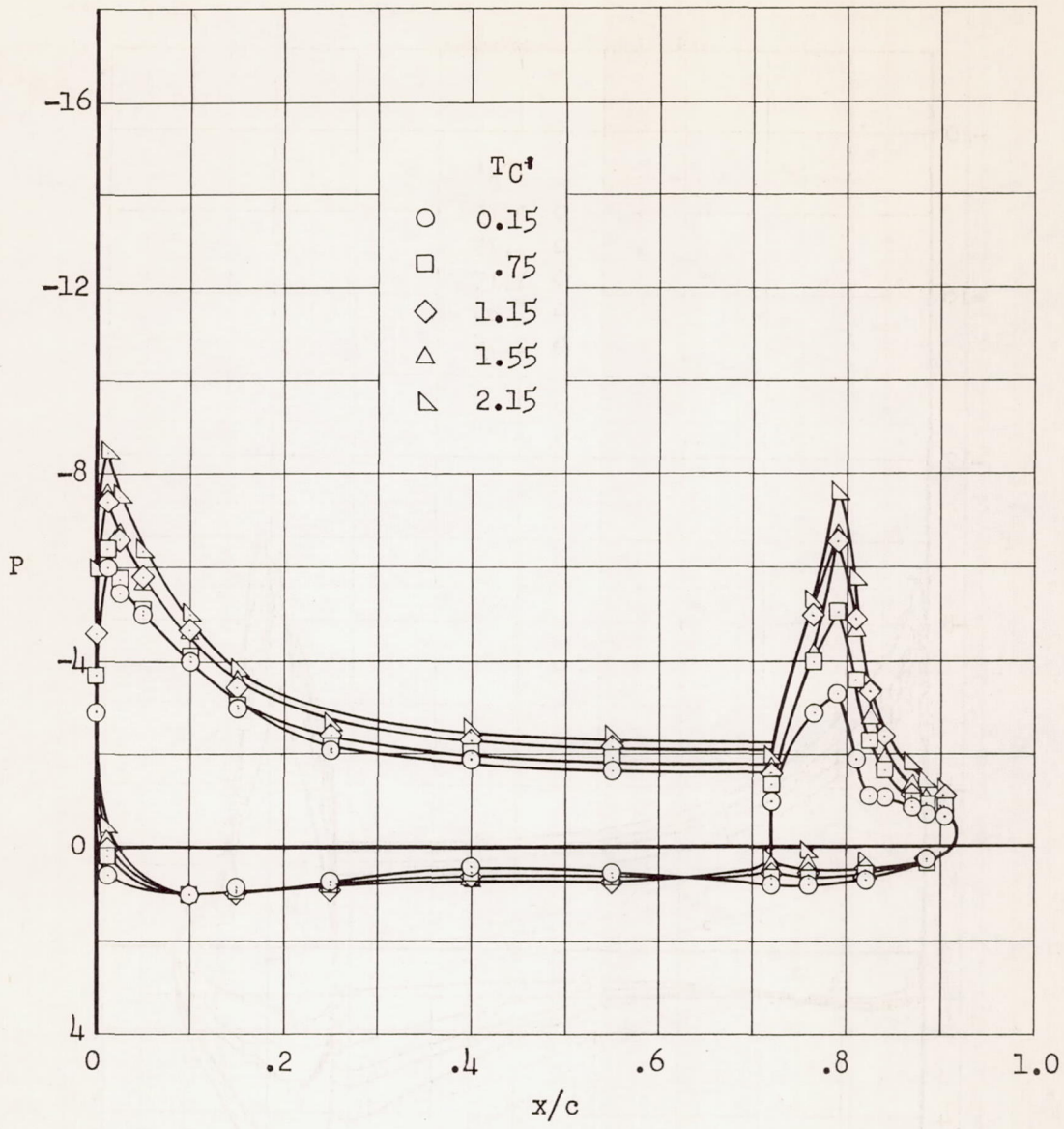

(d) The 0.583-semispan station.

Figure 13.- Concluded.

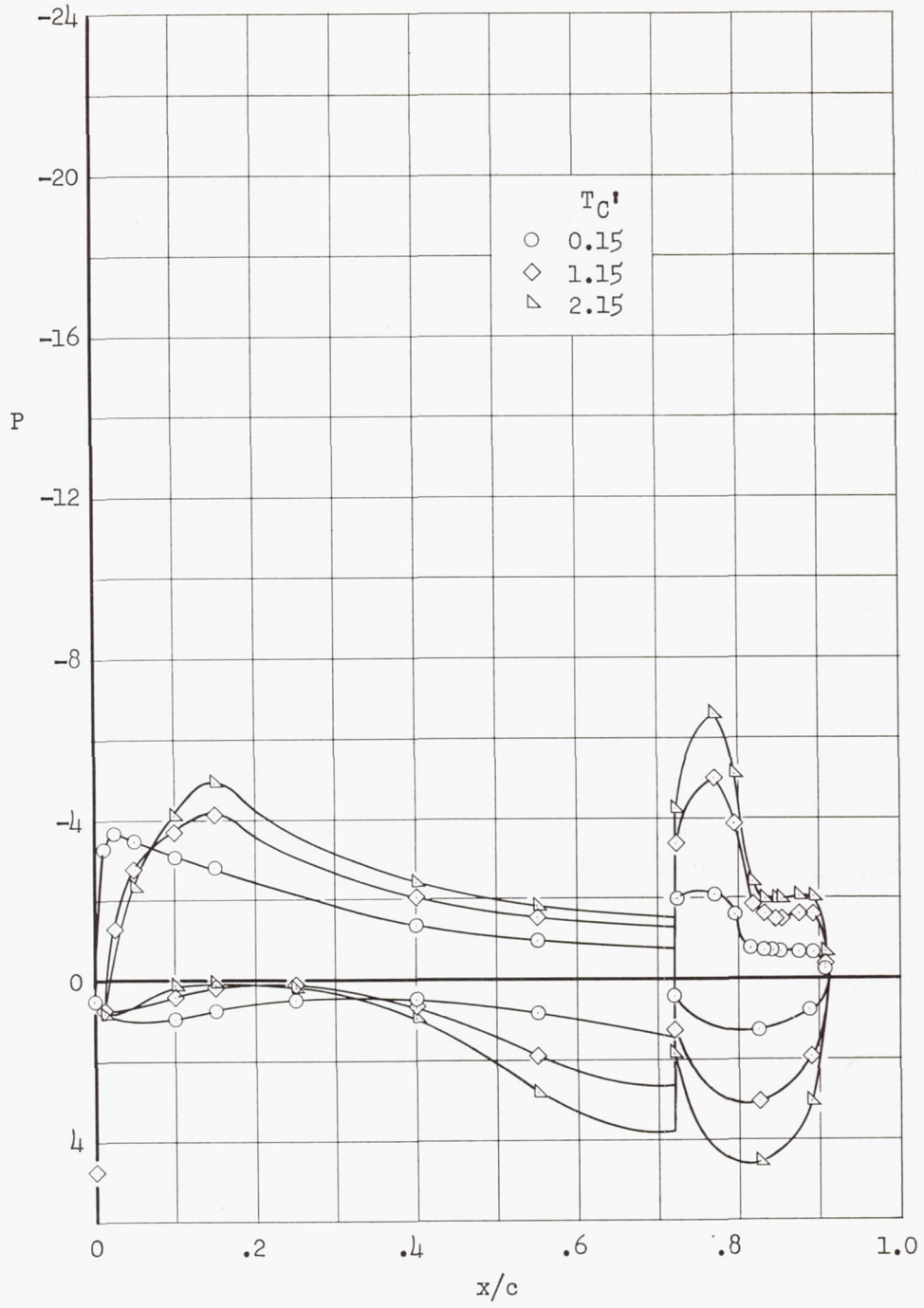

(a) The 0.186-semispan station.

Figure 14.- Effect of thrust on the chordwise distribution of pressure coefficient on the left wing; $\delta_f = 60^\circ$; $\delta_a = 30^\circ$; $C_{Q_f} = C_{Q_a} = 0$; $i_t = -3^\circ$; $\alpha_u = 0^\circ$.

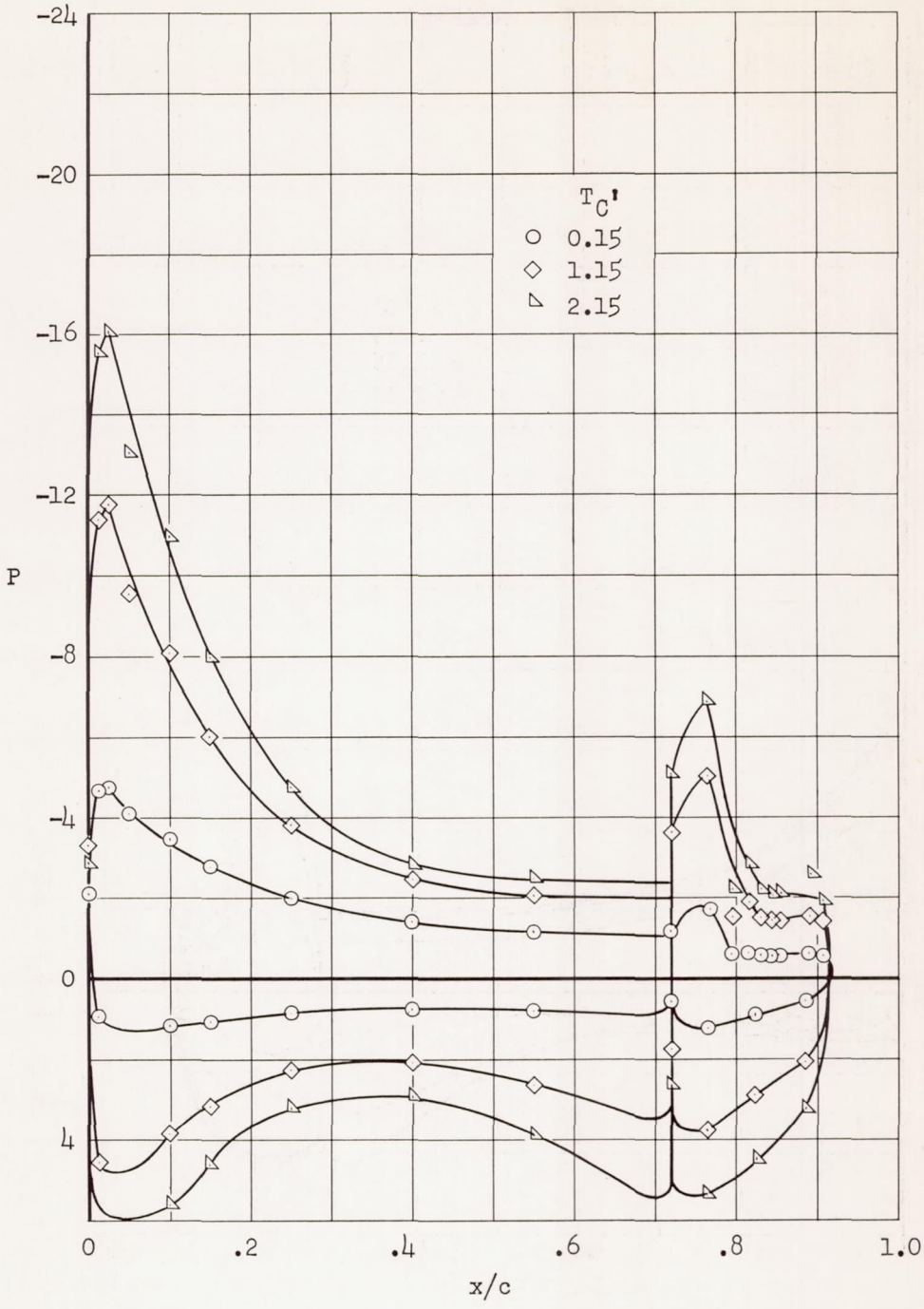

(b) The 0.343-semispan station.

Figure 14.- Continued.

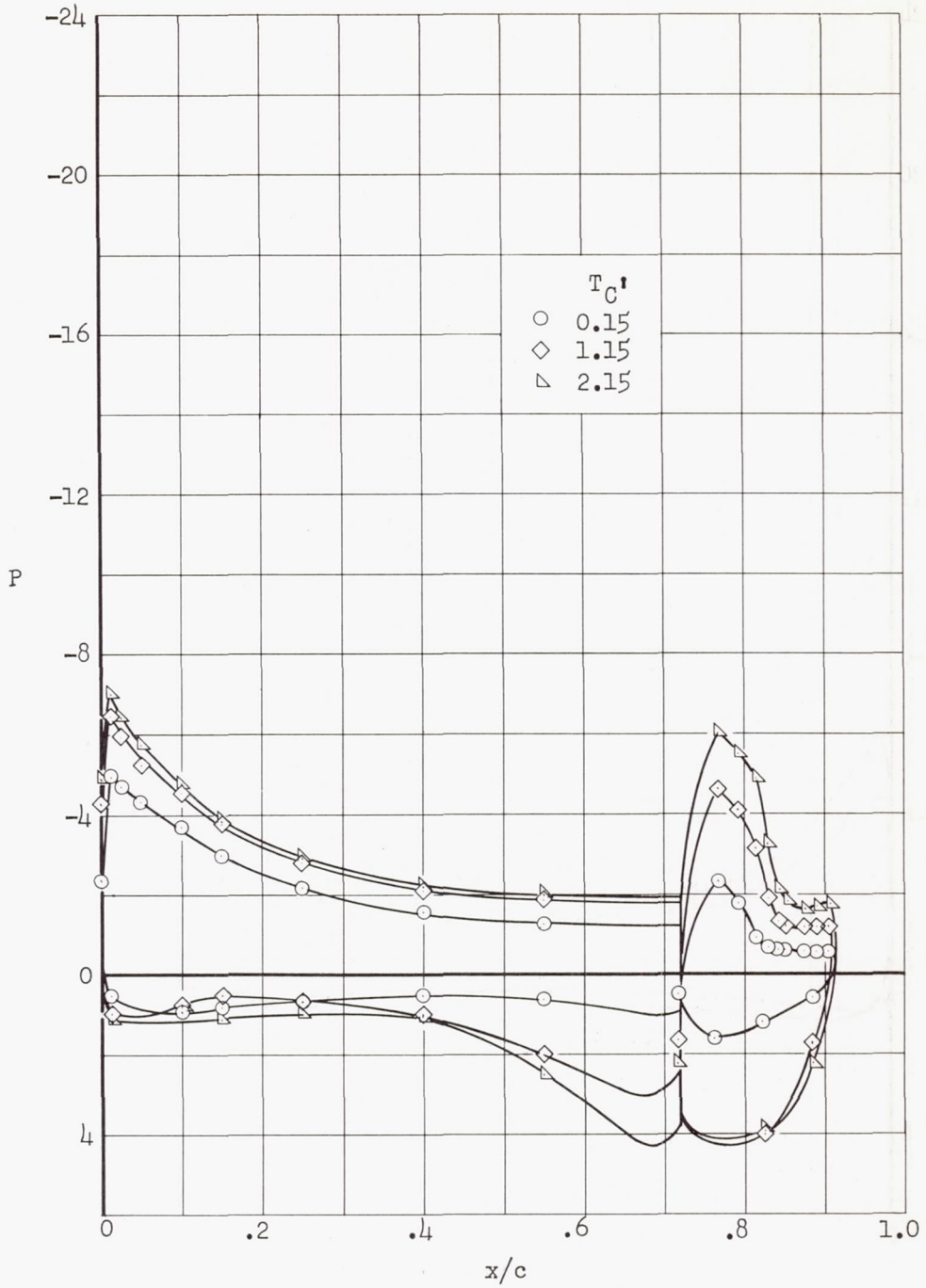

(c) The 0.454-semispan station.

Figure 14.- Continued.

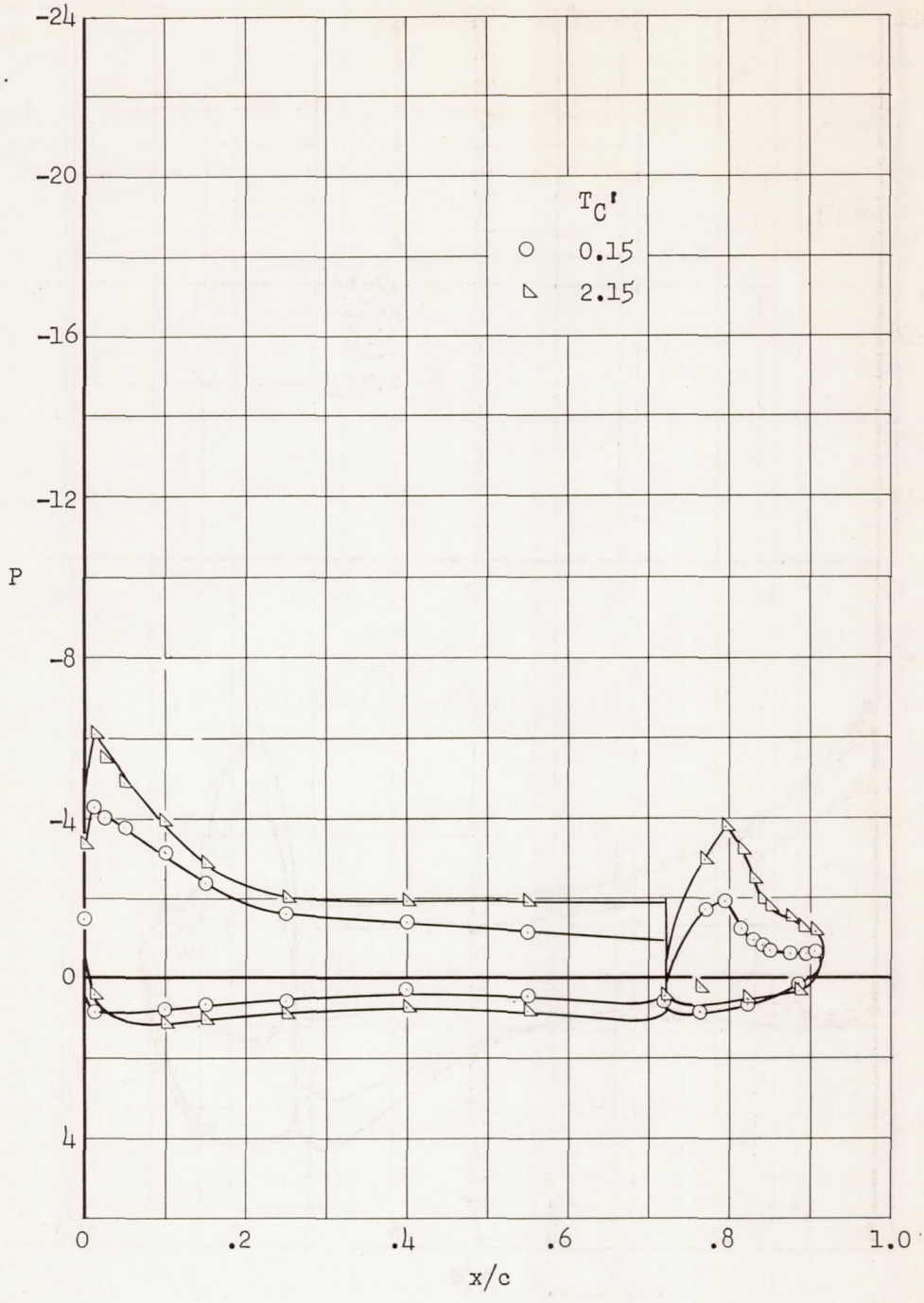

(d) The 0.583-semispan station.

Figure 14.- Concluded.

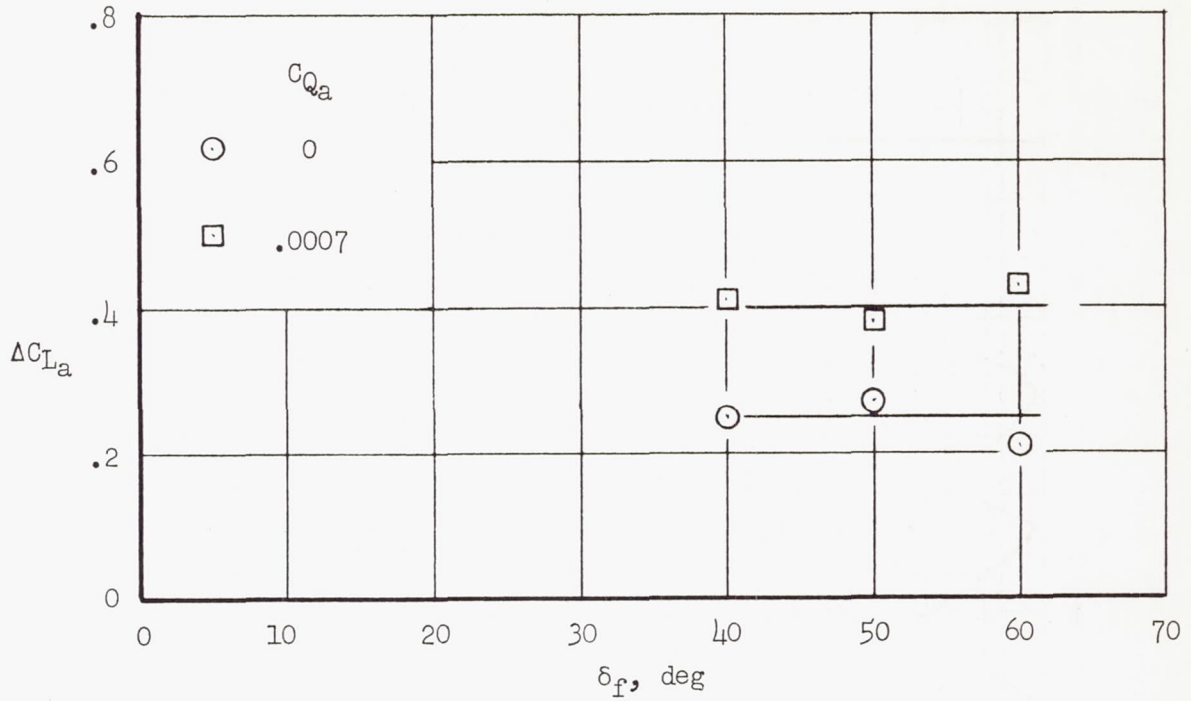

(a) Propellers and nacelles off.

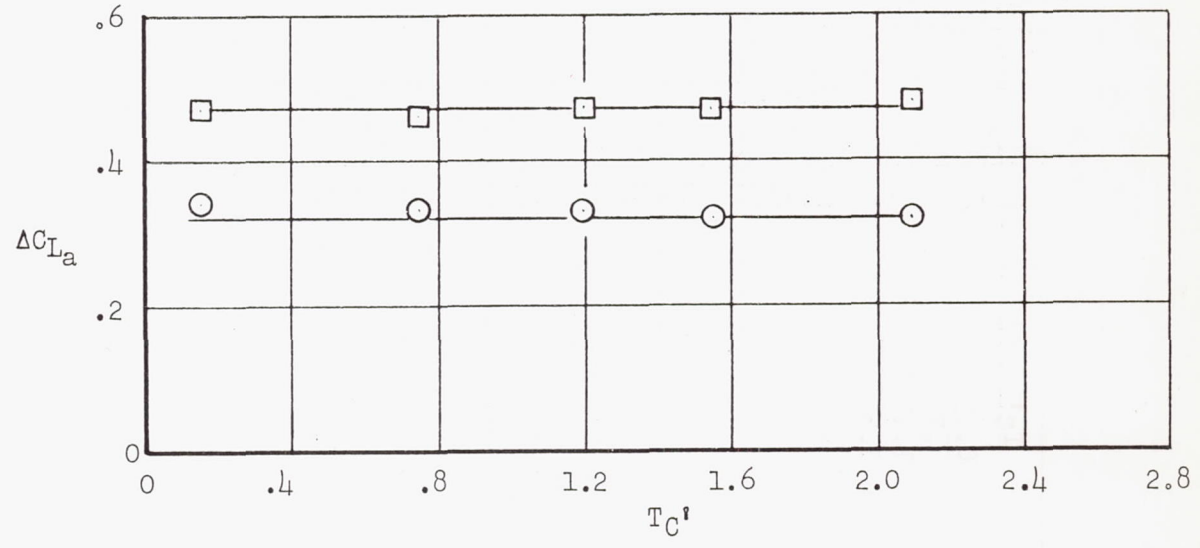

(b) $\delta_f = 60^\circ$

Figure 15.- The lift-coefficient increment due to 30° aileron deflection; $\alpha_u = 0^\circ$.

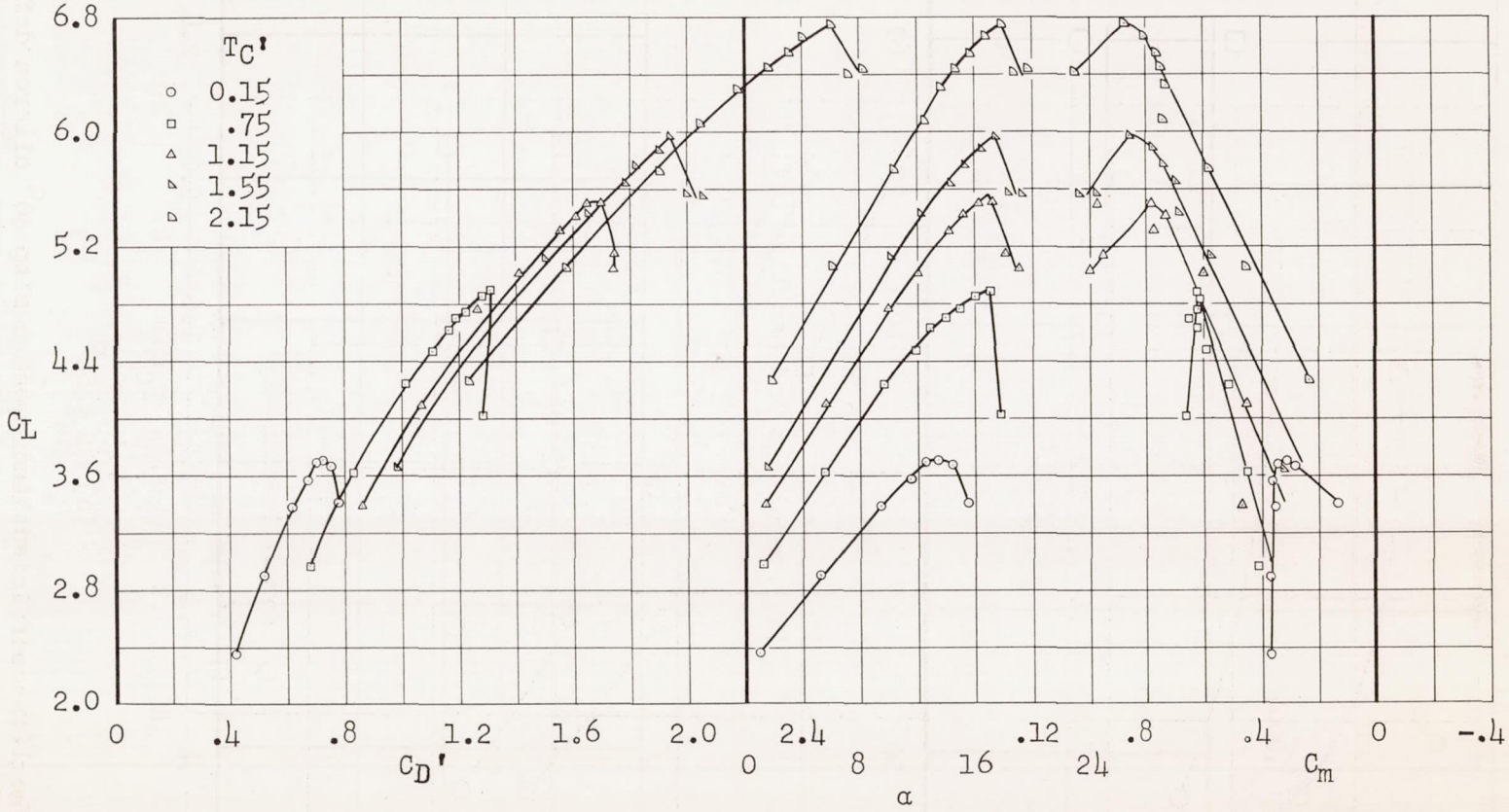

Figure 16.- Aerodynamic characteristics of the model with a simulated leading-edge flap; $\delta_f = 60^\circ$; $\delta_a = 30^\circ$; $C_{Q_f} = 0.0028$; $C_{Q_a} = 0.0007$; $i_t = -3^\circ$.

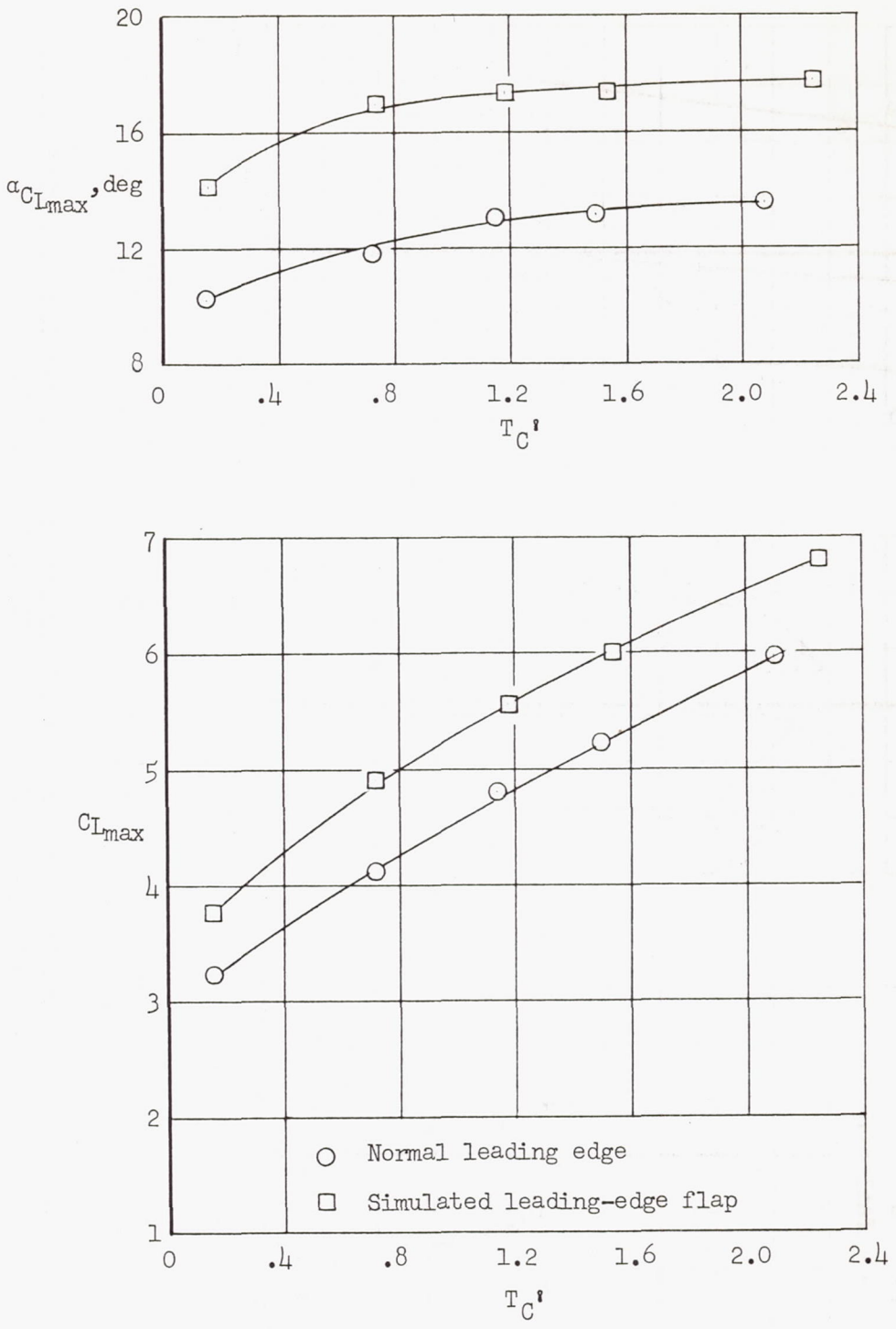

Figure 17.- Effect of a simulated leading-edge flap on $C_{L_{max}}$ and $\alpha_{C_{L_{max}}}$; $\delta_f = 60^\circ$; $\delta_a = 30^\circ$; $C_{Q_f} = 0.0033$; $C_{Q_a} = 0.0007$; $i_t = -3^\circ$.

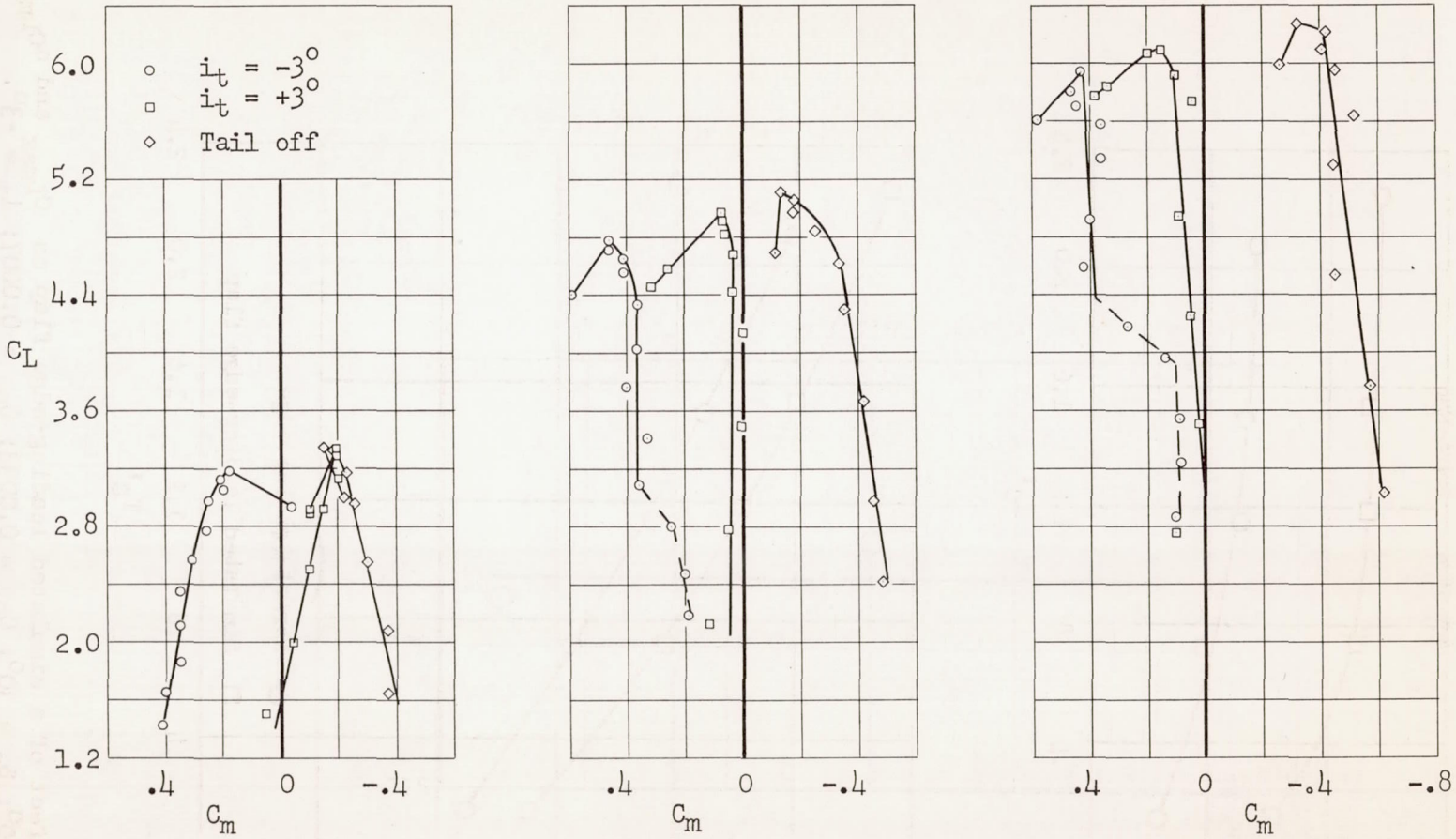

(a) T_C' = 0.15 (b) T_C' = 1.15 (c) T_C' = 2.1

Figure 18.- Effect of tail incidence on the pitching-moment characteristics of the model; $\delta_f = 60°$; $\delta_a = 30°$; $C_{Q_f} = 0.0033$; $C_{Q_a} = 0.007$.

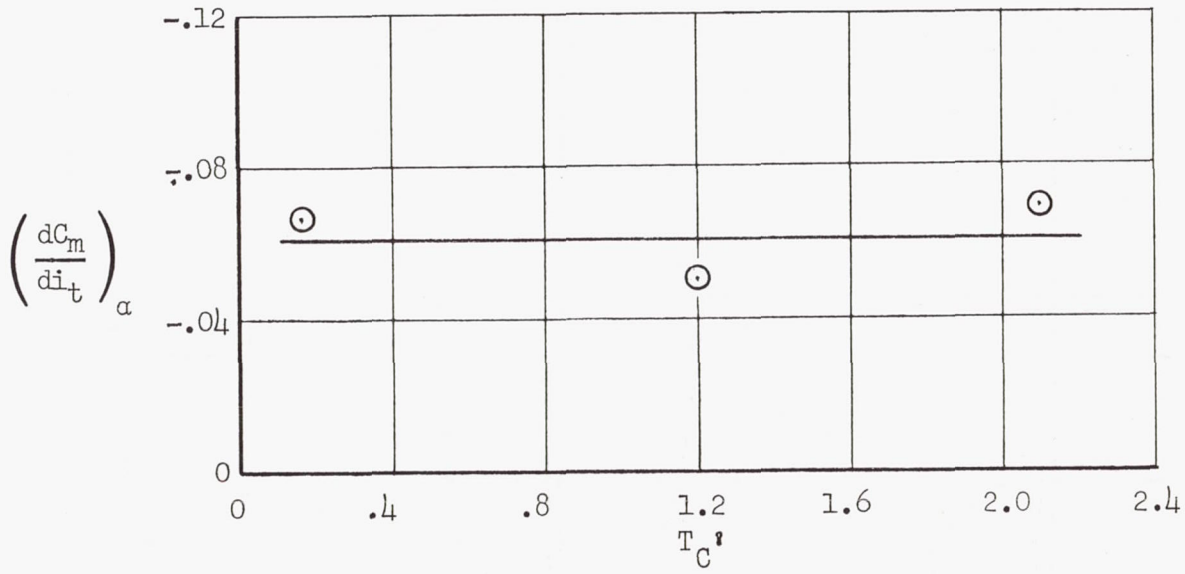

(d) $\left(\frac{dC_m}{di_t}\right)_\alpha$

Figure 18.- Concluded.

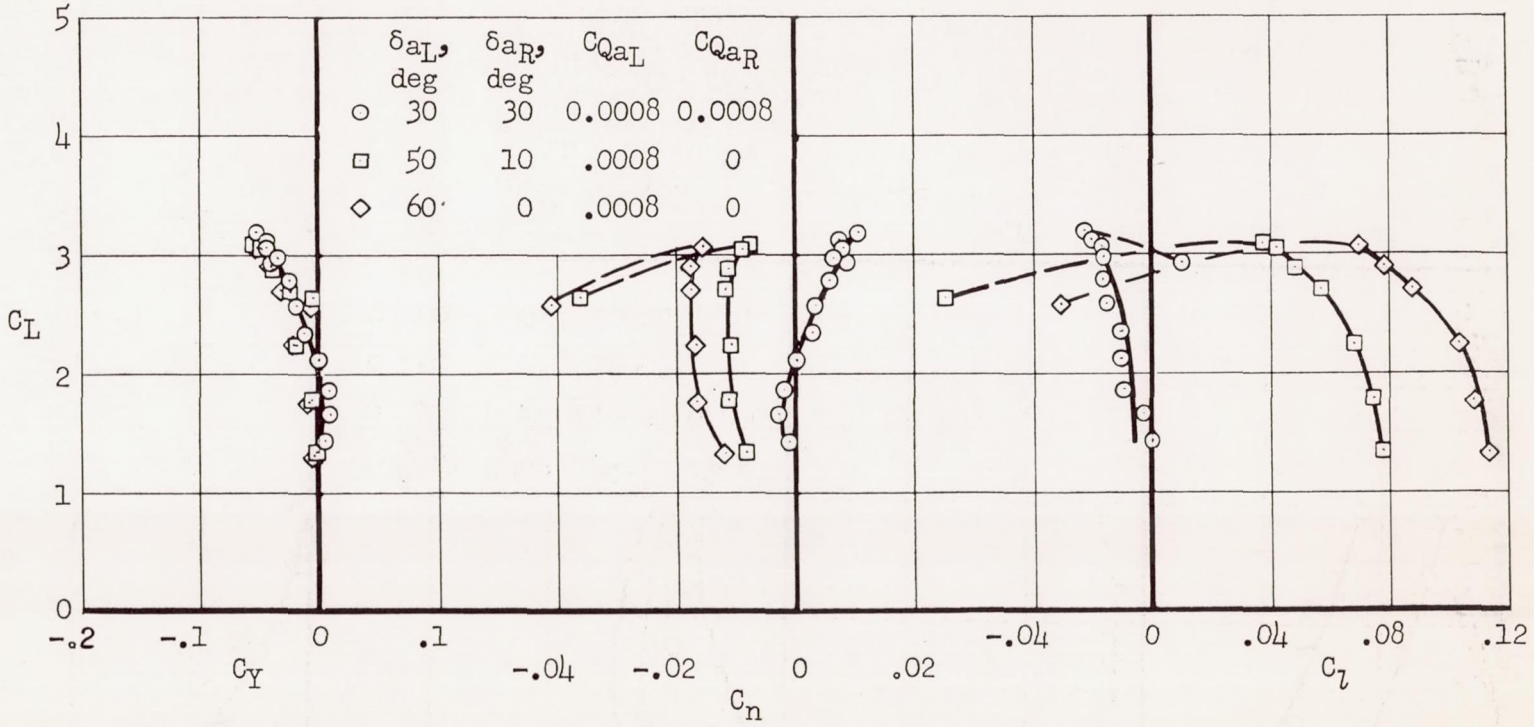

(a) $T_C' = 0.15$

Figure 19.- Lateral and directional characteristics of the model with ailerons deflected; $\delta_f = 60^\circ$; $C_{Q_f} = 0.0028$; $i_t = -3^\circ$.

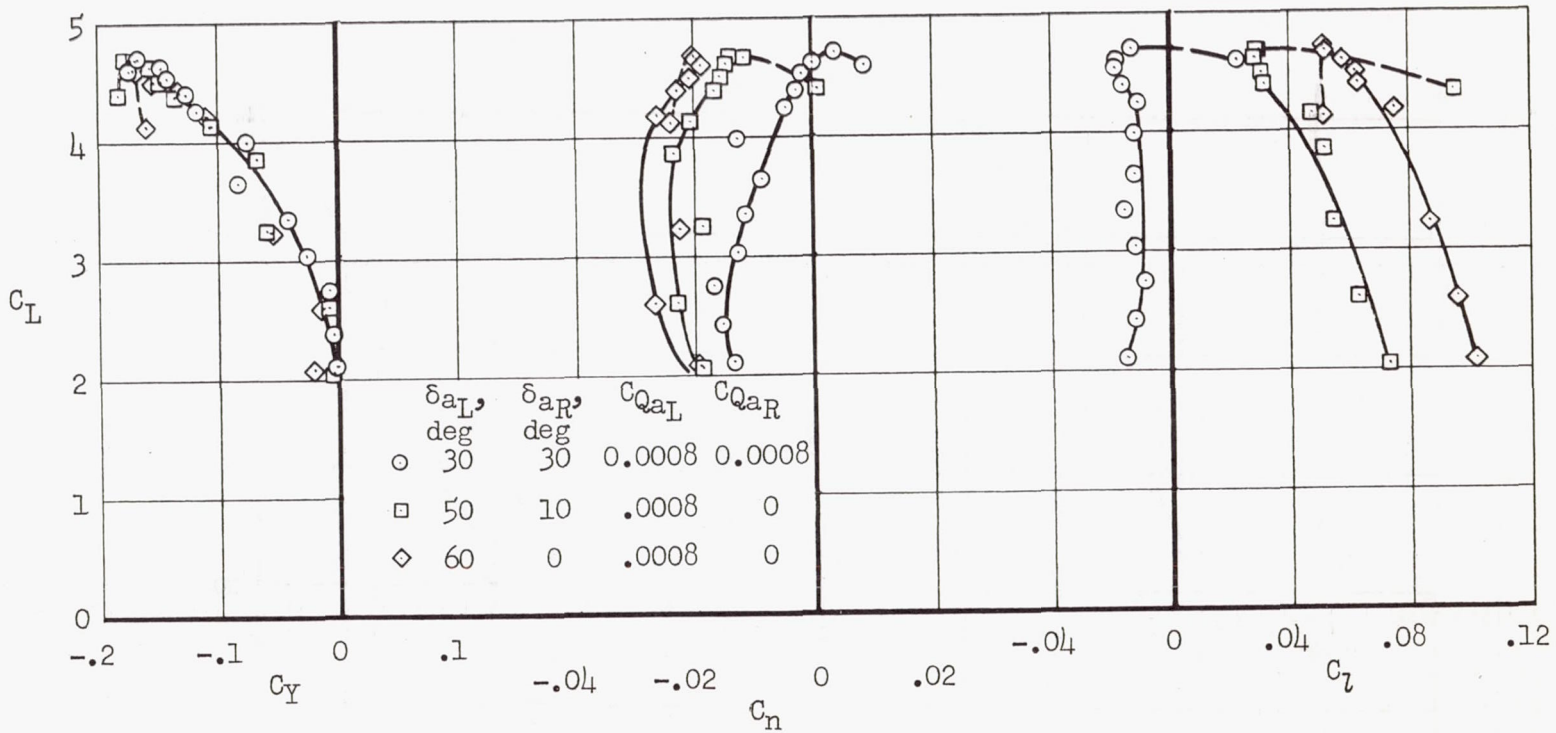

(b) $T_C' = 1.15$

Figure 19.- Concluded.

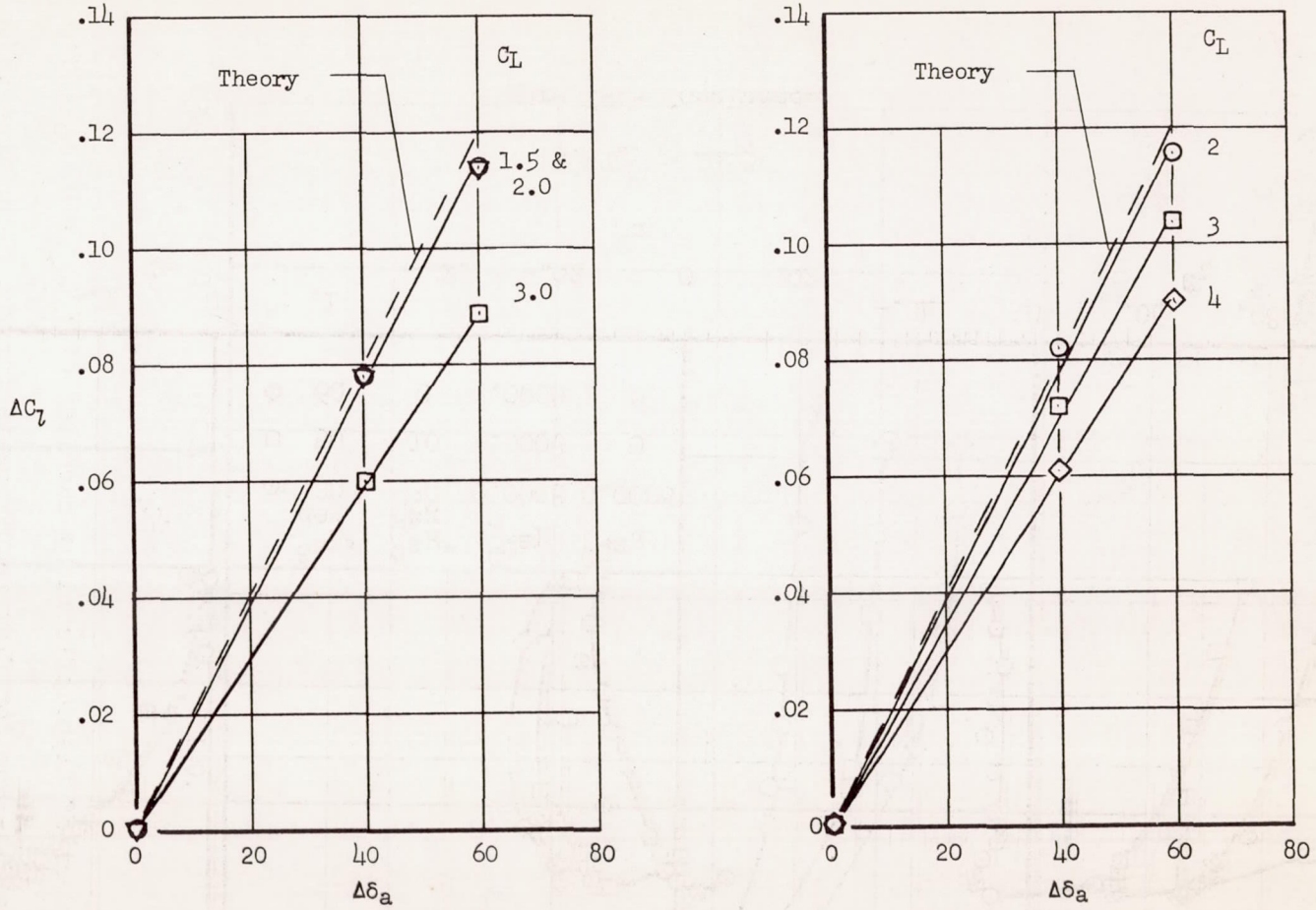

(a) $T_C' = 0.15$

(b) $T_C' = 1.15$

Figure 20.- Comparison of aileron effectiveness with theory; $\delta_f = 60^\circ$; $C_{Q_f} = 0.0027$; $C_{Q_{a_L}} = 0.0008$; $C_{Q_{a_R}} = 0$; $i_t = -3^\circ$.

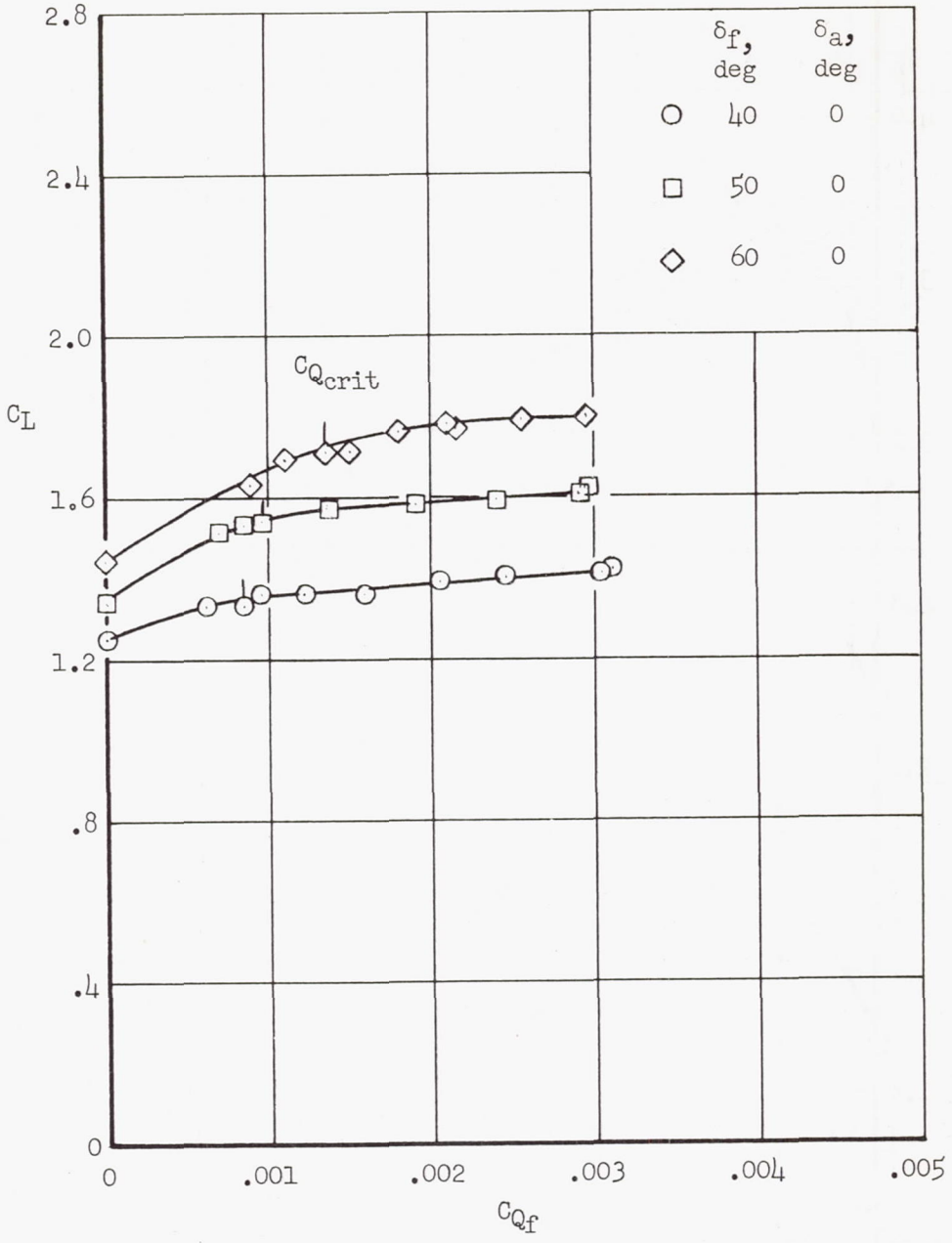

(a) Effect of flap deflection; nacelles off; $C_{Q_a} = 0$, $\alpha_u = 0^\circ$.

Figure 21.- Suction flow requirements for the flap; $i_t = -3^\circ$.

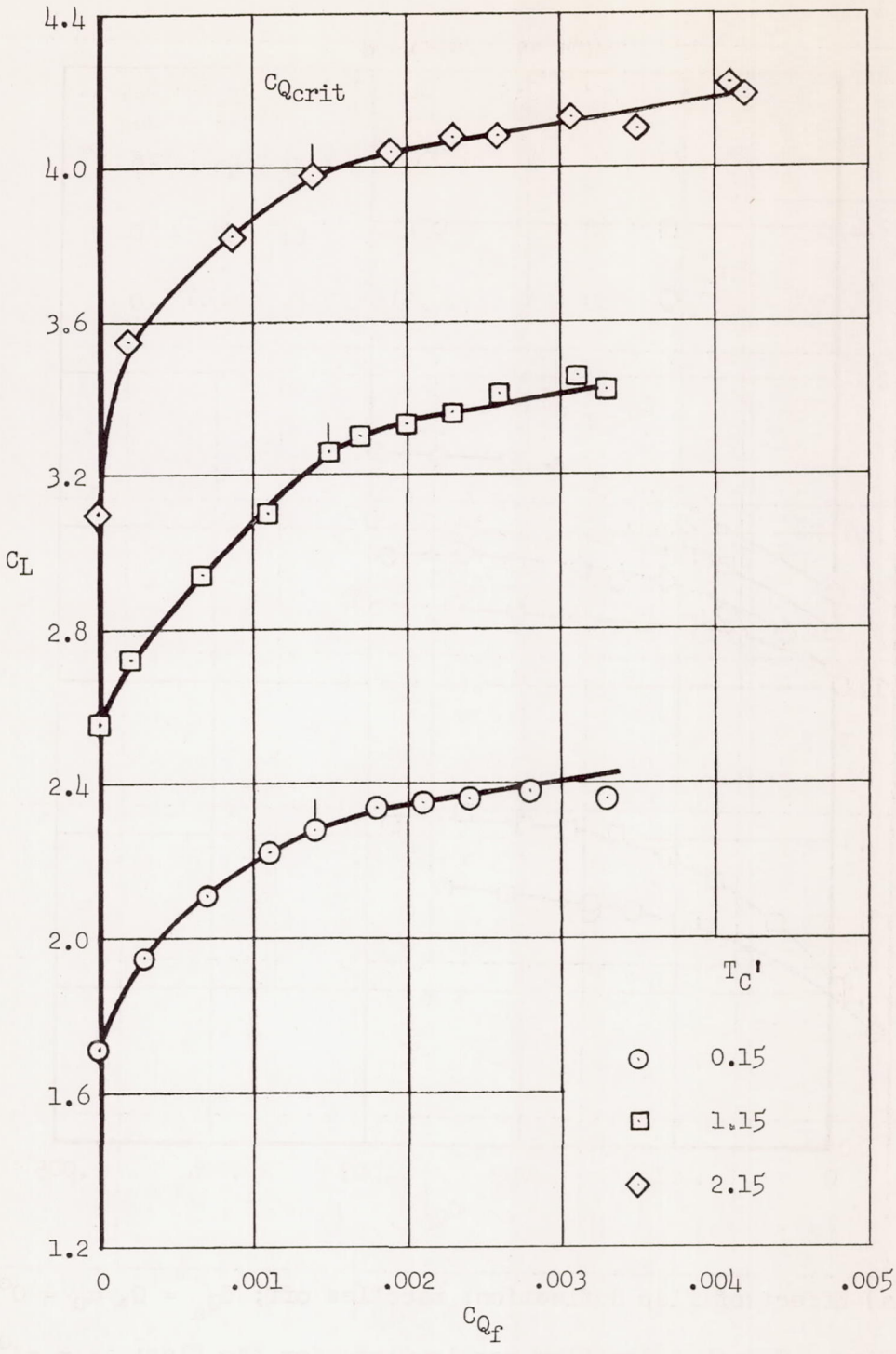

(b) Effect of thrust; $\delta_f = 60^\circ$; $\delta_a = 30^\circ$; $C_{Q_a} = 0.0013$; $\alpha_u = 0^\circ$.

Figure 21.- Continued.

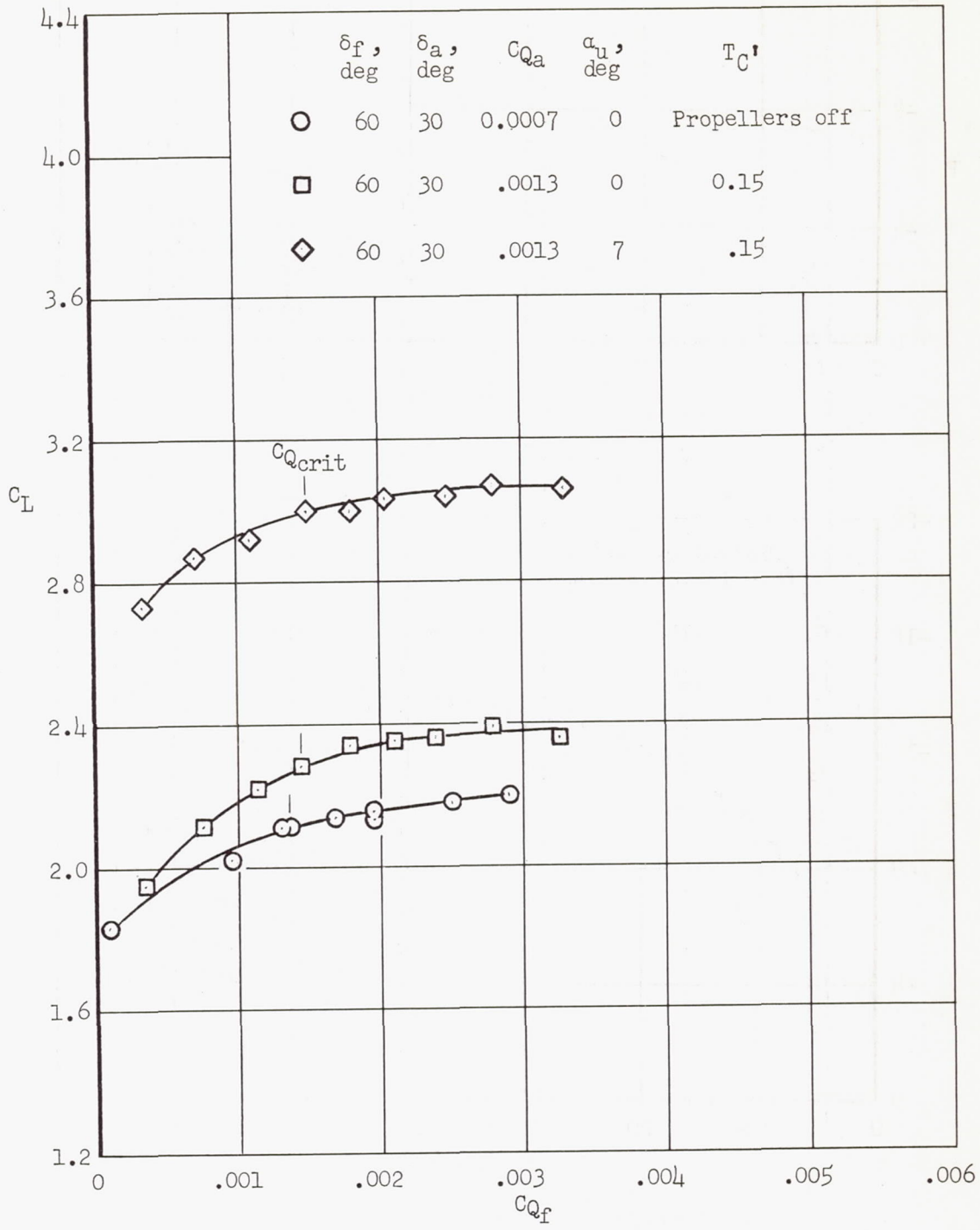

(c) Effect of angle of attack and aileron deflection.

Figure 21.- Concluded.

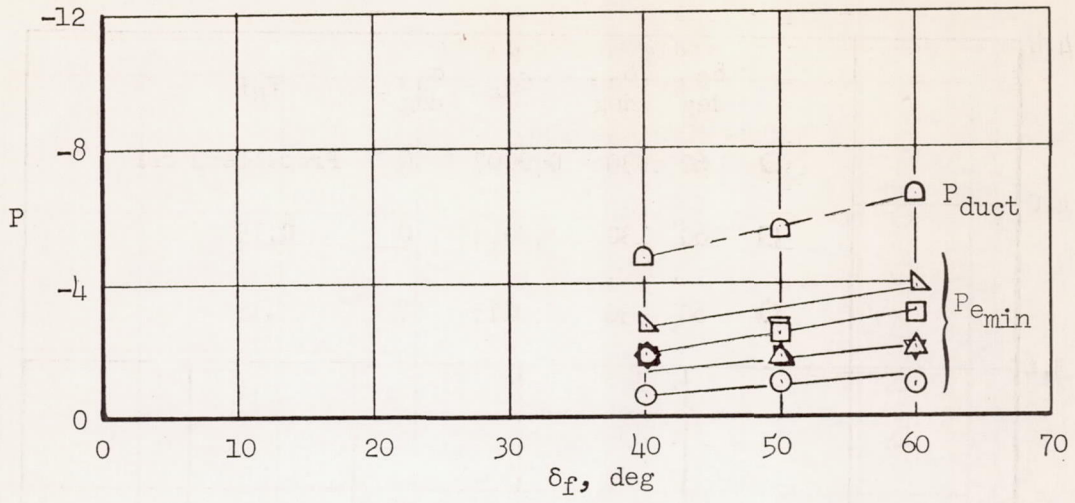

(a) Propellers and nacelles off.

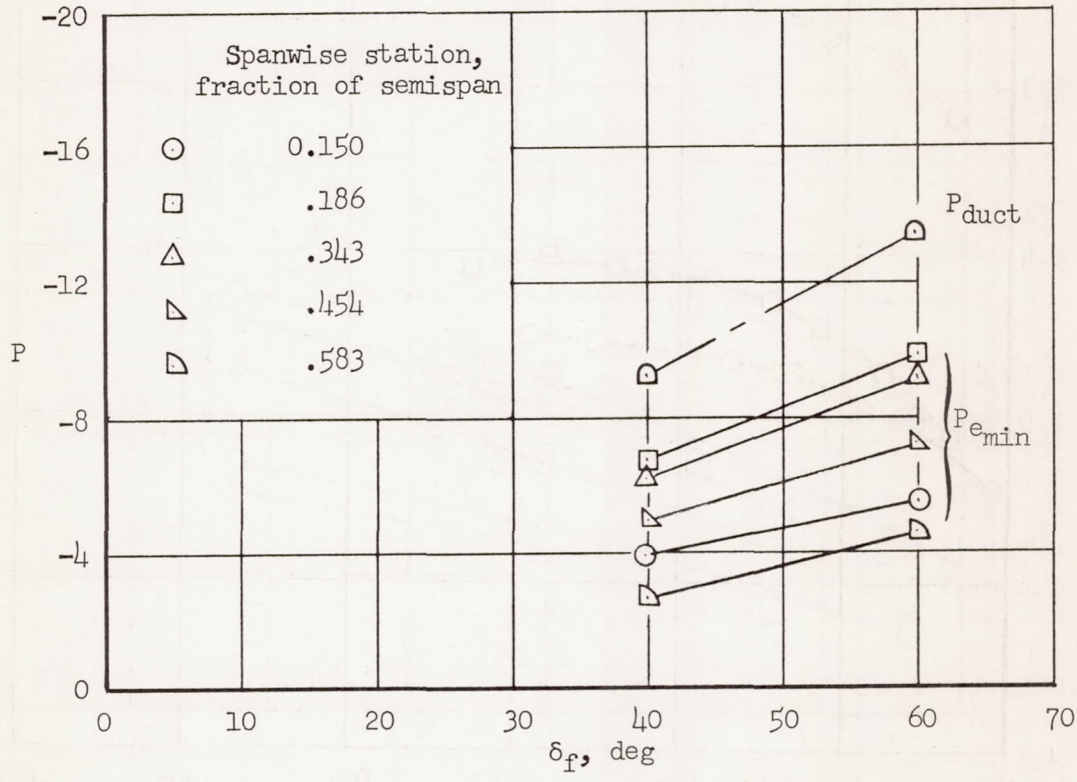

(b) Propellers and nacelles on; $T_C' = 1.15$.

Figure 22.- Flap duct and external surface pressures at $C_{Q_{f_{crit}}}$; $\delta_a = 30^\circ$; $C_{Q_a} = 0.0007$, $\alpha_u = 0^\circ$.

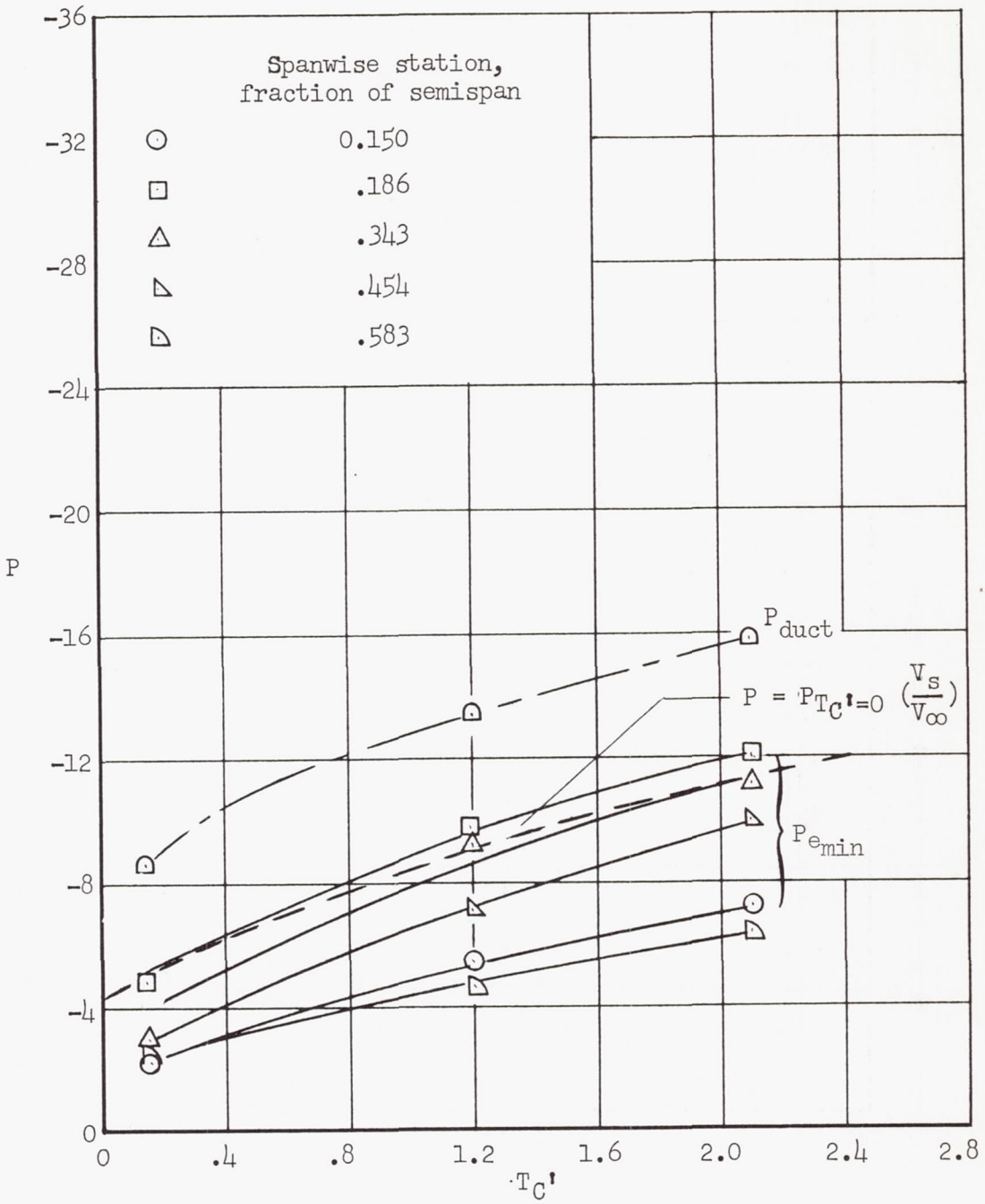

(c) $\delta_f = 60^\circ$

Figure 22.- Concluded.

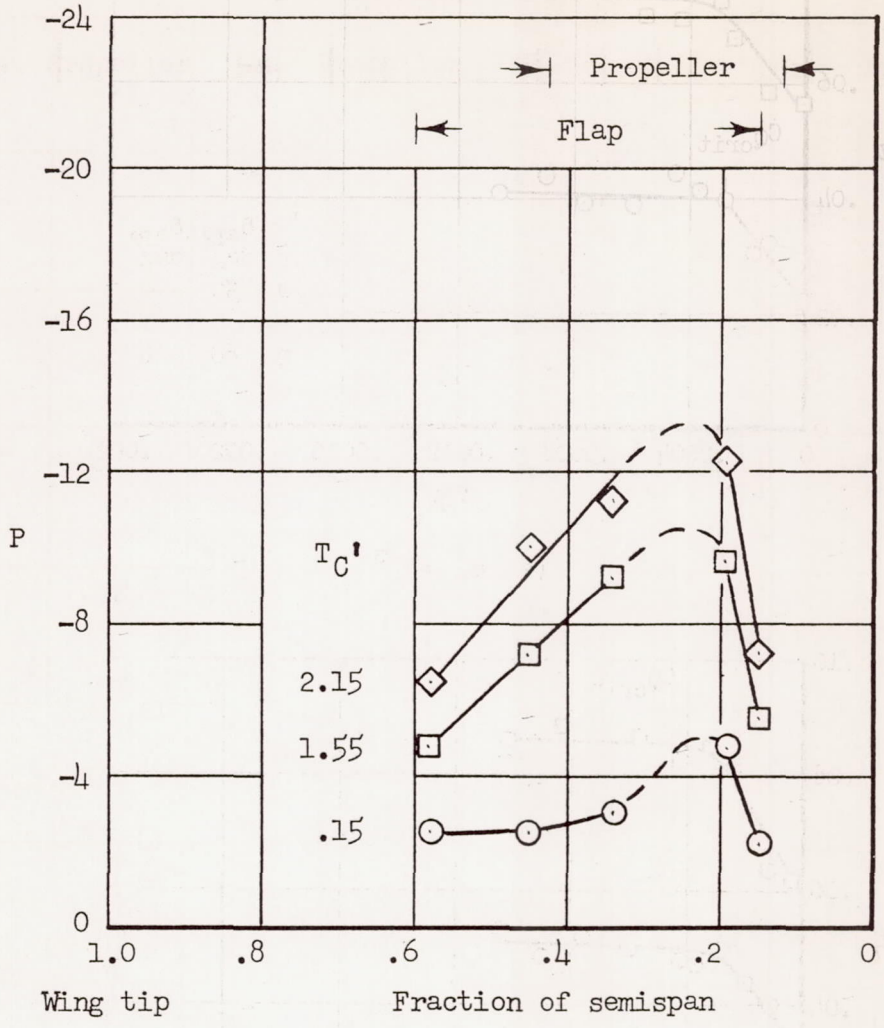

Figure 23.- Spanwise variation of minimum pressures on the left flap; $\delta_f = 60^\circ$; $\delta_a = 30^\circ$; $C_{Q_f} = 0.0015$; $C_{Q_a} = 0.0007$; $i_t = -3^\circ$; $\alpha_u = 0^\circ$.

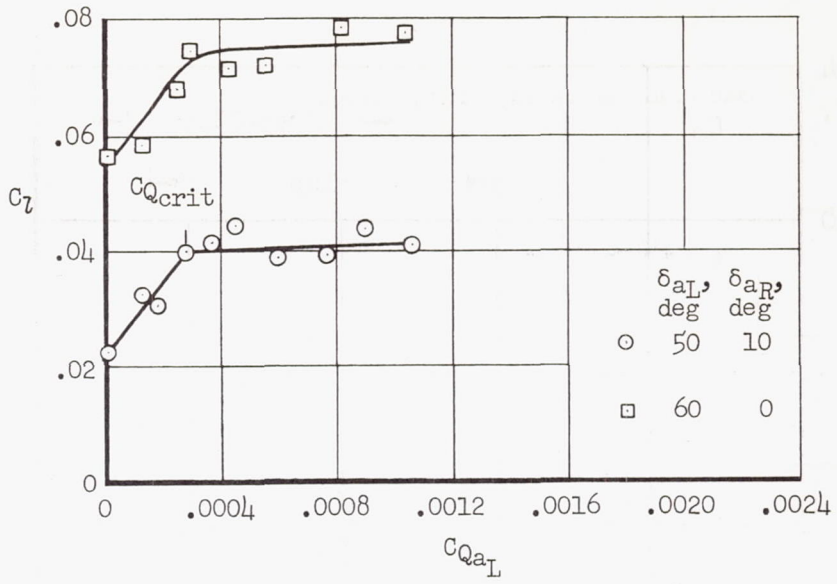

(a) $\alpha_u = 7^\circ$

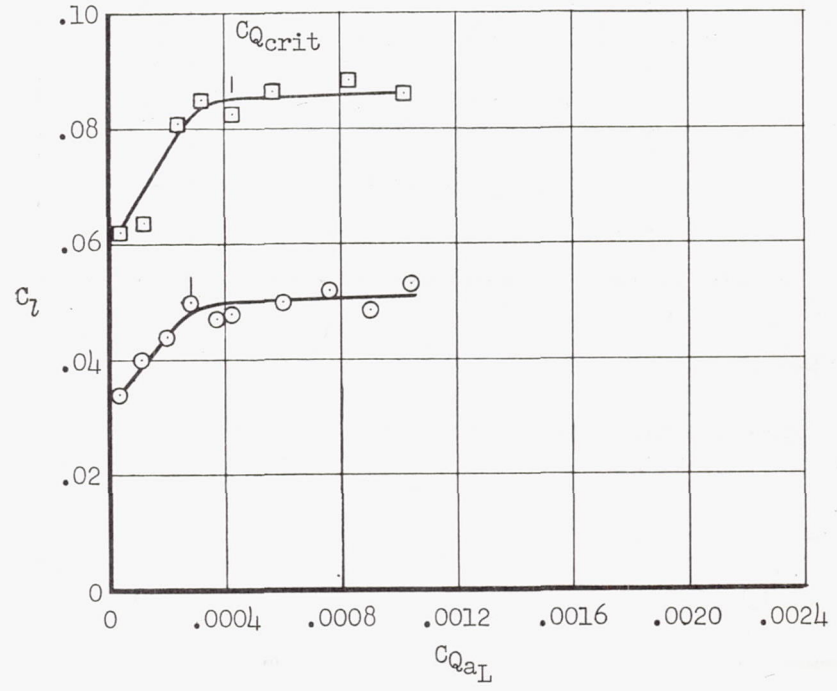

(b) $\alpha_u = 0^\circ$

Figure 24.- Aileron suction flow requirements; $\delta_f = 60^\circ$; $C_{Q_f} = 0.0028$; $i_t = -3^\circ$; $T_C' = 1.15$.

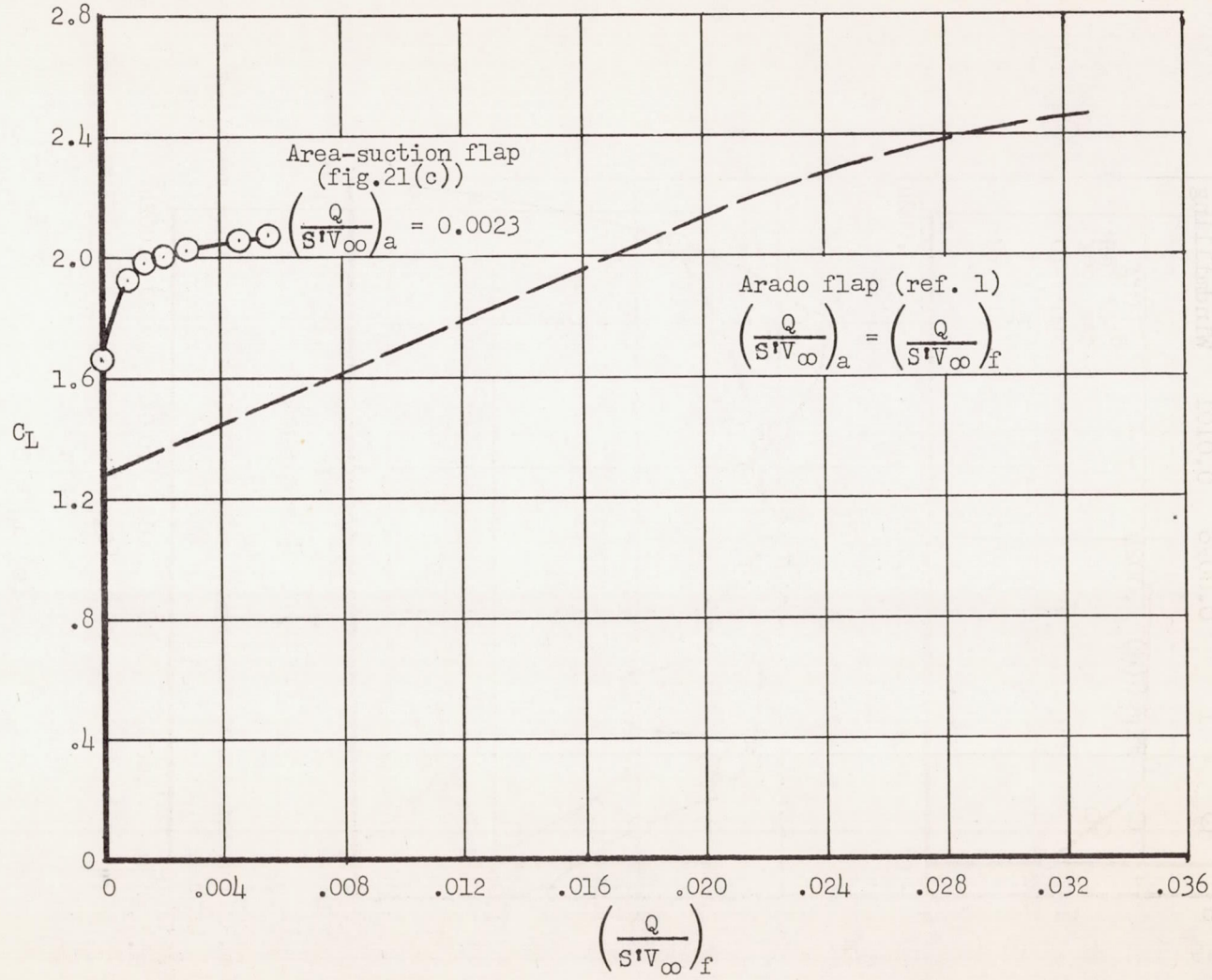

Figure 25.- Comparison of the suction flow requirements of the area-suction flap of this report with the Arado type boundary-layer-control system of reference 1; $\delta_f = 50^\circ$; $\delta_a = 30^\circ$; $\alpha_u = 0^\circ$.

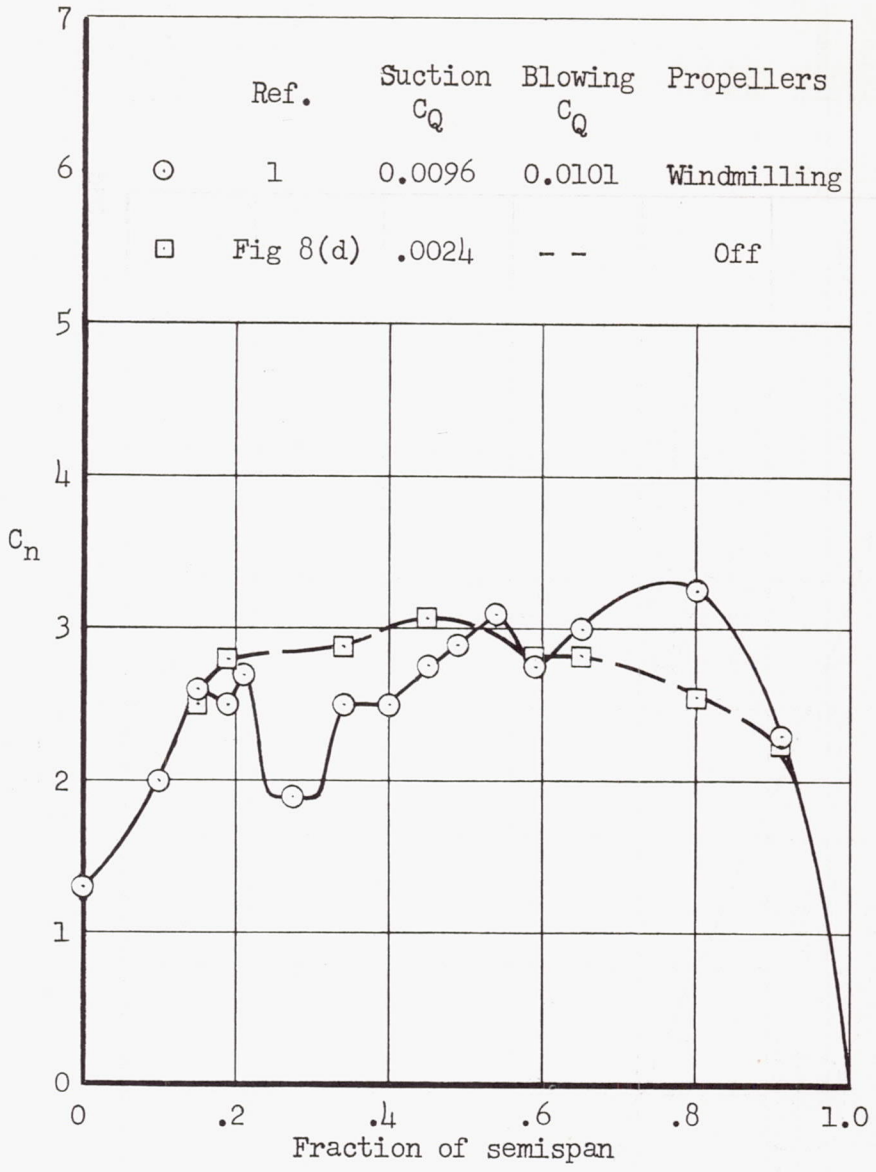

Figure 26.- Comparison of the span load distribution of the model of this report having suction flaps with the model of reference 1 having a combination suction-blowing (Arado) system; $\delta_f = 50^\circ$; $\delta_a = 30^\circ$; $C_L = 2.7$.